EXPERIMENT DESIGN FOR (TH,PU)O_2 POWER REACTORS

DEVELOPMENT OF APPLICABLE BENCHMARK EXPERIMENTS FOR (TH,PU)O_2 POWER REACTOR DESIGNS USING TSUNAMI ANALYSIS

BY STEPHANIE ELAINE LANGTON, B.ENG

A Thesis Submitted to the School of Graduate Studies in Partial Fulfillment of the Requirements for the Degree Master of Applied Science

McMaster University MASTER OF APPLIED SCIENCE (2013) Hamilton Ontario (Engineering Physics)

TITLE: Development of Applicable Benchmark Experiments for (Th,Pu)O_2 Power Reactor Designs Using TSUNAMI Analysis AUTHOR: Langton, S.E. (McMaster University) SUPERVISOR: Dr. A. Buijs NUMBER OF PAGES: xi,119

Abstract

When simulating reactor physics experiments, uncertainties in nuclear data result in a bias between simulated and experimental values. For new reactor designs or for power reactor designs the bias can be estimated using a set of experiments. However, the experiments used to estimate the bias must be applicable to the power reactor design of interest. Similarity studies can be performed to ensure this is the case. Here, potential experiments in the ZED-2 heavy water critical facility at Chalk River Laboratories were developed that would be applicable to the multiplication factor bias calculation of three thoria plutonia fuelled power reactor designs. The power reactor designs that were analyzed were the CANDU 6 with 37-element fuel bundles and 43-element fuel bundles, and a Canadian SCWR design with 78-element fuel assemblies. The power reactors were simulated using the code package SCALE 6.1 under burnup conditions that were determined using the lattice code DRAGON 3.06H and the diffusion code DONJON 3.02A. The intermediate results from DRAGON and DONJON were used to compare the benefits of various reactor designs. Various critical core configurations were then simulated in the ZED-2 reactor using the SCALE 6.1 package. The similarities between the potential ZED-2 reactor experiments and the power reactors were analyzed. These results were used to design a set of experiments having sufficiently high completeness that they can be used as part of a bias calculation using the generalized linear least squares method. To do so a methodology was developed to guide the experiment set design process in which the fuel type, lattice arrangements, and coolant type are modified and the effects on the sensitivity coverage analyzed. A set of six experiments was designed for which all of the power reactor designs had a completeness of 0.7 or higher.

Acknowledgments

I would first like to thank Dr. A. Buijs for his supervision and guidance throughout this project. Also, thank you to Dr. D. R. Novog for his assistance throughout my time as a graduate student. In addition, I would like to thank my parents Catherine Bell and Max Langton and my grandparents Verna and Gerry Bell for their support (financial and otherwise) and for making sure I was happy and healthy. Also, thank you to Ken for always being there for me and helping when I get too stressed out. Finally, thank you to my friends and colleagues in the Engineering Physics department for their assistance in technical matters and for making the past two years a lot of fun.

This work was supported by the National Science and Engineering Research Council (NSERC) of Canada, under grant numbers 125519967 and 165755410.

Contents

List of Figures

List of Tables

The following thesis is the work of Stephanie E. Langton. Any prior work pertaining to the subject has been duly referenced.

Chapter 1

Introduction

When developing a new power reactor design, or when modifying an existing design with a new fuel type, it is essential that the analysis codes used be validated for any new conditions introduced. Such validation can be performed (in part) through comparison with experimental results from a test reactor facility. In order to ensure that the test reactor results can be reasonably applied to the power reactor simulation, similarity factors can be examined. The focus of this thesis is on the similarity of test reactor experiments and power reactor designs using thorium fuel. Specifically, experiments involving (Th,Pu)O_2 fuel in the ZED-2 (Zero Energy Deuterium) heavy water critical facility located at Chalk River Laboratories (CRL) are used as the experiments in the similarity studies [1]. First the similarity of the ZED-2 reactor to the CANadian Deuterium-Uranium (CANDU) reactor developed by Atomic Energy Canada Limited (AECL) is examined with 37-element and 43-element bundles and thoria plutonia fuel elements. Next a supercritical water reactor (SCWR) design is used in the similarity study. In order to increase the similarity between the test reactor and the power reactor and to develop a potential benchmark set of experiments, various ZED-2 fuelling patterns and thoria plutonia fuel types are analyzed.

1.1 Thorium Fuelled Power Reactors

In most power reactors currently operating, fuel containing a certain percentage of U-235 is used as the fissile material. The CANDU reactor uses fuel consisting of natural uranium, which contains approximately 0.71% U-235 by weight. Other reactor designs, such as the Pressurized Water Reactor (PWR), use uranium fuel that has been enriched to a greater U-235 weight percentage.

However, uranium is not the only fuel type that can be used to successfully operate a nuclear reactor. Specifically, reactors fuelled with thorium oxide fuel are an option that may be beneficial for several reasons. Th-232, the thorium isotope found in nature, is not in itself a fissile material but is instead known as a fertile material. This means that fission must be induced by neutron irradiation from a starter fissile

material incorporated into the fuel, which then results in the production of the fissile U-233 through the process shown below [2].

$$\text{Th-232} + n \rightarrow \text{Th-233} \tag{1.1}$$

$$\text{Th-233} \rightarrow \text{Pa-233} + \beta \tag{1.2}$$

$$\text{Pa-233} \rightarrow \text{U-233} + \beta \tag{1.3}$$

This conversion process means that as the reactor operates and the starter fissile material depletes, Th-232 breeds U-233, helping slow the overall depletion of fissile material.

One of the main benefits of using thorium fuels is that there is a much higher abundance of thorium than uranium deposits (approximately 3 to 4 times higher) [3], making it a desired option for countries that are not rich in uranium. In addition, thorium fuel decreases the possibility of weapons proliferation in two ways. First, existing weapons grade plutonium can be used in the thorium cycle as the starter material. This is also true of civilian grade plutonium. A second way in which the thorium cycle decreases the possibility of weapons proliferation is that spent fuel from the thorium reactor contains U-232, which is produced through (n,2n) reactions. The decay of U-232 produces high energy gamma ray emission (the most significant being the 2.6 MeV gamma ray emitted from the decay of Tl-208) that would cause a high dose to anyone exposed [4]. This makes the extraction of fissile U-233 from the spent fuel difficult due to the shielding that would be required when handling the spent fuel. Adding to this difficulty is the fact that the removal process of the U-232 contaminants from the U-233 is difficult in itself.

1.1.1 CANDU Reactor

The thorium fuel cycle is of specific interest for CANDU reactor designs due to the inherent fuel-flexibility of this reactor type. The high neutron economy, fuel channel design, and on-power refuelling of the CANDU reactor mean that existing CANDU reactors could be used directly with thorium fuel bundles [5].

1.1.2 Canadian Supercritical Water Reactor

Thorium fuel is the reference fuel for the current Canadian Supercritical Water Reactor. The SCWR is a fourth generation reactor that is currently in the conceptual design stage. In its most basic definition the SCWR is any nuclear reactor in which

water in the supercritical regime is used as the primary coolant. Water in the supercritical regime (Pressure≥22.1 MPa, Temperature≥647 K [2]) is neither a liquid nor a gas, but possesses characteristics of both.

The benefit of using supercritical water as a reactor coolant is that it offers a large increase in thermodynamic efficiency from ≈33% in current reactors to ≈44% or higher [2]. This is because while reactors with subcritical water coolant are limited in their heat uptake by the critical heat flux, reactors with supercritical water coolant are not [6], allowing for the temperature of the coolant to be raised significantly higher. By increasing the temperature of the coolant the thermodynamic efficiency is also increased.

An additional benefit of the Canadian SCWR is that it uses a direct thermodynamic cycle. This also contributes to the increase in efficiency [7].

1.2 Similarity Studies

When performing reactor physics calculations, a common requirement is the computation of the effective multiplication factor of the reactor core, k_{eff}, which is equal to the ratio of the number of neutrons generated in one generation to the number generated in the previous generation. An alternate way of describing the multiplication factor is as the ratio of the production rate to the loss rate of neutrons. In order to maintain a constant reactor power level, the multiplication factor of a reactor core must be equal to unity.

The multiplication factor of a reactor is calculated using tabulated nuclear data that includes the nuclear cross sections (effective nucleus interaction areas) and other important values such as the number of neutrons emitted per fission (note, however, that here all of the nuclear data will commonly be referred to as cross section data). The nuclear data used in the calculations have associated uncertainty values resulting from the experimental processes used to evaluate them. These uncertainties are in the form of both variances in a particular cross section and covariances between cross sections. The variance of a value is a representation of statistical uncertainty in a result (i.e. the square of the standard deviation). The covariance between two values is a representation of statistical uncertainties shared between the two systems. In the current case, covariances would arise as a result of shared experimental processes (and hence shared uncertainties) [8].

The ultimate result of the uncertainties in the nuclear data is a difference between the k_{eff} calculated using simulations and the actual value of k_{eff}. This difference is known as the bias in the k_{eff}. Note that the bias itself also has an uncertainty

resulting from uncertainties in the experiment results.

Accurately determining the value of the bias is required in order to validate the calculation method that is being used. While for a test reactor experiment it is simple to analyze the bias between the simulation and the experiment (assuming exact knowledge of the geometry and materials is available), for power reactors or for new reactor designs, it is not so simple; for power reactors it is not feasible to simulate the exact composition of the core and for reactor designs there is no data with which to compare. Thus, the calculation method can instead be validated through the use of sufficiently applicable experiments that can be used to determine the bias. In order to determine which experiments are applicable to the validation, a similarity study may be performed. The choice of applicable experiment sets is the focus of the work performed here.

Chapter 2

Theory and Related Research

In the work performed here, a lattice cell code and diffusion code were used to develop Monte Carlo code models used in sensitivity studies. The process by which this was completed will be given in Chapter 3. An outline of the mathematical basis behind each code is provided in the current chapter. This is followed by a brief summary of research related to the work performed.

2.1 Lattice Cell Theory: DRAGON

Infinite lattice models of the fuel channels in power reactors are created using a lattice code developed at École Polytechnique de Montréal called DRAGON [9]. DRAGON is a code that performs neutronics calculations on two or three dimensional geometries using the neutron transport equation. In order to maintain some flexibility in its use, this code is divided into a number of modules. Some of the most important module functions are listed below, as described in the user manual [9]:

- ♢ Read microscopic cross sections
- ♢ Perform tracking calculations
- ♢ Solve for multi-group flux
- ♢ Perform burnup calculations
- ♢ Homogenize and condense microscopic and macroscopic cross sections

2.1.1 Lattice Cell Models

When examining the layout of nuclear reactors, there is a repetition of certain fuel structure geometries. Together, the geometry structures make up what is called the lattice of the reactor core, where each repeated structure is a unit cell. The unit cell differs by reactor type; for the pressurized water reactor (PWR) it consists of a fuel element surrounded by moderator/coolant, while for the CANDU reactor design, it consists of a single fuel bundle in its fuel channel surrounded by moderator. The width of the region defined by the unit cell is known as the lattice pitch of the reactor. An example of a typical lattice cell for a CANDU reactor with a 37-element bundle is shown below along with a 2x3 subsection of the full lattice.

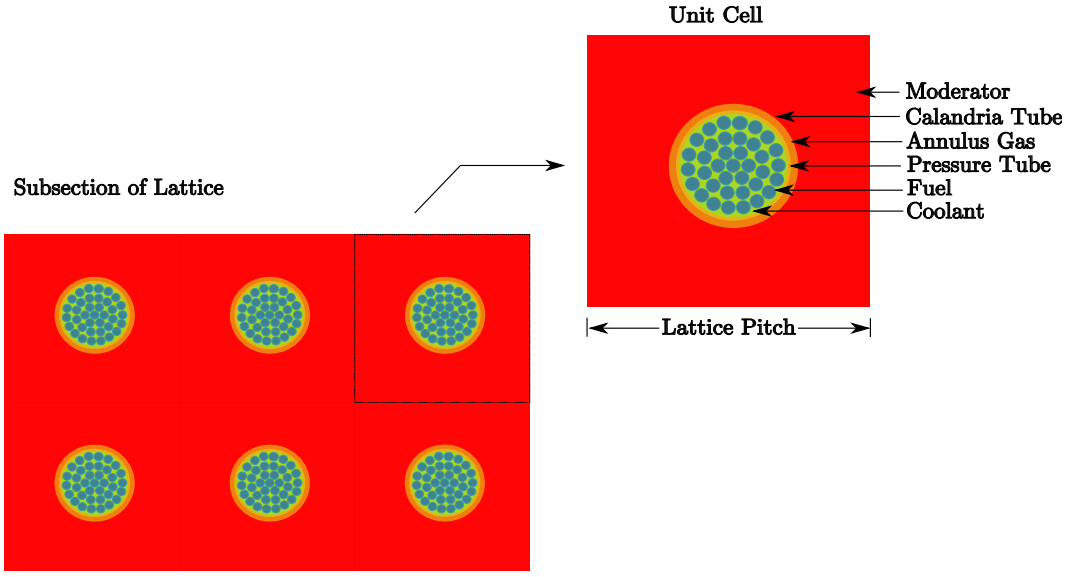

Figure 2.1: Typical Lattice Cell for 37-Element CANDU Bundle

In reactor physics, calculations are often performed over a single lattice cell only, as a representation of the entire core. This is because the complexity of the neutron transport equation makes it computationally expensive to perform calculations over a larger region. Due to the repetitive and symmetric nature of the unit cell, boundary conditions can be applied at each edge of the lattice cell in order to make the single cell calculation represent an infinite lattice of identical cells. For a large core region, representing the core as an infinite lattice is a reasonable approximation, however, if desired, corrections can be applied to account for leakage in a finite core. There are several possible boundary conditions that can be applied to simulate an infinite lattice. Some possible boundary conditions are listed below [10]:

♢ White Boundary: The incoming neutron flux at every boundary point is

isotropic

♢ Reflective Boundary: For every neutron that exits the surface at one location, a neutron will be reflected back in at the same location and the same speed but at a reflected angle.

♢ Periodic Boundary: For every neutron that exits the surface at one location, a neutron will enter the surface at the same velocity but at the opposite surface boundary (i.e. exits left, enters right).

DRAGON is not limited to calculations over a single unit cell with boundary conditions applied. Supercell geometries, consisting of more than one unit cell, added reactivity devices, etc. can also be created to develop a more thorough representation of the core. However, developing more complicated geometries has a trade-off in computational expense, and for the purposes of the study performed here only the single unit cell case was analyzed.

2.1.2 Solution to the Neutron Transport Equation

The neutron transport equation describes the number of neutrons at an energy E, in direction $\widehat{\Omega}$, and in an arbitrary volume V within a system. The equation is derived based on the balance of the gain and loss mechanisms for neutrons [11].

Gain Mechanisms:

♢ Neutron source

♢ Scattering from a different energy or direction into the energy and direction of interest

♢ Leakage into the volume

♢ Neutron production by fission

Loss Mechanisms:

♢ Absorption

♢ Scattering to a different energy or direction of motion

♢ Leakage out of the volume

Through derivations in [11], it is shown that the final integro-differential neutron transport equation can be expressed as:

$$\frac{1}{\upsilon}\frac{\partial\phi}{\partial t} + \widehat{\Omega}\cdot\bigtriangledown\phi + \Sigma_t\phi(\vec{r},E,\widehat{\Omega},t) = \int_{4\pi} d\widehat{\Omega}' \int_0^\infty dE'\Sigma_s(E'\rightarrow E,\widehat{\Omega}'\rightarrow\widehat{\Omega})\phi(\vec{r},E',\widehat{\Omega}',t) + \chi(E,\widehat{\Omega})\int_{4\pi} d\widehat{\Omega}' \int_0^\infty dE'\nu(E')\Sigma_f(E')\phi(\vec{r},E',\widehat{\Omega}',t) + s(\vec{r},E,\widehat{\Omega},t) \tag{2.1}$$

where υ represents the neutron speed, ϕ is the angular neutron flux, t is the time, $\widehat{\Omega}$ is the direction unit vector, E is the neutron energy, r is the neutron position, Σ_s is the macroscopic scattering cross section, Σ_t is the total macroscopic cross section, Σ_f is the macroscopic fission cross section, $\chi(E,\widehat{\Omega})$ is the fission spectrum describing the energy distribution of fission neutrons at the specified energy and angle, and $s(\vec{r},E,\widehat{\Omega},t)$ is the neutron source term.

In the case of a steady state system, the partial differential term representing the change in the number of neutrons with time will be eliminated. In addition, in the case where there is no external fission source independent of the flux, the term $s(\vec{r},E,\widehat{\Omega},t)$ is removed and the equation becomes an eigenvalue problem. Under these conditions the only system for which a solution would exist is a critical system (the number of neutrons in each generation is constant). In order to ensure a solution for systems that may not be critical, an effective multiplication factor k_{eff} is incorporated as a divisor in the fission term. This factor is a representation of how far the system is from critical.

$$\widehat{\Omega}\cdot\bigtriangledown\phi + \Sigma_t\phi(\vec{r},E,\widehat{\Omega}) = \int_{4\pi} d\widehat{\Omega}' \int_0^\infty dE'\Sigma_s(E'\rightarrow E,\widehat{\Omega}'\rightarrow\widehat{\Omega})\phi(\vec{r},E',\widehat{\Omega}') + \frac{\chi(E,\widehat{\Omega})}{k_{eff}}\int_{4\pi} d\widehat{\Omega}' \int_0^\infty dE'\nu(E')\Sigma_f(E')\phi(\vec{r},E',\widehat{\Omega}') \tag{2.2}$$

For simplicity the source terms on the right hand side of the transport equation can be grouped into one source term $Q(\vec{r},E,\widehat{\Omega},t)$ such that:

$$\widehat{\Omega}\cdot\bigtriangledown\phi + \Sigma_t\phi(\vec{r},E,\widehat{\Omega}) = Q(\vec{r},E,\widehat{\Omega}) \tag{2.3}$$

The neutron transport equation describes the exact balance of neutrons within a system. However, difficulty arises when attempting to solve this equation because of its complexity; there are six independent variables in this equation, and the macroscopic cross sections depend on position as well as energy. Thus, in order to solve the equation for the neutron flux, approximating methods are required. There are several possible methods of solving the neutron transport equation. The one used and presented here is the collision probability method [12].

The collision probability method for solution of the neutron transport equation uses collision probability matrices that describe the probability that a neutron born in one region of the geometry will not be absorbed until it has reached another region of the geometry and will therefore be included in the flux calculation for that region [13]. Using these matrices of collision probabilities, in conjunction with a discretized version of the neutron transport equation in space and energy, the neutron flux in each region can be calculated.

When implementing the collision probability method in DRAGON, first a tracking module is used that will generate appropriate integration points for the current geometry. It then uses these values as well as the cross section data to determine collision probability matrices. Finally, it calculates the flux using collision probability matrices as described below.

In order to use the collision probability method, the integro-differential form of the neutron transport equation must first be manipulated into a different form known as the integral transport equation [14]. The final form of the integral transport equation is shown below for the case in which the flux and cross sections are independent of energy and the source is isotropic $Q(\vec{r},\widehat{\Omega}) = \frac{1}{4\pi}q(\vec{r})$. A derivation of this form of the transport equation can be found in [12].

$$\phi(\vec{r},\widehat{\Omega}) = e^{-\tau(R_s)}\phi(\vec{r}_s,\widehat{\Omega}) + \frac{1}{4\pi}\int_0^R e^{-\tau(R')}q(\vec{r'})dR' \tag{2.4}$$

Here, $\tau(R)$ represents the optical path and is defined as:

$$\tau(R) = \int_0^R \Sigma(\vec{r} - R'\widehat{\Omega})dR' \tag{2.5}$$

where $\vec{r}$ is the position at which the flux is being calculated, $\vec{r'}$ is another position in the geometry. $\vec{r}_s$ represents a point on surface S where boundary conditions are applied, $R = |\vec{r} - \vec{r'}|$ is the the distance between the evaluated position and another position in the geometry, and $R_S = |\vec{r} - \vec{r}_S|$ is the distance between the evaluated position and the surface S. Integrating over all solid angles yields the scalar flux [12]:

$$\phi(\vec{r}) = \int_S \frac{e^{-\tau(R_S)}}{R_S^2}(\widehat{\Omega}\cdot N_-)\phi_-(\vec{r}_S,\widehat{\Omega}')d^2r' + \int_V \frac{e^{-\tau(R)}}{4\pi R^2}q(\vec{r'})d^3r' \tag{2.6}$$

where

$$d^3r = R^2 d^2\widehat{\Omega}dR \tag{2.7}$$

$$\widehat{\Omega}\cdot N_- d^2r = R_s^2 d^2\widehat{\Omega} \tag{2.8}$$

Here ϕ_- represents the incoming angular flux at the surface of S. Similarly ϕ_+ would represent the outgoing angular flux.

Having defined the integral form of the transport equation, the next step is to discretize the equation so that it can be used in a numerical computation. To do so, the geometry is divided into small volumetric regions V_i and it is assumed that the cross sections and source terms are constant in each volumetric region. Similarly, the boundary surface S is divided into N_S regions of area S_α. The incoming and outgoing fluxes at the surface S_α can then be represented as limited series expansions of half-range spherical harmonics $\psi^v(\widehat{\Omega}, \vec{N}_\pm)$, where there are N_v spherical harmonics, and $\vec{N}_\pm$ forms the unit vector base on the surface S_α. Here $\phi^\mu_{\pm,\alpha}$ represents the incoming and outgoing components of the average angular flux on each surface. Boundary conditions can be used to relate the incoming and outgoing flux components.

$$\phi_\pm(\vec{r}_S, \widehat{\Omega}) = \frac{1}{4\pi} \sum_{\nu=0}^{N_\nu} \phi^\nu_\pm \psi^\nu(\widehat{\Omega}, \vec{N}_\pm) \tag{2.9}$$

$$\phi^\nu_{\pm,\alpha} = \frac{4}{S_\alpha} \int_{S_\alpha} d^2r \int_{(\widehat{\Omega}\cdot\vec{N}_\pm)>0} d^2\Omega (\widehat{\Omega}\cdot\vec{N}_-)\psi^\nu(\widehat{\Omega}, N_\pm)\phi_\pm(\vec{r}_s, \widehat{\Omega}) \tag{2.10}$$

The final versions of the discretized average flux in region i and the average outgoing angular flux on the surfaces S_α can be shown to be the following assuming the incoming flux is constant on each surface, i.e. $\phi^\nu_{-,\alpha}(r_s) = \phi^\nu_{-,\alpha}$. A more thorough derivation can be found at [12].

$$\begin{aligned} V_i\phi_i = &\sum_{\alpha=1}^{N_S}\sum_{\nu=0}^{N_\nu} \int_{V_i}\int_{S_\alpha} \frac{e^{-\tau(R_S)}}{4\pi R_S^2} (\widehat{\Omega}\cdot\vec{N}_-)\phi^\nu_{-,\alpha}\psi^\nu(\widehat{\Omega}, \vec{N}_-) d^3r' d^2r + \\ &\sum_{j=1}^{N_V} \int_{V_i}\int_{V_j} \frac{e^{-\tau(R)}}{4\pi R^2} q_i d^3r' d^3r \end{aligned} \tag{2.11}$$

$$\begin{aligned} \frac{S_\alpha}{4}\phi^\nu_{+,\alpha} = &\sum_{\beta=1}^{N_S}\sum_{\mu=0}^{N_\nu} \int_{S_\alpha}\int_{S_\beta} \frac{e^{-\tau(R_S)}}{4\pi R_S^2} (\widehat{\Omega}\cdot\vec{N}_+)\psi^\nu(\widehat{\Omega}, \vec{N}_+)(\widehat{\Omega}\cdot\vec{N}_-)\psi^\mu(\widehat{\Omega}, \vec{N}_-)\phi^\mu_{-,\beta} d^2r d^2r' + \\ &\sum_{j=1}^{N_V} \int_{S_\alpha}\int_{V_i} \frac{e^{-\tau(R)}}{4\pi R^2} (\widehat{\Omega}\cdot\vec{N}_+)\psi^\nu(\widehat{\Omega}, \vec{N}_+) q_j d^3r' d^2r \end{aligned} \tag{2.12}$$

From this discretized version of the flux, four types of collision probabilities with a physical interpretation are seen. Mathematically these are defined as [12]:

$$\tilde{p}_{ij} = V_i p_{ij} = \int_{V_i}\int_{V_j} \frac{e^{-\tau(R)}}{4\pi R^2} d^3r' d^3r \tag{2.13}$$

$$\tilde{p}_{i\alpha}^{\nu} = V_i p_{i\alpha}^{\nu} = \int_{V_i}\int_{S_\alpha} \frac{e^{-\tau(R_S)}}{4\pi R_S^2}(\widehat{\Omega}\cdot\vec{N}_-)\psi^{\nu}(\widehat{\Omega},\vec{N}_-)d^3r'd^2r \tag{2.14}$$

$$\tilde{p}_{\alpha i}^{\nu} = \frac{S_\alpha}{4} p_{\alpha i}^{\nu} = \int_{S_\alpha}\int_{V_i} \frac{e^{-\tau(R)}}{4\pi R^2}(\widehat{\Omega}\cdot\vec{N}_+)\psi^{\nu}(\widehat{\Omega},\vec{N}_+)d^2r'd^3r \tag{2.15}$$

$$\tilde{p}_{\alpha\beta}^{\nu\mu} = \frac{S_\alpha}{4} p_{\alpha\beta}^{\nu\mu} = \int_{S_\alpha}\int_{S_\beta} \frac{e^{-\tau(R_S)}}{4\pi R_S^2}(\widehat{\Omega}\cdot\vec{N}_-)\psi^{\mu}(\widehat{\Omega},\vec{N}_-)(\widehat{\Omega}\cdot\vec{N}_+)\psi^{\nu}(\widehat{\Omega},\vec{N}_+)d^2rd^2r' \tag{2.16}$$

Physically, the collision probabilities represent [15] :

- ♢ p_{ij}: probability a neutron born in region i will have its first collision in region j without leaving the cell (i.e. without crossing an S_α boundary)
- ♢ $p_{i\alpha}^{\nu}$: probability a neutron born in region i will leave the cell by surface S_α
- ♢ $p_{\alpha i}^{\nu}$: probability a neutron entering the cell from surface S_α will have its first collision in region i without leaving the cell
- ♢ $p_{\alpha\beta}^{\nu\mu}$: probability a neutron entering from surface S_α will leave the cell by surface S_β

In DRAGON, numerical integration of the probability matrix equations is performed by generating a finite number of neutron paths over which to integrate, instead of integrating over the entire volume and for all angles. This is done using a tracking module in which the number of tracking line angles and the number of parallel tracking lines in the geometry are chosen. These tracking lines represent the path of a neutron in the geometry.

Substituting the collision probability matrices into equations 2.11 and 2.12 yields a solution to the transport equation using the collision probability method for the average flux and the average outgoing flux on a surface. Having determined the collision probability matrices, these equations can be solved through iteration of the k_{eff} and the fluxes [12]:

$$\phi_i = \sum_{\alpha=1}^{N_s}\sum_{\mu=0}^{N_\nu} p_{i\alpha}^{\mu}\phi_{-,\alpha}^{\mu} + \sum_{j=1}^{N_V} p_{ij}q_j \tag{2.17}$$

$$\phi_{+,\alpha}^{\nu} = \sum_{\beta=1}^{N_s}\sum_{\mu=0}^{N_\nu} p_{\alpha\beta}^{\nu\mu}\phi_{-,\beta}^{\mu} + \sum_{j=1}^{N_V} p_{\alpha j}^{\nu}q_j \tag{2.18}$$

Note that here a one-group approach was taken to the derivations. However, these same final equations apply for every energy group and the flux for all groups can be solved in parallel.

2.1.3 Resonance Self-Shielding

An important factor that must be considered when performing calculations using multi-group cross section data is a phenomenon called resonance self-shielding. Before moving forward in the definition of resonance self-shielding, first consider the figure below showing the total cross section of Th-232 (data obtained from [16]).

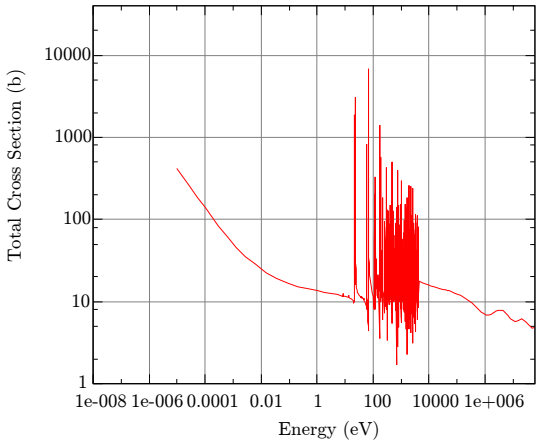

Figure 2.2: Th-232 Total Cross Section

From the image above, it is clear that there is a region from approximately 10 to 1000 eV in which the cross section experiences peaks as the energy changes. These peaks are known as resonances and the region in which they occur is called the resonance region. At approximately 1000 eV, the sharp peaks suddenly disappear. The reason for this is not that there are no longer resonances, but rather that the resonances begin overlapping and cannot be resolved through measurement. This is called the unresolved resonance region.

For neutron energies in and close to a resonance, the neutron flux is depressed due to the increased absorption. In some cases, the reduction of the neutron flux is sufficient to cause an overall decrease in the rate of absorption F in the nuclei at that energy despite the increase in the cross section [17]. This can be seen from the equation:

$$F = \Sigma_a(E)\phi(E) \tag{2.19}$$

This effect is called energy self-shielding due to the fact that the absorption of neutrons at the resonance energies causes a shielding effect to the rest of the absorbing nuclei against the neutrons with energies in that region by reducing the rate of collisions [11]. Self-shielding occurs for heavy nuclides that are in high concentrations in the fuel (otherwise the flux depression would not be sufficient to decrease the rate of absorption).

A second self-shielding effect is spatial self-shielding. This effect is based on the same principle as energy self-shielding and is caused by the location of nuclides containing resonance regions in a heterogeneous geometry. For example, if there is a moderating material and a fuel material, the nuclei near the surface of the fuel (which has resonances) will absorb a large number of neutrons at the resonance energy due to the high flux. This will cause a flux depression, so that the center of the fuel will have a lower neutron absorption rate for the same reason as previously described. Thus, the central fuel is shielded from neutrons in the resonance region.

In nuclear reactors, the effects of self-shielding are important due to the presence of heavy nuclides such as uranium and thorium. The localized depressions in flux within the resonance energy regions and the resulting self-shielding effects must be taken into account in order to develop an accurate model of the reactor. However, the difficulty is as follows: when discretizing the neutron transport equation, the cross section data was divided into discrete averaged energy groups. The calculation of the neutron flux is then based on the data in these energy groups. For energy groups that contain resonances the self-shielding effects caused by flux depression need to be taken into account. In order to do so, the cross section data in the resonance regions are adjusted as follows so as to obtain a microscopic self-shielded cross section $\bar{\sigma}_{i,g}$. Here i represents a reaction type and g is an energy group [15].

$$\bar{\sigma}_{i,g} = \mu_g \frac{\int_{u_{g-1}}^{u_g} du \sigma_i(u)\phi(u)}{\int_{u_{g-1}}^{u_g} du \phi(u)} \tag{2.20}$$

Where u_{g-1} and u_g are the lethargy limits of group g, μ_g is a factor called the super-homogeneisation factor, $\phi(u)$ is the averaged neutron flux , and σ_i is the microscopic cross section.

The difficulty with the above equation is that the neutron flux is unknown. Approximations are used to estimate the flux in order to calculate the resonance corrected cross section.

The main method used in DRAGON to correct for self-shielding effects and determine this self-shielded cross section is called the Stamm'ler model.

2.1.3.1 Stamm'ler Model

The Stamm'ler method solves for the self-shielded cross section by first assuming that the neutron flux is the product of a resonant fine-structure $\rho_i(u)$ function and a regular distribution function $\psi_i(u)$:

$$\phi_i(u) = \rho_i(u)\psi_i(u) \tag{2.21}$$

Based on this approximation, the resonant fine-structure function, and a term known as the resonance integral, which represents the average absorption cross section for the resonance averaged over the flux within the resonance energy, are determined. These are used to solve equation 2.20. To correct for effects due to heterogeneity that arise in some cases, a process known as the Livolant-Jeanpierre normalization is used [14].

There are other options available in DRAGON to perform the self-shielding calculations. These include the Stamm'ler model with Nordheim approximation and the Stamm'ler model with Nordheim approximation and Riemann integration [9].

2.1.4 Burnup Calculations

As fuel remains in a reactor for a period of time the fissile material depletes, fission products accumulate, and transmutation may occur. Thus, the fuel composition changes. DRAGON can be used to model this change in fuel composition with time by solving the Bateman equations, a model that describes the concentration of materials in a decay chain over time. For a case in which there is a decay chain consisting of n nuclides, the concentrations of the nuclides as the parent product decays can be described by [18]:

$$\frac{dN_1}{dt} = -\lambda_1 N_1 + R_1 \tag{2.22}$$

$$\frac{dN_i}{dt} = \lambda_{i-1} N_{i-1} - \lambda_i N_i + R_i, i = 2 \text{ to } n \tag{2.23}$$

Where the subscript i represents the daughter nuclide, the subscript $i-1$ represents the parent nuclide, N represents the nuclide concentration, t represents time, λ represents the decay constant of the nuclide, and R represents the rate of production of the nuclide in nuclei/cm^{2}s.

This equation can be solved analytically.

The burnup of fuel in a reactor is a measure of the fission energy produced per

unit mass of heavy nuclides in the fresh fuel M_h. It is therefore used as a metric for the age of the fuel and the fuel composition can be computed as a function of burnup. For a reactor operating at constant fission power P for a length of time t, the burnup B is:

$$B = \frac{P \times t}{M_h} \tag{2.24}$$

2.1.5 Cell Homogenization and Condensation

The diffusion code DONJON (which will be described in the next section) uses as input the cell-averaged, group condensed macroscopic cross sections. Cell homogenization consists of averaging the macroscopic cross sections over the entirety of the unit cell. In order to do so, these values must be averaged using the flux distribution in the cell as a weighting function. Cell condensation consists of averaging the macroscopic cross sections over energy groups in order to lump them into fewer energy groups. Condensation and homogenization is done in DRAGON using a flux volume weighting method [9].

2.1.6 DRAGON Module Descriptions

DRAGON is a modular code, meaning that it uses separate code sections in order to complete specific tasks. The following is an outline of the modules that are used in the work performed here, listed in the order that they are used within a DRAGON calculation [9].

LIB: The LIB: module is used for the creation of a microscopic cross section file. In this module the user inputs the isotopic composition of each mixture used in the model. The module will then read microscopic cross section data. The microscopic cross section data can be in the formats: DRAGLIB, MATXS, WIMS-D4, or WIMS-AECL. Here, the WIMS-D4 format is used.

MAC: This module is used to create or modify a file containing the DRAGON macroscopic cross sections.

GEO: This module is used to describe the geometry of the current system. It can be a two-dimensional or three-dimensional geometry. For example, this module would be used to create the description of a CANDU lattice cell.

EXCELT/NXT: These modules are used to perform tracking calculations and generate integration points required to perform the collision probability method of

solving the transport equation (as described in Section 2.1.2).

SHI: The SHI: module is used to perform self-shielding calculations using the Stamm'ler model as described in Section 2.1.3.1.

ASM: The ASM: module is used to generate the collision probability matrix (Section 2.1.2).

FLU: The FLU: module uses the collision probability matrix generated by the ASM: module to calculate the flux.

EVO: The EVO: module is used when performing burnup calculations.

EDI: The EDI: module is the exiting module for DRAGON. It allows the user to specify the types of analysis that should be performed, such as computing reaction rates. This module also allows the user to store this data on a file.

CPO: The CPO: module is used to create COMPO formatted files which contain multi-group homogenized cross sections. These files can then be used as input to the DONJON diffusion code.

2.2 Diffusion Theory: DONJON

Having obtained the results for the burnup of a single lattice cell model using DRAGON, a diffusion code called DONJON [19] can be used to make a larger model of the core. DONJON is a code that was developed at École Polytechnique de Montréal. It determines the flux of the system by solving the diffusion equation, a simplification to the neutron transport equation. Using the diffusion equation as a simplification allows large areas of the reactor core to be modelled with much less computational expense. Thus, using DONJON, three-dimensional models of subsections of the core or even the entire core can be modelled [19]. In addition DONJON can be used to model core conditions such that the burnup of the fuel in the core is accounted for.

2.2.1 The Diffusion Equation

The diffusion approximation is a method of solving the neutron transport equation through discretization and some simplifying assumptions. First, the equation is written in terms of the angle-integrated flux, rather than the angular flux. Second, it uses the approximation that the angle-integrated neutron flux and neutron current

can be related through Fick's law as follows [11]:

$$\vec{J}(r,E) = -D(r,E) \bigtriangledown \phi(r,E) \tag{2.25}$$

Where D is the diffusion coefficient.

Fick's law is a mathematical representation of the fact that the neutron current will flow from regions of high neutron density to low neutron density. Note that this assumption is not always true; near the boundaries of the reactor core this assumption is incorrect. However, in general it is a reasonable approximation.

Applying the above two assumptions to the steady state neutron transport equation results in the diffusion equation.

$$- \bigtriangledown \cdot D(r,E) \bigtriangledown \phi(r,E) + \Sigma_t \phi(r,E) = \int_0^\infty dE' \Sigma_s(E' \rightarrow E)\phi(r,E') + \frac{\chi(E)}{4\pi k_{eff}} \int_0^\infty dE' \nu(E')\Sigma_f(E')\phi(r,E') + s(r,E) \tag{2.26}$$

Here it has been assumed that the fission neutrons are emitted isotropically.

A third simplification that is used in the diffusion approximation is that the neutron energies can be discretized into energy groups and the neutron flux can be solved for each energy group. In addition, the lattice cell properties are homogenized over each cell (as was described in Section 2.1.5) to simplify the calculation.

The final step that is required is to define interface and boundary conditions for each lattice cell. The diffusion equation is then solved through the use of numerical methods.

2.2.2 Time-Average Core

As a CANDU reactor operates, the channels are refuelled with a specified number of fresh bundles at certain time intervals (the dwell time) in order to maintain the power of the reactor. The refuelling occurs on-power and is therefore called online refuelling. After a long period of operation time, the CANDU reactor reaches a point where the global flux and power distribution is always close to an equilibrium state [20]. This equilibrium state, called a time-average core, is therefore a reasonable representation of the core after a long period of time.

The goal of the time-average model is to determine the average cross sections in each bundle. Using these, the time-average flux of the reactor can be calculated.

To calculate the time-average flux the values of the refuelling shift (number of bundles refuelled at each refuelling operation) and either the exit irradiation of the channel or the dwell time of the channel are required. The first step is then to determine the entrance and exit irradiations for each fuel bundle in the channel.

The irradiation accumulated by a bundle at a fixed position in the channel is equal to the flux multiplied by the time, the exit irradiation of the fuel at that position can be written as [20]:

$$\omega_{exit,cb} = \omega_{ent,cb} + \phi_{tav,cb} D_c \tag{2.27}$$

Where the subscript cb is used to represent a specific bundle and channel position in the core, the subscript c is a specific channel position, and ω_{ent} is the irradiation when the bundle enters the location. ω is the irradiation, D_c is the dwell time, and the subscript tav is used to represent the time-average value. Note that either the dwell time or the channel exit irradiation can be used as the independent variable in this equation due to the relation:

$$\omega_{exit,c} = \frac{1}{E_c} \sum_{b=1}^{N_c} (\phi_{tav,cb} D_c) \tag{2.28}$$

Here E_c is the number of shifts at refuelling and N_c is the total number of bundles in a channel. This is a simple derivation and can be found at [20].

The time-average cross sections can then be found by first noting that the total reactions in the time between refuellings is:

$$R_{x,cb} = \int_0^{D_c} \Sigma_{x,cb}(\omega) \phi_{cb}(t) dt \tag{2.29}$$

Where x represents any reaction and R is the total reactions in the bundle between refuellings. The time-average cross section is defined as a cross section that reproduces the total number of reactions but is independent of time. Thus the equation above can be rewritten as follows.

$$R_{x,cb} = \Sigma_{x,cb,tav} \int_0^{D_c} \phi_{cb}(t) dt \tag{2.30}$$

Equating (2.29) and (2.30) and using the fact that irradiation ω is equal to flux multiplied by time:

$$\Sigma_{x,cb,tav} = \frac{\int_{\omega_{ent,cb}}^{\omega_{exit,cb}} \Sigma_{x,cb}(\omega) d\omega}{\omega_{exit,cb} - \omega_{ent,cb}} \tag{2.31}$$

Using equation (2.31), all of the cross sections can be found for all bundle locations in the core and using the diffusion equation the time-average flux can then be determined as well as the multiplication factor of the core. Note that this is an iterative

process due to the dependence of the exit irradiation on the flux, the cross sections on the exit irradiation, and the flux on the cross sections.

To examine the core at an instantaneous point in time and simulate the refuelling ripple (the variations of the flux and power shape about the time-average shape resulting from refuelling [20]), a snapshot of the core can be taken with a particular fuelling sequence.

2.2.3 Batch Fuelling

Batch refuelling means that rather than continuously refuelling bundles in various channels throughout the core, a large number of channels are completely refuelled at the same time at the end of a time period called a cycle. Depending on the type of batch refuelling, the fuel that was in the locations being refuelled may be shuffled to other channels. This means that some channels may have fresh fuel and some may have what is called once-irradiated fuel (because it has been in the reactor for one cycle). Similarly, the fuel that was in the now once-irradiated fuel locations may be shifted to other channels, etc..

Reactors fuelled in batches cannot be modelled using the time-average core model. They have distinctly different burnup states depending on the point in the refuelling cycle and can be modelled at any time in the cycle. Often core results are analyzed for an averaged beginning of cycle (BOC) and end of cycle (EOC) state, assuming the reactor has been operational for a long period of time. DONJON does not explicitly do this, as it does the time-average model. Instead the user must specify a cycle time, and perform iterations until the core has reached its averaged BOC and EOC states.

2.2.4 DONJON Module Descriptions

The following is an outline of some of the important DONJON modules used here, listed in order that they are used in the DONJON calculations, as well as a brief description of each [19]. The structure of DONJON is very similar to that of DRAGON. The module names and descriptions reflect this similarity.

GEOD: The GEOD: module is used to create a geometry description. For example, this would consist of the description of the number of CANDU bundles in a channel and the number of channels considered.

USPLIT: This module is used to create an index containing the material mix-

ture types in the different sections of a split geometry.

CRE: This module is used to create a file containing the nuclear data properties as a function of burnup, interpolated from the table created in the XSCONS: module.

XSCONS: The XSCONS: module is used to create a table containing the burnup dependent nuclear data properties for the fuel. This is done using the COMPO files that were output from DRAGON.

INIRES: This module is used to read fuel bundle information.

REFRES: This module computes the cross references between the geometry of the simulation and the mixtures in the geometry.

TRIVAT: This is the tracking module for DONJON.

FLXAXC: This module determines an average flux value over the bundles in the core, as well as determining the flux shape.

REFUEL: This module is used to both compute the burnup values for a time-average core as well as to specify refuelling schemes (refuel or shuffle fuel in a channel).

INIMAC: This module is used to create a new file containing properties for each material region.

TRIVAA: This module is used to compute finite element system matrices based on the results of TRIVAT:.

FLUD: This module computes the solution to the diffusion equation using the matrices from TRIVAA:.

POWER: This module computes the bundle and channel powers in the region.

2.3 Monte Carlo and Sensitivity Theory: SCALE 6.1

The code package SCALE 6.1, available from the Radiation Safety Informational Computational Center [21], consists of a collection of modules that can be used for specific solutions. For example, it contains modules that have functions such as solving for the neutron flux and multiplication factor, finding the similarity between two systems, correcting for the bias between experiments and simulations, etc.

To solve for the neutron flux and multiplication factor, some of the modules in the SCALE 6.1 package, such as the KENO V.a module [46], use a stochastic method called the Monte Carlo method rather than the deterministic methods described previously.

2.3.1 Monte Carlo Method

The Monte Carlo method is a method of solving integral equations by calculating the value of the integrand at randomly generated points in the phase space of the integral. It is applicable not only to neutronics calculations, but can also be applied to many other areas of science such as particle physics, astrophysics, microelectronics, etc.. The method is oftentimes compared to the rolling of dice due to the randomness that is involved (the name Monte Carlo is a tribute to the city of the same name that is famous for its casinos).

In neutronics, the Monte Carlo technique is used to solve the neutron transport equation by following neutrons through a simulated geometry. To summarize the process, a set number of neutrons are randomly generated and followed from birth until death. Once all the neutrons have died, the neutrons are re-generated at locations chosen based on the number of fissions that took place with the previous set of neutrons. The new set of neutrons are then followed until death. The process is repeated for a set number of cycles or 'generations'.

2.3.1.1 Interaction Path Distance

When a neutron is generated, it is given a position, direction of motion, and energy. To determine how far the neutron travels before an interaction occurs, an equation is used that describes the probability that the neutron undergoes an interaction (absorption or scattering) at position s along its trajectory [22]:

$$P(s) = \Sigma_t(E)e^{-\Sigma_t(E)s} \tag{2.32}$$

Here the value Σ_t is the total cross section. The probability of an interaction occurring between the starting location (s=0) and the final position r is a random quantity between 0 and 1. Let this random number be represented by ξ.

$$\xi = \int_0^r \Sigma_t(E)e^{-\Sigma_t(E)s}ds \tag{2.33}$$

By manipulating the equation above and choosing a random number, the final position of the neutron can be calculated.

$$r = -\frac{1}{\Sigma_t(E)}\ln(\xi) \tag{2.34}$$

If it is found that the neutron exits the boundary of the volume of interest (i.e. a region defined with a particular material) before interacting, then the neutron is placed on the boundary and the process above is repeated. However, if the length r is within the boundary then an interaction is simulated at this location.

2.3.1.2 Interactions

When a neutron interaction occurs, there are three possibilities: absorption, inelastic scattering, and elastic scattering. The interaction that occurs is chosen through a random selection process and based on the selection, different procedures are taken [22].

If an absorption occurs then the original neutron disappears and is 'dead'. However, if the type of absorption is a fission then new neutrons are created at this location to be used in the next generation. The average number of neutrons that are generated from fission is not an integer value. Thus, another procedure involving random number generation is used to decide how many neutrons are generated.

If a scattering interaction occurs (elastic or inelastic), the neutron experiences a change in energy and direction and its trajectory continues.

2.3.1.3 Re-initializing

At the end of a generation, the number of neutrons created by fission is compared to the number of neutrons at the start of the generation (this ratio is the multiplication factor). In order to ensure the number of neutrons used in subsequent generations does not become progressively larger or progressively smaller, fission neutrons are either randomly added or randomly dropped from the simulation such that the neutrons per generation is approximately constant.

2.3.1.4 Results from Monte Carlo

The processes described above for tracking neutrons are performed for a large number of neutrons and neutron generation cycles. For each generation the multiplication factor is re-calculated. By repeating the process for a large number of cycles, the multiplication factor calculated should converge to the most accurate value.

In order to determine the flux in the simulation, the simulation geometry is di-

vided into regions and tallies are used, which count the number of a certain occurrence. There are several different tally methods for determining the flux in the simulation. A common method, and the one used in KENO V.a, is the track-length estimator method in which the total distance traveled by each neutron through each pre-defined region is counted and added to a total.

2.3.2 Resonance Self-Shielding

Monte Carlo codes such as the KENO V.a module of the SCALE 6.1 code package have the option of performing calculations in which continuous energy cross sections are used and therefore no self-shielding corrections are required. However, due to the computational expense of continuous energy calculations and due to the inability of KENO V.a to calculate the adjoint solution in continuous energy mode, all of the computations performed here use multi-group cross sections, which require self-shielding corrections.

There are several methods available for correcting for the effects of resonance self-shielding, as described in Section 2.1.3. In SCALE 6.1 there are three primary options: the Bondarenko method, the Nordheim Integral Method, and a third method developed by Oak Ridge National Laboratory called the CENTRM/PMC method [23].

2.3.2.1 Bondarenko Method

The Bondarenko method is used to solve for the self-shielding cross sections based on a number of assumptions. First it uses a Narrow Resonance (NR) approximation to estimate the flux as a function of the cross section in an infinite homogeneous medium as simply [24]:

$$\phi(u) \approx \frac{1}{\Sigma_t(u)} \tag{2.35}$$

In addition it uses an equivalence theory to account for heterogeneity. These approximations can then be used to develop a simple model for the self-shielded flux and to correct the cross sections for resonance self-shielding.

The Bondarenko method produces accurate results for higher energy resonances where the NR approximation is satisfied, however it is not applicable for lower energy, wider resonances.

2.3.2.2 Nordheim Integral Method

The Nordheim Integral method is in general an improvement to the Bondarenko method however it still offers some difficulties. This method does not use the NR approximation. Instead it assumes that there is a two region model consisting of an absorber and a moderator. It then solves for the two-region form of the integral neutron transport equation for this model. By doing so it can develop cross sections that account for self-shielding effects. [23]

The difficulties with the Nordheim Integral method are that the absorber can contain only one resonance material. In addition systems with multiple absorber regions cannot be treated.

2.3.2.3 CENTRM/PMC Method

The CENTRM/PMC Method is a method developed for the SCALE package [23]. This method is the most accurate of the three discussed as it eliminates many of the difficulties encountered with the other models.

The CENTRM/PMC method generates cross section data corrected for self-shielding by first solving for the continuous energy neutron flux-spectra using a deterministic method. This is done using user-defined 1D simplified geometry descriptions of each unit cell in the model. It then uses the flux-spectra as weight functions in order to determine corrected cross section data. In the unresolved resonance range, the CENTRM/PMC method uses tabulated Bonarenko method results. The self-shielded cross section data produced is stored in a library that can then be used in higher dimensional models and in Monte Carlo calculations.

2.3.3 Sensitivity Analysis

In order to perform a similarity analysis (which will be described in subsequent sections), it is necessary to first perform a sensitivity analysis. A sensitivity analysis consists of determining the sensitivity of the calculated k_{eff} to changes in the nuclear data. This is important because the nuclear data used in these calculations were found empirically and have associated uncertainties. The method that is used in the SCALE 6.1 package to determine the sensitivities is called adjoint based linear perturbation theory.

Perturbation theory is used to determine the change in the multiplication factor caused by small changes in either the core geometry or the composition of the core.

The benefit of this method is that it eliminates the need to perform the criticality calculation for every perturbed stated analyzed. Instead the perturbed core is expressed in terms of the flux and the adjoint flux of the original unperturbed core.

2.3.3.1 Adjoint Flux

Before entering into an explanation of perturbation, it is important to first define a quantity called the adjoint flux.

If M is an operator then the adjoint to the operator, $M^\dagger$, is defined as an operator that satisfies the following relation:

$$(M^\dagger f, g) = (f, Mg) \tag{2.36}$$

Where f and g are any functions that satisfy the boundary conditions *f(r)=g(r)=0*. The bracket notation used is for the inner product of two functions [11]:

$$(f, g) = \int_V d^3 r f^*(r) g(r) \tag{2.37}$$

Where $f^*(r)$ is the complex conjugate of *f(r)*.

The steady state neutron transport equation can be represented in operator notation as the eigenvalue problem:

$$M\phi = \frac{1}{k_{eff}} F\phi \tag{2.38}$$

Where M and F are operators. The adjoint flux is then defined as the solution to the equation:

$$M^\dagger \phi^\dagger = \frac{1}{k_{eff}} F^\dagger \phi^\dagger \tag{2.39}$$

It can be shown that physically the adjoint flux is a representation of the importance of a neutron event. For this reason it is sometimes called the neutron importance [11]. The adjoint flux can be found using the KENO V.a module using multi-group Monte Carlo techniques.

2.3.3.2 Perturbation

Mathematically, small perturbations in the core can be represented by perturbations on the affected operators [11]:

$$M' = M + \delta M \tag{2.40}$$

$$F' = F + \delta F \tag{2.41}$$

And this then changes the multiplication factor by:

$$k'_{eff} = k_{eff} + \Delta k_{eff} \tag{2.42}$$

The resultant equation for the perturbed core is:

$$M'\phi' = \frac{1}{k'_{eff}} F'\phi' \tag{2.43}$$

Rather than repeat the full core calculation to obtain ϕ' and k'_{eff}, it can be shown that these values can be obtained on the basis of perturbation theory. The derivation of this method follows below.

First, take the dot product of the equation above with the adjoint flux of the original core:

$$(\phi^\dagger, M\phi') + (\phi^\dagger, \delta M\phi') = \frac{1}{k'_{eff}}((\phi^\dagger, F\phi') + (\phi^\dagger, \delta F\phi')) \tag{2.44}$$

Using the definition of the adjoint, the following is true:

$$(\phi^\dagger, M\phi') = (M^\dagger\phi^\dagger, \phi') = (\frac{1}{k_{eff}} F^\dagger\phi^\dagger, \phi') = \frac{1}{k_{eff}}(\phi^\dagger, F\phi') \tag{2.45}$$

Now using :

$$\rho' = \rho + \Delta\rho \tag{2.46}$$

where ρ is the reactivity of the core and is equal to:

$$\rho = 1 - \frac{1}{k_{eff}} \tag{2.47}$$

Equations 2.46 and 2.47 find that $\Delta\rho$ is equal to:

$$\Delta\rho = \frac{1}{k_{eff}} - \frac{1}{k'_{eff}} \tag{2.48}$$

Using equations (2.45) and (2.48), the equation (2.44) can be rearranged as follows to solve for the change in reactivity.

$$\frac{1}{k_{eff}}(\phi^\dagger, F\phi') = \frac{1}{k'_{eff}}(\phi^\dagger, F\phi') + (\phi^\dagger, (\frac{1}{k'_{eff}}\delta F - \delta M)\phi')) \tag{2.49}$$

$$\Delta\rho = \frac{(\phi^\dagger, (\frac{1}{k_{eff}}\delta F - \delta M)\phi')}{(\phi^\dagger, F\phi')} \tag{2.50}$$

It is at this point that the concept of perturbation theory is used. Remembering that it was assumed that the perturbation was small, this equation can be expanded as follows into an equation that is not dependent on the perturbed flux.

$$\Delta\rho = -\frac{(\phi^\dagger, (\frac{1}{k_{eff}}\delta F - \delta M)\phi)}{(\phi^\dagger, F\phi)} - \frac{(\phi^\dagger, (\frac{1}{k}\delta F - \delta M)\delta\phi)}{(\phi^\dagger, F\phi)} + \frac{(\phi^\dagger, (\frac{1}{k}\delta F - \delta M)\phi)(\phi^\dagger, F\delta\phi)}{(\phi^\dagger, F\phi)^2} + ... \tag{2.51}$$

For first order perturbation only the first term is used and the result for the perturbation is:

$$\Delta\rho \approx \frac{(\phi^\dagger, (\frac{1}{k_{eff}}\delta F - \delta M)\phi)}{(\phi^\dagger, F\phi)} \tag{2.52}$$

Note that this equation does not include ϕ'. The equation above was shown for one energy only. For multi-group equations, this equation can be generalized into the matrix equation [11]:

$$\Delta\rho \approx \frac{(\underline{\phi}^\dagger, (\frac{1}{k_{eff}}\underline{\delta F} - \underline{\delta M})\underline{\phi})}{(\underline{\phi}^\dagger, \underline{F}\underline{\phi})} \tag{2.53}$$

2.3.3.3 Explicit Sensitivity

The result from equation (2.53) is highly useful as it allows for the response to a small perturbation in the core to be analyzed using only the results of the original core calculation. The perturbation analysis can then be used to determine the sensitivities of the reactor multiplication factor to various changes in the core. There are two types of sensitivities to be considered: explicit and implicit sensitivities. By summing these two sensitivity coefficients, a total sensitivity is found.

Explicit sensitivities are those that apply when the effects of resonance self-shielding are not significant. The relationship between the percent change in the k_{eff} of the reactor and the percent change in the perturbed quantity is assumed to be proportional, with a proportionality factor called the explicit sensitivity coefficient.

For example, for a small change in macroscopic cross section at a certain point in phase space r the relationship between the multiplication factor and the cross section changes is [25]:

$$\frac{\Delta\Sigma(r)}{\Sigma(r)} S_{k,\Sigma(r)} = \frac{\Delta k_{eff}}{k_{eff}} \tag{2.54}$$

where $S_{k,\Sigma(r)}$ is the sensitivity coefficient. Using partial derivatives, the relative sensitivity coefficient can be defined as:

$$S_{k,\Sigma(r)} \equiv \frac{\Sigma(r)}{k_{eff}} \frac{\partial k_{eff}}{\partial \Sigma(r)} \tag{2.55}$$

This can be transformed in terms of the reactivity using the approximation for a small perturbation:

$$\partial\rho \approx \frac{\partial k_{eff}}{k_{eff}^2} \tag{2.56}$$

The sensitivity is then:

$$S_{k,\Sigma(r)} = k_{eff}\Sigma(r)\frac{\partial\rho}{\partial\Sigma(r)} \tag{2.57}$$

Substituting the results for $\Delta\rho \approx \partial\rho$ from perturbation theory shown in (2.52) the sensitivity coefficient equation (2.57) yields the following result for the sensitivity coefficient.

$$S_{k,\Sigma(r)} = k_{eff}\Sigma(r)\frac{(\phi^\dagger, (\frac{1}{k_{eff}}\frac{\delta F[\Sigma(\xi)]}{\partial\Sigma(r)} - \frac{\delta M[\Sigma(\xi)]}{\partial\Sigma(r)})\phi)}{(\phi^\dagger, F[\Sigma(\xi)]\phi)} \tag{2.58}$$

where ξ represents the phase space vector and the square brackets denote an integration over space, direction, and energy. Recall that the round bracket notation represents the inner product. The sensitivity due to individual cross sections can then be calculated by modifying the equation using the discrete ordinates formulation for solving the transport equation. The result is an equation for the sensitivity of reaction x, isotope i, energy group g, and computational region z [25]:

$$S_{k,\Sigma^i_{x,g,z}} = \frac{T^i_{1,x,g,z} + T^i_{2,x,g,z} + T^i_{3,x,g,z}}{D} \tag{2.59}$$

The T terms are:

$$T^i_{1,x,g,z} = -\Sigma^i_{x,g,z}V_z\sum_{j=0}^{NMOM}(2l+1)\tilde{\phi}^{\dagger j}_{g,z}\tilde{\phi}^j_{g,z} \tag{2.60}$$

$$T^i_{2,x,g,z} = \frac{1}{k}V_z\bar{\nu}^i_{g,z}\Sigma^i_{f,g,z}\phi_{g,z}\sum_{g'=1}^{G}\phi^\dagger_{g',z}\chi_{g',z} \tag{2.61}$$

$$T^i_{3,x,g,z} = \sum_{j=0}^{NMOM}V_z\sum_{g'=1}^{G}\tilde{\phi}^{\dagger j}_{g',z}\tilde{\phi}^j_{g',z}\Sigma^{l,i}_{x,g'\to g,z} \tag{2.62}$$

where l is the Legendre order that corresponds to the j^{th} real valued flux moment, $\tilde{\phi}^j_{g,z}$ is the j^{th} component of the flux moment, $\tilde{\phi}^{\dagger j}_{g,z}$ is the j^{th} component of the adjoint flux moment, $NMOM$ is the total number of real valued flux moments corresponding to the Legendre order expansion performed, V_z is the volume of the region, and $\Sigma^{l,i}_{x,g'\to g,z}$ is the l^{th} moment of the transfer cross section from energy g' to g.

The denominator term D from equation (2.59) is:

$$D = \frac{1}{k} \sum_{i=1}^{I} \sum_{z=1}^{R} V_z \sum_{g=1}^{G} (\bar{\nu}^i_{g,z} \Sigma^i_{f,g,z} \phi_{g,z}) \sum_{g'=1}^{G} (\chi^i_{g',z} \phi^\dagger_{g',z}) \tag{2.63}$$

Where $\bar{\nu}^i_{g,z}$ is the average number of fission neutrons emitted, $\chi^i_{g',z}$ is the average fraction of fission neutrons emitted into energy group g', $\Sigma^i_{f,g,z}$ is the macroscopic fission cross section for the isotope, energy group, and region, I is the total number of isotopes, R is the total number of regions, and G is the total number of energy groups.

Note that not all of the T terms are required for all sensitivity calculations. The terms required for each calculation are summarized in [26].

2.3.3.4 Implicit Sensitivities

Implicit sensitivities are sensitivities that are required for models in which the effects of resonance self-shielding are significant. They provide a correction to the explicit sensitivity to account for the fact that a change in a particular cross section may cause a change in a different self-shielded cross section as a result of the change in the flux.

The implicit sensitivity for each reaction is calculated by first finding the total implicit sensitivity by changing the number density of a nuclide. Modifications are then made to the total implicit sensitivity to find the sensitivity to each reaction. An in-depth description of the implicit sensitivity coefficient formulae can be found at [25].

2.3.3.5 Total Sensitivities

The total sensitivity coefficient can be found by simply taking the sum of the explicit and implicit sensitivity coefficients:

$$(S_{k,\Sigma^i_{x,g}})_{complete} = (S_{k,\Sigma^i_{x,g}})_{explicit} + (S_{k,\Sigma^i_{x,g}})_{implicit} \tag{2.64}$$

2.3.4 Uncertainty

The sensitivities that are calculated using the above method can then be used to determine the uncertainty in the multiplication factor (both the total uncertainty, and the contribution to the uncertainty from each nuclide/reaction pair). Using the SCALE 6.1 code package, the determination of the uncertainty is performed by the Sensitivity Analysis Module for SCALE (SAMS). [25]

Let α=α_m, m=1,2,...,M represent a matrix containing the nuclear data, where M is the product of the number of nuclide/reaction pairs with the number of energy groups. Then develop the matrix $C_{\alpha\alpha}$ which contains the relative variances and covariances.

$$C_{\alpha\alpha} = \frac{COV(\alpha_m, \alpha_p)}{\alpha_m \alpha_p}, m = 1, 2, ..., M, p = 1, 2, ..., M \tag{2.65}$$

Here the notation COV(,) represents the covariance of α_m and α_p. Covariance is defined as [27]:

$$COV(\alpha_m, \alpha_p) = E[(\alpha_m - E[\alpha_m])(\alpha_p - E[\alpha_p])] \tag{2.66}$$

Here the notation *E[X]* represents the expected value of the variable X. For a continuous random variable f(x):

$$E[f(x)] = \int_{-\infty}^{\infty} f(x)p(x)dx \tag{2.67}$$

where *p(x)* is the probability density function.

The variance in the system is then computed as:

$$\sigma_k^2 = S_k C_{\alpha\alpha} S_k^T \tag{2.68}$$

where T represents the transpose of the matrix.

In the SAMS calculations, this value is not actually computed directly. It is instead computed using the contribution to the covariance from each nuclide/reaction to nuclide/reaction for all energy groups.

$$\sigma^2_{k^{i,j}_{x,y}} = S_{k,\alpha^i_x} C_{\alpha^i_x,\alpha^j_y} S^{\dagger}_{k,\alpha^j_y} \tag{2.69}$$

where i and j are isotopes, and x and y are reactions (these are all held constant).

The total variance of the system is then computed by adding all of the variances ($\sigma^2_{k^{i,j}_{x,y}}$ where i=j and x=y) and adding two times all of the covariances ($\sigma^2_{k^{i,j}_{x,y}}$ where $i \neq j$ and/or $x \neq y$). The covariances are added twice because for $i \neq j$ and/or $x \neq y$, only data for one of $C_{\alpha^i_x,\alpha^j_y}$ and $C_{\alpha^j_y,\alpha^i_x}$ are present in the covariance libraries used by SAMS. This means that the $C_{\alpha,\alpha}$ matrix would be triangular. Multiplying by two accounts for this omission in the final variance value calculated.

2.3.5 Similarity Analysis

Having determined the formulae required to find the complete sensitivity coefficients, an explanation of the similarity analysis process can now follow. Quantitative measures of the similarity between two systems, similarity parameters, are developed and discussed below. The parameters focused on in the current work are the global integral index c_k, which represents the similarity of nuclear data uncertainties in the experiment and application, and the completeness parameter R, which represents how well a set of benchmark experiments cover the sensitivities of the application. [26]

2.3.5.1 Index c_k

The integral index c_k is a measure of the similarity in the nuclear data uncertainties that the simulations of the experiment and application incur. Here the term 'application' is used to represent the system of interest (i.e. the power reactor design). As was mentioned in previous sections, the nuclear data that is used in the simulations performed has an associated tabulated uncertainty. This method of assessing similarity propagates these uncertainty values to the k_{eff} that was calculated through the use of the sensitivity coefficients. The result is a measure of the similarity between two systems as a result of nuclear data uncertainty.

Using the definition of the complete sensitivity defined previously, an $I \times M$ matrix S_k containing the sensitivity of the k_{eff} to the α values can be constructed, where I is the number of systems analyzed and M is the product of the number of nuclide/reaction pairs with the number of energy groups. An uncertainty matrix can then be created by taking the product of the sensitivity matrix, the covariance matrix, and the transpose of the sensitivity matrix, in an analogous way to that presented in Section 2.3.4. Note that here the result is an uncertainty matrix that contains the variance values σ_i^2 for each individual system (diagonal elements), as well as the covariance between the systems σ_{ij}^2, whereas in Section 2.3.4 the result was a single value for the variance of one system [26].

$$C_{kk} = S_k C_{\alpha\alpha} S_k^T \tag{2.70}$$

The similarity coefficient representing the correlation between the k_{eff} values of each system resulting from nuclear data uncertainties can then be defined as:

$$c_k = \frac{\sigma_{ij}^2}{\sigma_i \sigma_j} \tag{2.71}$$

Each c_k value that is calculated represents the similarity index between two of the systems being analyzed (i and j). A similarity index valued at 1 indicates that

there is complete similarity between the uncertainties of the systems and the bias of system i is the bias of system j. A similarity index of 0 shows that there is no similarity between the system and -1 shows there is complete dissimilarity.

2.3.5.2 Completeness Parameter

The completeness parameter R is a measure of how well a set of benchmark experiments covers the sensitivities of the application under consideration. It is defined as:

$$R = \frac{S_a}{S_t} \tag{2.72}$$

where the values of S_a and S_t are:

$$S_a = \sum_n \sum_x \sum_j |dS^{a,n}_{x,j}| \tag{2.73}$$

$$S_t = \sum_n \sum_x \sum_j |S^{a,n}_{x,j}| \tag{2.74}$$

$$d = \begin{cases} 1 & if N^n_{x,j} \geq nixlim \\ 0 & if N^n_{x,j} < nixlim \end{cases} \tag{2.75}$$

$$N^n_{x,j} = \text{number of experiments where } |S^{e,n}_{x,j}| > |senfac \times S^{a,n}_{x,j}| \tag{2.76}$$

Here, a represents the application, S is the sensitivity of the multiplication factor to the cross section of nuclide n, reaction x, and energy group j. N represents the number of systems where (for a particular nuclide/reaction/energy) the magnitude of the sensitivity of the experiment is greater than that of the application multiplied by the desired coverage factor (between 0 and 1). Finally, *nixlim* represents the minimum number of systems with sensitivities above the specified coverage factor required for the experiment sensitivities to be included in the R calculation.

As an example, assume that in a similarity study between a set of 15 benchmark experiments and an application, the specified coverage factor *senfac* is 0.7, *nixlim* is 1, and the resulting completeness R is 0.8. This indicates that the ratio of the sum of the application sensitivities covered by the experiments to the sum of all of the application's sensitivities is 0.8, where at least 1 experiment with a specific sensitivity within 70% of the application's sensitivity (in absolute value) is required for the sensitivity to be considered covered. Note that each of the 15 benchmark experiments may cover different sensitivities depending on their sensitivity spectrum (i.e. some may cover sensitivities in the thermal region and others in the fast region). It is the cumulative effect of the combination of the regions covered by all experiments that is important to the completeness.

Equation (2.72) indicates that for a sensitivity to be deemed covered by an experiment, it must be greater (within a coverage factor) than the application's sensitivity. The cross section sensitivities are a measure of the importance of a specific cross section to the calculation of the k_{eff} [28]. Thus, for cross sections with larger sensitivities (higher importance) it is more important to accurately know the value of the cross section. This is clear from equation (2.55) for the explicit sensitivity. A higher sensitivity means that a small change in the cross section has a large effect on the k_{eff}. By using experiments that have sensitivities that are at least as large (within a coverage factor) as those for the application, the goal is to ensure the importance of a cross section is not underestimated.

The nature of equation (2.72) accounts for the necessity to ensure cross sections with larger sensitivity are particularly important to cover. It is defined such that sensitivities of a larger magnitude have a greater weight in the completeness calculation.

2.3.5.3 Similarity Analysis Summary

To summarize, the following steps are required in order to calculate the similarity between an experiment and an application and to further analyze a benchmark set of experiments:

1. Calculation of the flux and multiplication factor for experiments and application

2. Calculation of the adjoint flux for experiments and application

3. Calculation of the sensitivity coefficients for experiments and application using the adjoint flux

4. Calculation of the similarity integral indices between application and each individual experiment using the sensitivity coefficients

5. Calculation of the completeness parameter for a set of experiments and the application (if a benchmark set is being analyzed)

2.3.6 Bias Calculation

The goal of a similarity study is to compile a set of experiments that have a sufficient similarity to the application of interest that a procedure is applicable to determine the bias of the calculation. There are several methods available for calculating the bias in computations. These include a traditional trending analysis, global validation, and the GLLS data adjustment method. A traditional trending analysis is a method generally used for criticality safety studies rather than reactor analysis. It consists of determining the multiplication factor bias in a number of applicable experiments and extrapolating to determine the bias of the application [29]. Global validation is a technique used in reactor analysis in which a mock-up experiment is used to directly estimate the biases [30]. The method focused on here is the generalized linear least squares (GLLS) method which consists of a nuclear data adjustment. This is described in the section below, as it is implemented in the Tool for Sensitivity/Uncertainty analysis of Response Functionals using Experimental Results (TSURFER) module [32] of the SCALE 6.1 package. Note that none of these validation procedures were performed in the current work because of a lack of required experimental data (the experimental k_{eff} values must be included). However, the ultimate goal of the similarity study performed here would be to gather and execute a benchmark set of experiments that could be used to validate the applications.

2.3.6.1 TSURFER Generalized Linear Least Squares (GLLS) Method

Given a set of I experiments, each has an experimental multiplication factor (m) and a simulated multiplication factor (k), both of which have uncertainties associated with them. The uncertainty in the experimental multiplication factor is dependent on the accuracy of the experiment performed (i.e. the geometry measurements, material densities, etc.). The uncertainty in the simulated multiplication factor is a result of uncertainty propagation from the nuclear data and statistical uncertainty in the calculation method. The absolute difference between the experimental and simulated multiplication factors is the bias $k-m$. In TSURFER, the GLLS approach is employed in which the cross section data and the experiment multiplication factors are adjusted such that the bias of each experiment is eliminated (the contribution of the uncertainty due to the calculation method is assumed to be negligible). The adjusted nuclear data can then be applied to an application if applicable.

A GLLS adjustment is a method used to fit a linear combination of functions of x to a set of data points (x_i, y_i) [31]. As its name suggests, it is a generalization to the common linear least squares method used to fit a straight line to a set of data points. In TSURFER, the GLLS method is used to fit a new set of nuclear data so that certain constraints are met. The first constraint is that the adjustments are

made such that they are within the uncertainty of the unadjusted values. This is ensured by minimizing a χ^2 factor [32]:

$$\chi^2 = \left[\frac{\alpha' - \alpha}{\alpha}\right]^T C_{\alpha\alpha}^{-1} \left[\frac{\alpha' - \alpha}{\alpha}\right] + \left[\frac{m' - m}{m}\right]^T C_{mm}^{-1} \left[\frac{m' - m}{m}\right] \tag{2.77}$$

where α is a matrix containing the nuclear data, α' is a matrix containing the adjusted nuclear data, m is the experimental multiplication factor, and m' is the adjusted experimental multiplication factor. The matrices $C_{\alpha\alpha}$ and C_{mm} contain the uncertainty data for the nuclear data and the experimental multiplication factors respectively.

The second constraint in the TSURFER GLLS adjustment is that for each experiment the multiplication factor found for the simulation using the adjusted data is equal to the adjusted experimental multiplication factor:

$$k'(\alpha') = k + S_{k\alpha}\Delta\alpha = m' \tag{2.78}$$

Where $k'(\alpha')$ is the simulated multiplication factor for each experiment using the adjusted nuclear data, $S_{k\alpha}$ is a matrix of sensitivities for each experiment, and $\Delta\alpha$ is a matrix containing the relative adjustment applied $\left[\frac{\alpha'-\alpha}{\alpha}\right]$.

From these two constraints, the only possible set of adjustments to the nuclear data and the experimental multiplication factor are [32]:

$$\Delta\alpha = -\left[C_{\alpha\alpha} S_{k\alpha}^T C_{dd}^{-1}\right] d \tag{2.79}$$

$$\Delta m = \left[C_{mm} F_{m/k}^T C_{dd}^{-1}\right] d \tag{2.80}$$

where $F_{m/k}$ is a diagonal matrix containing the ratios k/m and,

$$C_{dd} = S_{k\alpha} C_{\alpha\alpha} S_{k\alpha}^T + F_{m/k} C_{mm} F_{m/k}^T \tag{2.81}$$

$$d = \left[\frac{k(\alpha) - m}{k(\alpha)}\right] \tag{2.82}$$

Once the new nuclear data has been determined based on the experiments, this can then be used to adjust the application multiplication factor using its sensitivity coefficients and determine the bias of the application. The uncertainty in the bias of the application can also be determined based on calculated reduced nuclear data uncertainties and reduced experiment k_{eff} uncertainties. However, for a bias calculation of the application to be reasonable, not just any set of experiments is applicable. When choosing a benchmark set to use for this procedure, it is important to ensure the application sensitivities are adequately covered by the benchmark set, as described in Section 2.3.5.2. In the GLLS method, the cross section data itself

is being adjusted based on the benchmark set. Thus, if sensitivities that are high in the application are low in the benchmark experiments, a small adjustment to the cross section would have a small effect on the benchmark k_{eff} but a larger effect on the application k_{eff}. This means that the importance of that cross section to the application's bias is not being adequately represented. Thus, for a GLLS study, the completeness parameter is the index of interest.

It is suggested that a completeness of 0.7 or larger [32] is necessary for an adjustment procedure to be performed in TSURFER. However, this is only an estimate; further work is underway to determine if this is sufficient.

One of the benefits of a GLLS analysis is that experiments with a high similarity index c_k are not necessarily a requirement (although a high similarity is still useful). Thus, a multitude of experiments that have been performed in the past can be combined to help to develop a set, reducing the number of new experiments that must be performed.

Although the above derivation explained the GLLS method in terms of determining the bias in the multiplication factor, this method can in fact be used to directly determine the bias of any integral response value (i.e. the coolant void reactivity). To do so, sensitivities can be computed for the integral response of interest and these can be used in the equations above.

2.3.7 SCALE 6.1 Module Descriptions

The SCALE 6.1 code package contains a number of modules that are used for different features. The following is an outline of the modules that are required in order to perform a similarity study such as the one completed in the present research. The modules are linked together by a driver module that is specified in the input file.

2.3.7.1 TSUNAMI-3D

When performing a similarity study, the first step is to determine the sensitivity coefficients of each case. This is done using the SCALE driver TSUNAMI-3D (Tools for Sensitivity and Uncertainty Analysis Methodology Implementation in Three Dimensions). A diagram showing the modules that are invoked by the TSUNAMI-3D control sequence is shown in the figure below:

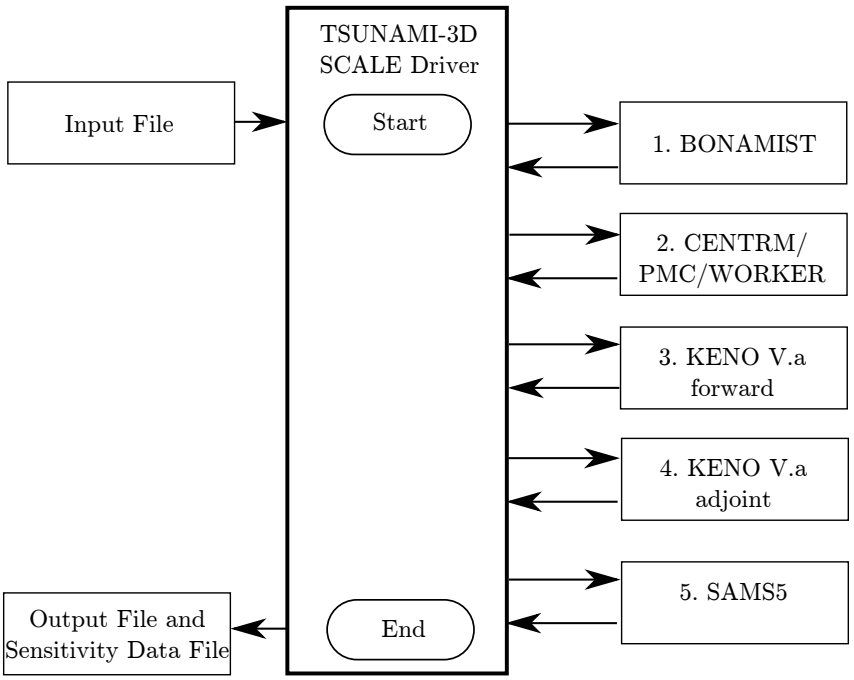

Figure 2.3: Modules Implemented in TSUNAMI-3D [33]

Descriptions of each module are as follows [33]:

BONAMIST: This module is used to compute the unresolved resonance cross sections using the Bondarenko method.

CENTRM/PMC/WORKER: These modules are used together to compute a problem specific cross section library that corrects for the effects of resonance self-shielding. The CENTRM module computes the problem specific continuous energy fluxes. The PMC module uses these fluxes to develop problem-specific multi-group cross sections that incorporate the effects of self-shielding using the method described in Section 2.3.2. The WORKER module then produces a cross section library that can be used by KENO V.a.

KENO V.a forward: This module is used to compute the flux and multiplication factor in the reactor using the Monte Carlo method.

KENO V.a adjoint: This module is used to compute the adjoint flux that is required for the sensitivity calculations. The calculation is also performed using the Monte Carlo method.

SAMS5: This module is used to perform the sensitivity and uncertainty calculations as described in Section 2.3.3.

2.3.7.2 TSAR

The TSAR (Tools for Sensitivity Analysis of Reactivity responses) module of the SCALE 6.1 code package is a control module used to compute the sensitivity coefficients for eigenvalue-difference responses (i.e. the difference between the multiplication factor of two systems). For example, the coolant void reactivity is one such eigenvalue-difference response value. The sensitivities for these responses are determined using the sensitivity coefficient values for each system (calculated by the TSUNAMI-3D module) and determining the sensitivity coefficient for the difference between the values.

2.3.7.3 TSUNAMI-IP

The TSUNAMI-IP (Tools for Sensitivity and Uncertainty Analysis Methodology Implementation Indices and Parameters) module of the SCALE 6.1 code package is a control module that is used separately from the TSUNAMI-3D module. It uses the output sensitivity data computed in the SAMS5 module for all experiments and applications being compared and computes similarity parameters [26].

2.3.7.4 TSURFER

The TSURFER (Tools for Sensitivity/Uncertainty analysis of Response Functionals using Experimental Results) module of the SCALE 6.1 code package is a control module used to perform a bias calculation.

2.4 Related Work

The following section outlines work of a related nature to that performed here. First, prior work upon which the current project was based is outlined. Next, benchmark set similarity analyses that have been performed are briefly examined.

2.4.1 Prior Work

T. Zhu (2011) [34] performed a study in which the sensitivities and uncertainties associated with the simulation of experiments using (Th,Pu)O_2 fuel in the ZED-2 reactor were examined. The core configuration used in these experiments consisted of one channel with (Th,Pu)O_2 fuel bundles and 63 other channel locations filled with natural uranium ZEEP rods. Zhu found that the experiments exhibited biases in the range of 0.188 to 2.3 mk [34]. Uncertainties resulting from nuclear data are in the range of 6.9 to 7.5 mk. The nuclear data that contributes most to the uncertainty are the U-238 (n,γ), U-235 ($\bar{\nu}$) and H-2 (n,2n) cross sections. The original KENO V.a geometry models for the ZED-2 experiments that were used by T. Zhu have also been used in the work performed here.

2.4.2 Similarity Analysis

The concept of ensuring similarity between a set of experiments and an application for bias calculations has been the focus of a number of studies, particularly from Oak Ridge National Laboratory. In general the goal of these analyses is to determine limits on particular calculated values that provide a simple indication as to whether a set of experiments is sufficient to determine the bias for a particular application. For the cases mentioned here, this has been done for the purposes of criticality safety studies. However, the results of these studies are assumed to be extendable to reactor analysis.

A study was performed by Broadhead et al (1999) [35] in which sensitivity and uncertainty techniques were applied to a validation study. In particular the GLLS approach was used to examine the range of applicability of benchmark experiments to a bias calculation procedure. Based on the study it was recommended that 5-10 experiments with a c_k ¿0.9 or 10-20 with a c_k of 0.8-0.9 should be used for adequate convergence of the GLLS method. However, it was noted that for experiments with a c_k of 0.8-0.9, the use of 10-20 experiments was not always adequate for convergence. The completeness parameter was indicated as the determining factor as to whether the set was sufficient, and further analysis of this parameter was recommended. The recommended c_k ranges were later modied by Broadhead et al (2003) [29] based on a study of thermal systems to 15 to 20 experiments with a c_k of 0.9 or higher.

In volume 2 of the above study [36], the value of using the GLLS analysis method for experiments with a low c_k between 0.2 and 0.6 was introduced. Again, it was suggested that for the use of a GLLS analysis, further development of the completeness parameter is required, particularly for experiments with lower c_k values.

The completeness of a set of experiments was analyzed in a study by Broadhead

et al (2000) [37]. Here it was determined that a completeness of approximately 0.8 was sufficient for a set of experiments to be applicable to a GLLS adjustment. However, further fine tuning of this limit was suggested.

Chapter 3

Methodology

The work performed here consists of two main stages. The first is the development of quarter core 3D models of power reactor designs with burned fuel for use in a Monte Carlo code. This implies the development of core models simulating the state of the reactor after a long period of operation. The second is a sensitivity and uncertainty analysis of the power reactor designs as well as the development of guidelines for accumulating a potential experiment set for use in a bias calculation procedure based on a similarity analysis. These guidelines were applied to gather a set of potential ZED-2 reactor experiments that are applicable to the power reactor designs. The methods used for each stage are outlined here.

3.1 Burned Fuel Core Models

In order to examine the similarity between systems, it is necessary to have computer simulations of each system. The simulation package that was used for the similarity study was the SCALE 6.1 code package, which consists of a number of modules as described in Section 2.3.7. The ZED-2 reactor experiments contain unirradiated fuel with known and well defined compositions, and can therefore be directly modelled as KENO V.a geometries for the TSUNAMI-3D driver code module of SCALE 6.1. However, operating power reactors contain irradiated fuel at various burnup states throughout the core. Burned fuel has a different fuel composition from fresh fuel as a result of the decrease in fissile material, and build up of fission products. Thus, it is important to ensure that when analyzing the similarity between a test reactor and power reactor, the power reactor is modelled in a state that is representative of the core with irradiated fuel in order to provide as accurate an analysis as possible.

To obtain core models that simulate the reactor after a long period of operation, three computer code systems were used (the functions of which are described in Chapter 2 of this thesis). First, the lattice code DRAGON 3.06H was used to develop models of a single cell in an infinite lattice for each reactor design and calculate the fuel burnup over a specified period of time. The results from this code gave the fuel composition with respect to time. Next the diffusion code DONJON 3.02A was used to build full core and quarter core models of the various power reactors being

analyzed. From DONJON, the burnup as a function of position in the core was determined. By combining and discretizing the results from the above two codes, core models of the power reactors after a long period of operation can be developed for use with the KENO V.a and TSUNAMI modules of the SCALE 6.1 code package.

The diagram below provides a summary of the process of developing the core model for the SCALE 6.1 code package.

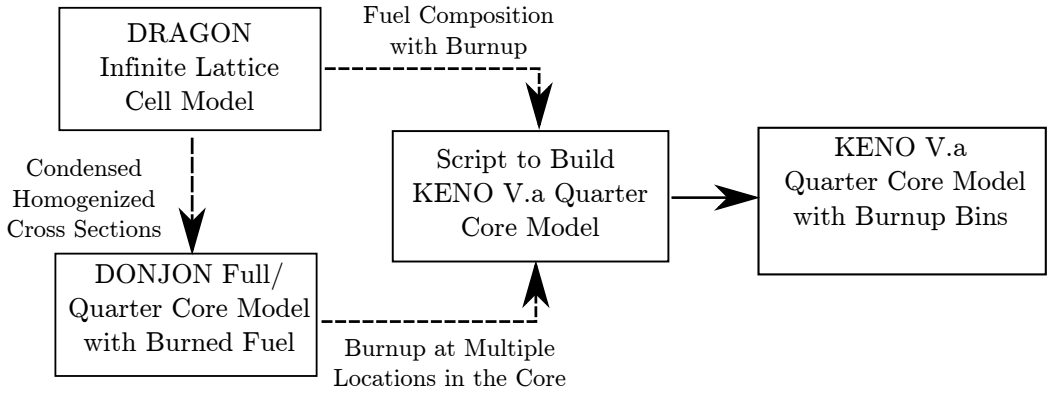

Figure 3.1: KENO V.a. Core Model Flow Chart

The core development process varied slightly between the online refuelled CANDU-type reactors and the batch-fuelled SCWR. These are described in more detail below.

3.1.0.1 Online-Refuelled CANDU Core

To develop a Monte Carlo 3D model of the CANDU core, a script was used to automatically build the KENO V.a case (materials and geometry) based on the DRAGON and DONJON input and output files. In this way, having developed the DRAGON and the DONJON models, it is ensured that the KENO V.a model constructed has the same materials and geometry as the DRAGON and DONJON models for every aspect except the fuel.

First, from the DRAGON input file, the geometry of the fuel bundle and all materials used in the bundle other than that of the fuel itself were extracted. Next, from the DONJON input file the bundles per channel and geometry of the channel arrangement were determined. The next step was to determine the fuel composition as a function of location in the core. This was done by taking the DONJON results for a snapshot of the time-average core that list the bundle burnup as a function of position. These were then combined with the DRAGON results to determine the

composition of each of the rings of fuel in the bundle as a function of burnup.

Due to computational limits, making a KENO V.a model where every bundle in the core has a different composition was not possible. Thus, a method of truncating the number of burnups analyzed was employed in which each bundle in the core was filed in a 'burnup-bin'.

Using the script mentioned above, the desired number of burnup-bins B was chosen by the user. The burnup of the bundle with the maximum burnup and that of the bundle with the minimum burnup were then determined. Between the minimum and maximum burnup, B evenly spaced burnup-bins were chosen. The bundles at every location in the core were then sorted into the appropriate burnup-bin. For a specific burnup bin, a unique composition was used for each ring of fuel in the bundle. The figure below helps to clarify the bundle-burnup definition for a case where B=6.

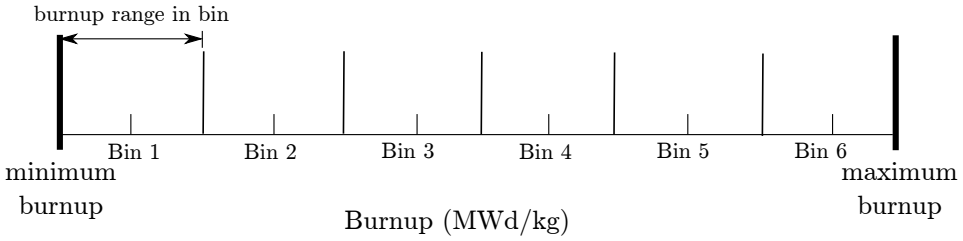

Figure 3.2: Burnup Bin Method

The core models designed here consist of six burnup bins, as this was found to offer a sufficient trade-off between computational time and accuracy. However, more or fewer burnup bins are possible with the current implementation.

3.1.0.2 SCWR Core

The method used to develop Monte Carlo quarter core models of the SCWR was similar to that of the CANDU reactors, however there are some differences. Rather than using multiple fuel bundles in each channel, the proposed SCWR uses a fuel assembly that is 5 m in length [38]. In order to create a representation of this core, the fuel channels were divided into ten sections 50 cm in length. For every two 50 cm sections along the channel, different coolant density conditions, etc. were used, making for a total of five channel positions with different material properties. Thus, for each burnup value defined, five different simulations must be performed. In order for the model to be computationally feasible, the number of burnup-bins must be decreased.

Here, three burnup-bins were defined, although more are possible with the script developed. Because the SCWR has a 3-batch cycle, this is a reasonable approximation. For each of the five channel positions, a different set of three burnup-bins was chosen. This makes for a total of fifteen channel segments with different compositions in the quarter core model. There is a slight difference in the way that the burnup-bins were defined for the SCWR compared to the method used for the CANDUs. Because it is known that there are approximately three main burnup groups (3-batch fuelling), for each vertical channel position the burnups of all of the channel sections were ordered from minimum to maximum, divided into three groups, and the average of each group was taken to be the burnup-bin. This was done in order to achieve a closer approximation to the burnup in the core.

3.2 Similarity Analysis and Benchmark Set Development

When referring to a similarity study, the goal is to determine the degree of similarity between two systems with respect to one of two things. The first is with respect to the nuclear data uncertainties: if two systems, such as a test reactor experiment and a power reactor, have nuclear data uncertainties that are very similar, then it can be assumed that they will have similar biases and the test reactor experiment may be applicable to a bias calculation procedure. The second is with respect to their cross section sensitivities: if a set of experiments effectively cover the cross sections of an application they can be applied to a bias calculation procedure.

Here, a methodology for building a set of experiments particularly for the purpose of a GLLS adjustment procedure is presented. The methodology developed provides the guidelines for ensuring an experiment is acceptable, and for designing new experiments to add to an experiment set. This methodology is based on a sensitivity and uncertainty analysis of the power reactor designs. To perform a sensitivity and uncertainty analysis, the TSUNAMI code modules of the SCALE 6.1 code package are used to determine the nuclide/reaction pairs with the largest sensitivities and the nuclide/reaction to nuclide/reactor covariance matrices that contribute the largest uncertainty to the computed multiplication factor. An analysis of similarity parameters is then performed to indicate the adequacy of the potential experiments. Although the multiplication factor is used as the integral response of interest here, the same methodology for building an experiment set could be applied to the development of experiment sets useful for calculating the bias in other integral response values.

Using the procedure guidelines, a set of potential ZED-2 reactor experiments was devised that have adequate sensitivity coverage for the power reactor designs simulated

here.

Chapter 4

Core Development and Results

The following outlines the results from each of the three steps in developing models of the power reactor designs after a long period of operation. These steps are the creation of lattice cell models in DRAGON, diffusion models in DONJON, and Monte Carlo models in KENO V.a.

4.1 Power Reactor Lattice Cell Calculations

To begin developing KENO V.a models of each of the applications of interest, infinite lattice models of each application were first required. These lattice cell models were simulated using the code DRAGON. The development and results from these models are given in the following sections.

Three power reactor types were used in the similarity studies: a 37-element CANDU 6 with (Th,Pu)O_2 fuel, a 43-element CANDU 6 with (Th,Pu)O_2 fuel, and an SCWR design. Thus, lattice cell models for each of the reactor types were required.

4.1.1 Cell Model Descriptions

4.1.1.1 CANDU Model Description

The (Th,Pu)O_2 fuelled CANDU reactor designs are very similar; the 37-element design uses the typical CANDU-type bundle geometry [9], while the 43-element design uses the CANFLEX bundle geometry [39]. The materials used in the fuel bundles are the same as those currently used in CANDU reactors, with the exception of the fuel. The goal of such a design is to allow for a simple replacement of the current uranium bundles with the proposed thorium bundles. The bundle geometries used for each bundle design are shown in the figure below:

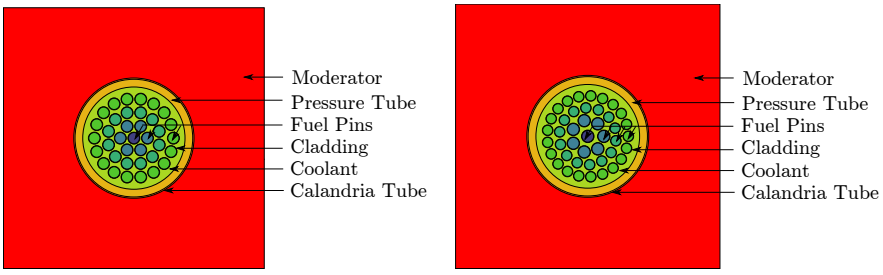

(a) 37-Element CANDU (b) 43-Element CANDU

Figure 4.1: CANDU-Type Bundle Geometries

The fuel used in the CANDU-type reactors in the current study is (Th,Pu)O_2 with approximately 1.745 wt% PuO_2. This was chosen because it is the same fuel as was used in experiments performed in the ZED-2 reactor [1]. The complete composition of the fuel is shown in the table below:

Table 4.1: CANDU (Th,Pu)O_2 Fuel Composition [1]

Nuclide	wt%
Th-232	86.051
Pu-238	0.002
Pu-239	1.181
Pu-240	0.303
Pu-241	0.045
Pu-242	0.008
O-16	12.410

Table 4.2 below specifies the pertinent DRAGON simulation parameters used in the DRAGON models.

Table 4.2: DRAGON Simulation Parameters

DRAGON Version	DRAGON 3.06
Cross Section Library	ENDF-B7 172 Group
Self-Shielding	Stamm'ler Method
Tracking Type	EXCELT
Number of Tracking Angles	10
Density of Integration Lines	30 cm^{-2}
Boundary Condition	Reflective

The geometry and meshing of the lattice cells developed in DRAGON are shown in Figures 4.2 and 4.3. The meshes represent the division of the lattice cell into

multiple regions for the self-shielding and flux calculations, where each region is shown with a different colour. For the self-shielding calculation a coarse mesh was used where each component of the cell (i.e. each fuel pin, ring of coolant, etc.) is a single region except the moderator which is two regions. For the flux calculation a finer mesh was defined where the fuel pins were divided into two regions, each ring of coolant, the pressure tube, and the calandria tube were divided into ten regions, and the moderator was divided into fifty regions.

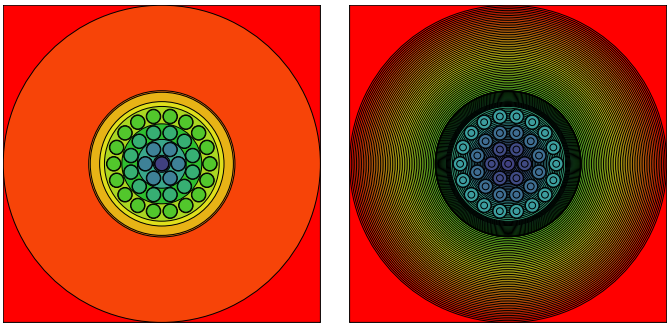

(a) Self-shielding (b) Flux

Figure 4.2: 37-Element CANDU Meshing

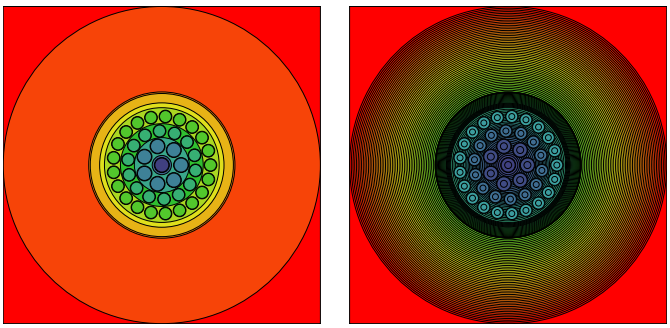

(a) Self-shielding (b) Flux

Figure 4.3: 43-Element CANDU Meshing

4.1.1.2 SCWR Model Description

A recently proposed Canadian Supercritical Water Reactor design that is analyzed here uses a 78-element fuel assembly. A single lattice cell consists of concentric rings of fuel pins with a central non-fuel pin and supercritical water coolant. These are then encased in a porous liner tube and insulator surrounded by the pressure tube. The geometry and material compositions used in the SCWR design were matched as closely as possible to those proposed by AECL. For detailed information please

see [40]. The sole difference between the AECL reference model and the model used here is the presence of yttria in the center pin and the insulator. Yttria is not available in the cross section libraries currently available for DRAGON and thus it was not possible to include it. Instead both the center pin and the insulator are assumed to be 100% ZrO_2.

The fuel channel geometry used for the SCWR is shown in the figure below.

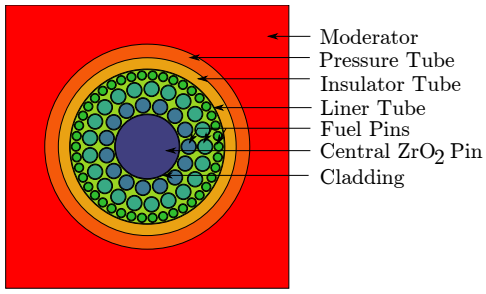

Figure 4.4: SCWR Fuel Channel Geometry

The fuel used in the proposed Canadian SCWR is a (Th,Pu)O_2 fuel with 13 wt% PuO_2. The composition of the fuel is shown in Table 4.3.

Table 4.3: SCWR (Th,Pu)O_2 Fuel Composition [40]

Nuclide	wt%
Th-232	76.46
Pu-238	0.32
Pu-239	5.96
Pu-240	2.63
Pu-241	1.75
Pu-242	0.81
O-16	12.07

For the DRAGON simulations, the same simulation parameters were used in the SCWR cases as were used in the previous CANDU cases (see Table 4.2) except the density of the tracking angles was increased to 40 cm^{-2} to keep the average tracking error on the surface below 1%. The meshing used is shown in Figure 4.5. For the SCWR lattice cell flux meshing, the center pin was divided into eight regions, each ring of fuel was divided into four regions, each ring of coolant was divided into ten regions, the insulator was divided into thirty regions, the liner tube was divided into ten regions, and the moderator was divided into twenty regions.

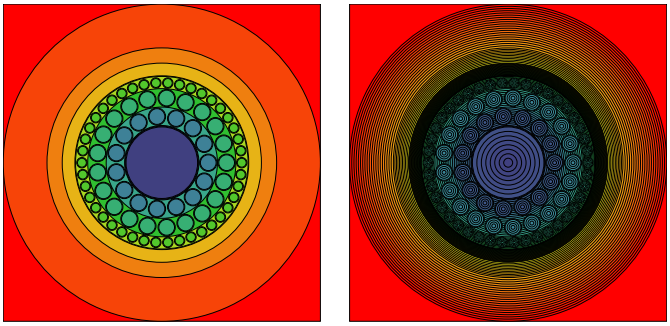

(a) Self-shielding (b) Flux

Figure 4.5: 78-Element SCWR Meshing

When using supercritical water as a coolant, the density of the coolant varies by a large amount from the inlet of the channel to the outlet of the channel. As a result, temperatures of other materials in the fuel channel also change. In order to account for these changes, an approximation was made that simulating five channel positions with different coolant densities, etc., was sufficient to represent the channel. The densities and temperatures used at each of the five channel positions were chosen by J. Pencer and can be found in [40]. The image below shows the division of the channel into ten positions with five different coolant densities, etc.

Figure 4.6: SCWR Channel Division

4.1.2 Results

4.1.2.1 CANDU Results

Having simulated the infinite lattice cell and updated the composition with burnup, the resulting k_∞ as a function of burnup is shown in Figure 4.7. This assumes a power of 34.4 kW/kg of heavy nuclides for the 37-element bundle and 36.028 kW/kg of heavy nuclides for the 43-element bundle.

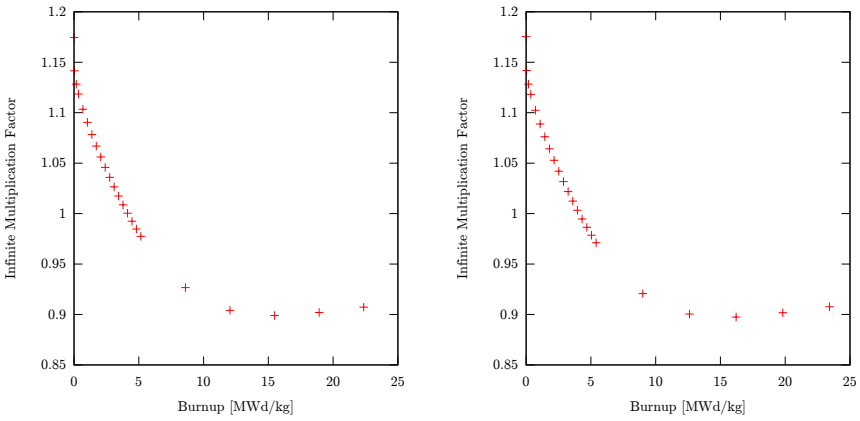

(a) 37-Element bundle (b) 43-Element bundle

Figure 4.7: Thoria Plutonia fuelled CANDU Burnup

The results find that there is little difference in the multiplication factor of the 37- and 43-element bundle geometries. For both, there is a decrease in the k_{eff} as a function of burnup until approximately 15 MWd/kg of heavy nuclides. This indicates that the increasing concentration of fissile U-233 resulting from Th-232 neutron absorption is not significant enough to sustain the reaction until this point.

One of the benefits of the 43-element CANFLEX type bundle compared to the 37-element CANDU bundle is a decrease in the peak linear element rating (LER). This decrease in the peak LER is seen for slightly enriched uranium fuel [41] and is also seen for the thoria plutonia fuel used here. The plots below show the linear element rating for each of the power reactors being analyzed. The linear element was found as a function of the burnup in the bundle using the equation:

$$LER_i = P_{i,rel} \times \frac{P_{dens} \times M_h}{L \times N_i} \tag{4.1}$$

Where i is the index for the current ring, P_{dens} is the power density in kW/kg (assumed to be constant), M_h is the mass of heavy elements in kg, L is the channel length, and N_i is the number of elements in the current ring. $P_{i,rel}$ is the relative power of ring i:

$$P_{i,rel} = \frac{\phi_{i,int} \times E_{i,fiss} \times \Sigma_{F_i}}{\sum_{a=1}^{I} \phi_{a,int} \times E_{a,fiss} \times \Sigma_{F_a}} \tag{4.2}$$

Where $\phi_{i,int}$ is the integrated flux in ring i, $E_{i,fiss}$ is the energy released from fission in ring i, Σ_{F_i} is the macroscopic fission cross section in ring i, and I is the number of rings.

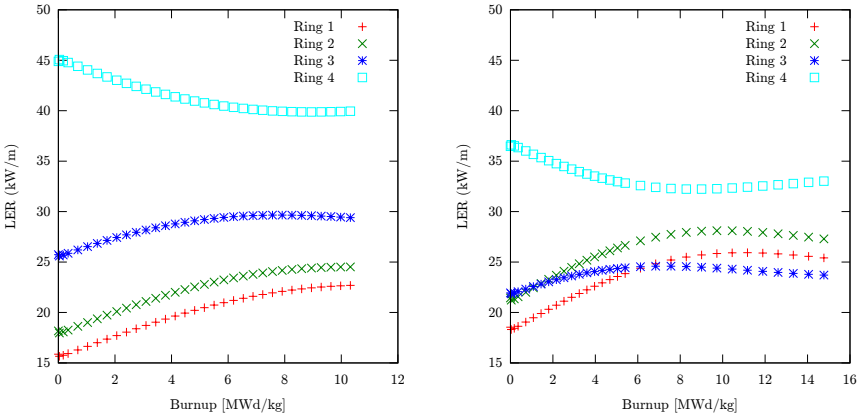

(a) 37-Element bundle (b) 43-Element bundle

Figure 4.8: DRAGON LER for CANDU bundles with (Th,Pu)O_2 fuel

Thus, the 43-element CANDU-type bundle LER was found be lower for the outer two rings than in the 37-element bundle and higher for the inner two rings. In both the 43- and 37-element bundles the outer ring has the highest LER for all burnups, indicating that the LER of this ring would be a limiting value. The fact that the outer ring of the 43-element bundle has a lower LER than the 37-element bundle means that the peak operating temperature is decreased, and there is less fission gas released [41].

4.1.2.2 SCWR Results

The figure below shows the k_∞ of the SCWR as a function of burnup for each channel position assuming a power of 28.0 kW/kg of heavy nuclides.

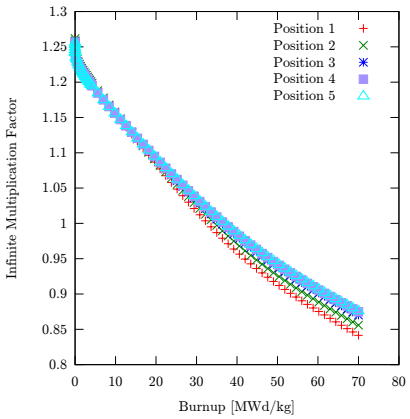

Figure 4.9: 78-Element SCWR Burnup

It is found that the decrease in k_∞ as a function of burnup depends on the channel position. Position 1, at the inlet of the channel, exhibits the largest decrease in k_∞ as a function of burnup, while Position 5, at the outlet of the channel, exhibits the smallest decrease in k_∞ as a function of burnup. In addition, it is found that for fresh fuel, the reactivity is higher at the channel inlet than the outlet, whereas for burned fuel the opposite effect is found.

The linear element rating for the SCWR was also calculated for each channel position. This is shown below.

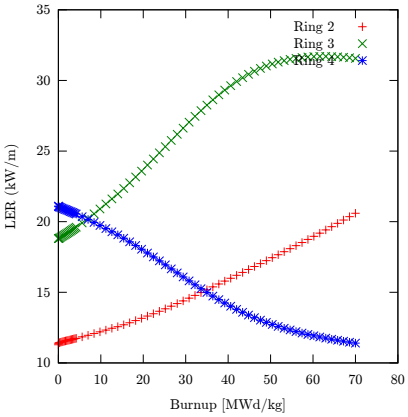

(a) Position 1

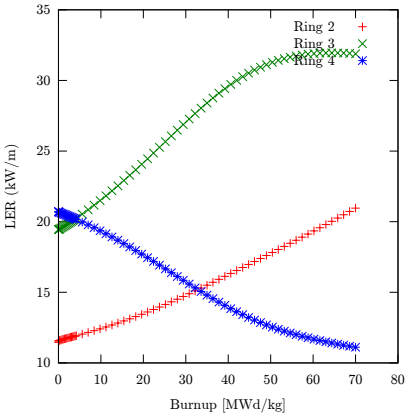

(b) Position 2

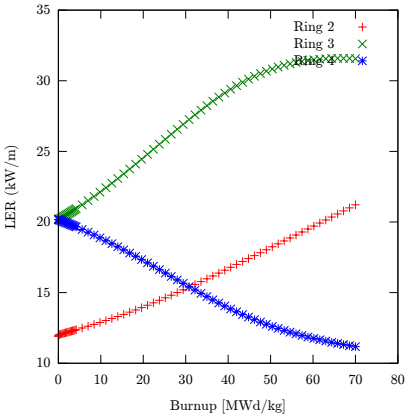

(c) Position 3

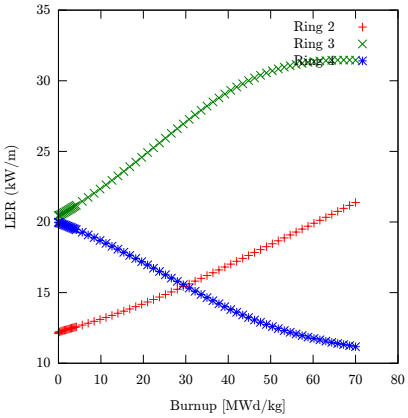

(d) Position 4

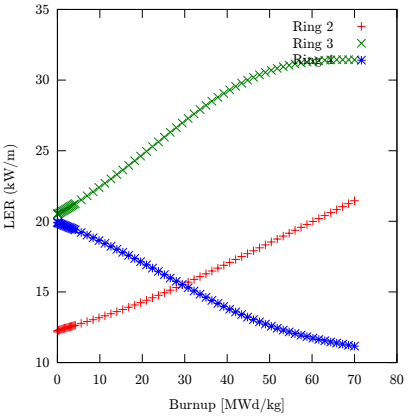

(e) Position 5

Figure 4.10: DRAGON LER for SCWR Channel Positions

There is little difference in the linear element rating between the channel positions. However, there is a fairly large difference between the fuel rings. The inner ring was found to have a relatively low LER that increases with burnup. The middle ring had the highest LER, also increasing with burnup. The outer ring had a high LER for fresh fuel, however the LER decreases with burnup.

4.1.3 Code Comparison

Due to the nature of the current study, it is of interest to perform a comparative analysis between the results found using DRAGON and results found using KENO V.a. This is because the DRAGON burnup results are to be used in the KENO V.a simulations. Thus, a comparison of the aforementioned DRAGON infinite lattice and an equivalent KENO V.a infinite lattice was performed for both the k_{eff}, as well as the coolant void reactivity (CVR). Coolant void reactivity is calculated as:

$$CVR = \rho_{void} - \rho_{cooled} \tag{4.3}$$

Where ρ_{cooled} is the reactivity with the coolant present and ρ_{void} is the reactivity when there is no coolant in the pressure tubes. In the simulations, a void condition has been achieved by setting the coolant density to 0.001 g/cm^3

For the KENO V.a models, the CENTRM/PMC method was used to correct the cross sectional data for self-shielding. Recall from Section 2.3.2.3 that when performing self-shielding correction calculations, a 1D unit cell is required with a simplified geometry. For a CANDU lattice cell, a difficulty arises when attempting to define an acceptable geometry for these purposes.

To describe the CANDU geometry for resonance self-shielding calculations, the bundle was defined as a series of concentric infinite cylinders. Each fuel annulus was defined such that it was of equal volume to the fuel rings, etc. An example of how to define such a geometry is illustrated in the figure below for an SCWR fuel channel.

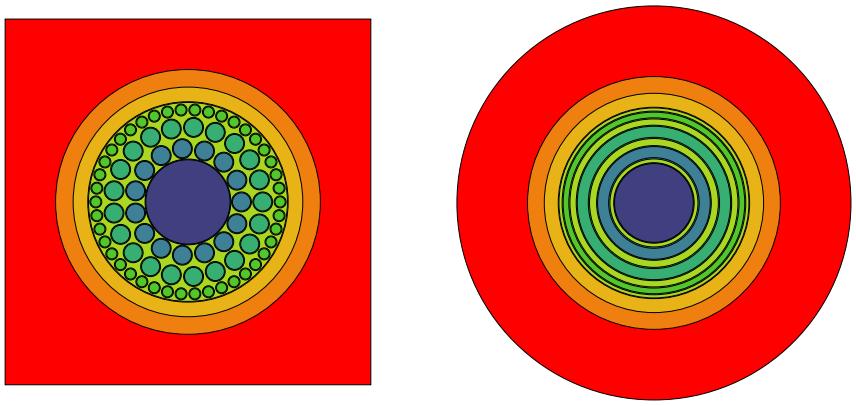

Figure 4.11: Illustration of Self-Shielding Geometry Definition in KENO V.a

Note that these simplified geometries are only used for the self-shielding corrections in order to create a cross section library. For the flux calculations, the KENO V.a model uses the same geometry as was used in the DRAGON simulations. The KENO V.a model was simulated for five burnups (where the composition at each burnup was taken from DRAGON). The results are shown below for the CANDU-type bundles and for the SCWR.

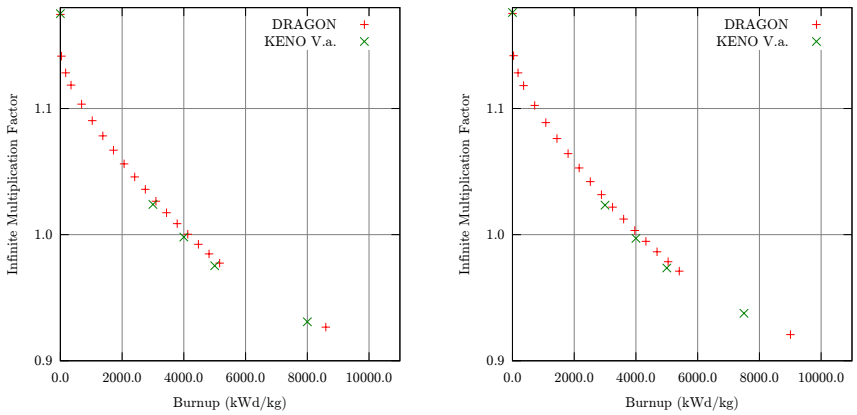

(a) 37-Element bundle (b) 43-Element bundle

Figure 4.12: DRAGON and KENO V.a k_∞ for (Th,Pu)O_2 CANDU bundles

The above figures show that the multiplication factors as a function of burnup computed using DRAGON and KENO V.a are in close agreement. The difference between the results is very small for fresh fuel (approximately 1 mk) but increases to approximately 5 mk.

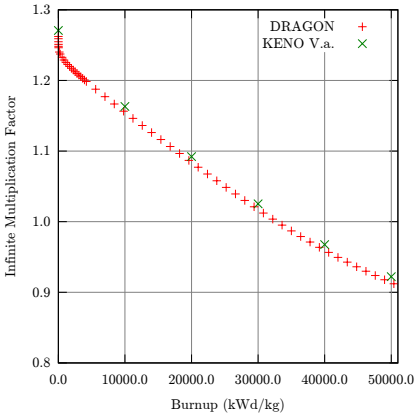

(a) Position 1

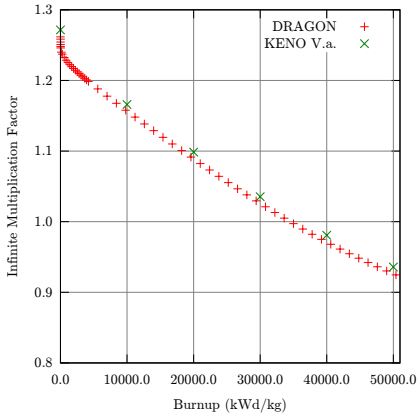

(b) Position 2

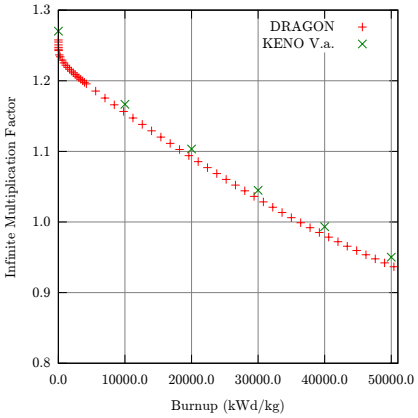

(c) Position 3

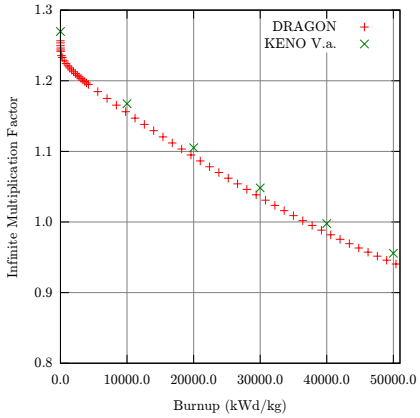

(d) Position 4

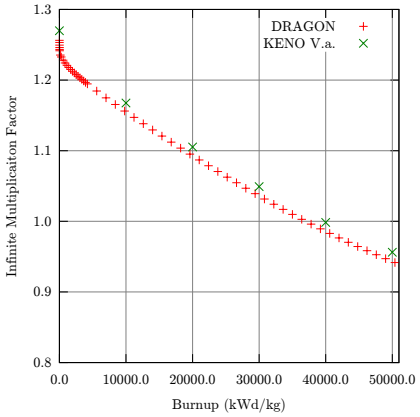

(e) Position 5

Figure 4.13: DRAGON and KENO V.a k_∞ for SCWR Channel Positions

There is a discrepancy between the DRAGON and KENO V.a results for the SCWR lattice cell. It is found that for the fresh fuel lattice there is a difference of approximately 10 mk between the two codes. It is hypothesized that the main cause for the discrepancies found between the two codes is the difference in resonance self-shielding correction methods employed by each of the codes, described in Section 2.1.3.1 and Section 2.3.2.3, and the annularization of the geometry for the KENO V.a models. Further analysis is required to confirm this hypothesis and a benchmark study is currently ongoing [38]. In addition, DRAGON uses a 172-group cross section library, while KENO V.a uses a 273-group library. This may also cause discrepancies in the results.

A comparison of the CVR for each of the cases is shown in the figures below. For the CANDU-type bundles, the CVR computed using each code is very similar for fresh fuel. As the fuel is burned and fission products are introduced, however, the KENO V.a results tend to be slightly higher than the DRAGON results, with a maximum difference of approximately 2 mk. For the SCWR it is found that for all channel positions the two codes have similar trends. However, for all of the channel positions the KENO V.a CVR is higher than the DRAGON CVR with a maximum difference of approximately 5 mk. Once again, it is hypothesized that the reason for the discrepancies is the self-shielding methods used in the calculations.

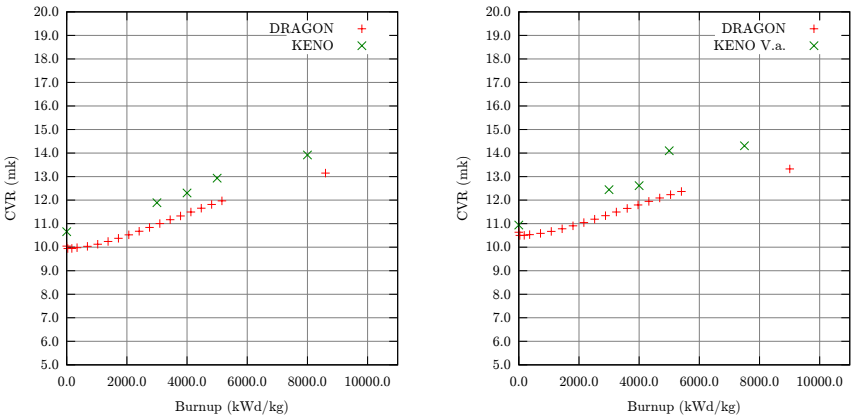

(a) 37-Element bundle

(b) 43-Element bundle

Figure 4.14: DRAGON and KENO V.a CVR for (Th,Pu)O_2 CANDU bundles

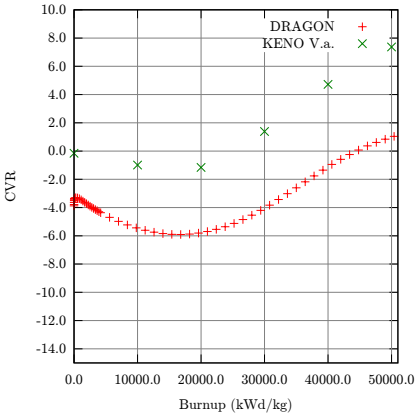

(a) Position 1

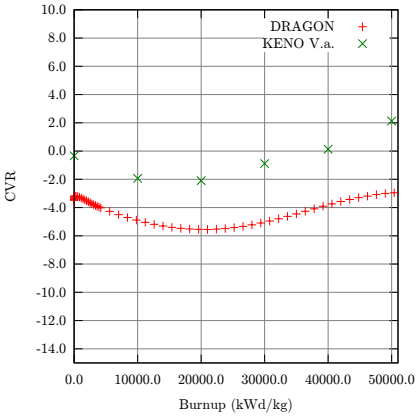

(b) Position 2

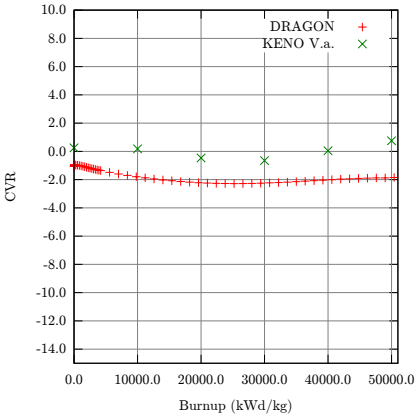

(c) Position 3

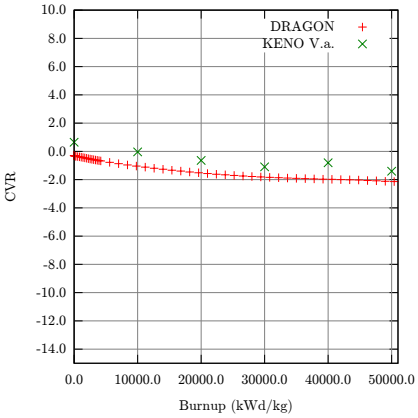

(d) Position 4

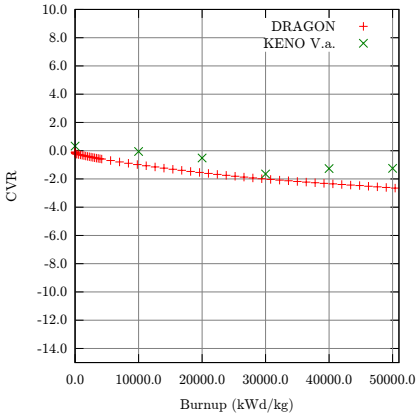

(e) Position 5

Figure 4.15: DRAGON and KENO V.a CVR for SCWR Channel Positions

4.2 Power Reactor 3D Diffusion Models

Having created infinite lattice cell models of each of the reactor types of interest using DRAGON, diffusion models of the cores were then created for DONJON. In order to perform a diffusion calculation, homogenized cross section data is required. This is available in the form of CPO files output from DRAGON. In order to increase the accuracy of the diffusion calculation, 6-group diffusion calculations have been performed here. The energy group boundaries that were used in the DRAGON homogenization scheme are listed in the table below. These energy group boundaries were used by W. Shen for an SCWR 2D benchmark using a 54-element fuel assembly and (Th,Pu)O_2 at 15 wt% PuO_2 [42]. Due to the similarity in the fuel type, the same energy boundaries were deemed applicable to the current analysis. The 6-group homogenization was chosen for the current analysis as a compromise between accuracy and computation time. Future analysis regarding the group energy boundaries would be beneficial.

Table 4.4: Multi-Group Energy Boundaries

Energy [eV]
0.3000
0.6250
1.0970
5.5308×10^3
8.2085×10^5

4.2.1 Model Descriptions

Descriptions of the DONJON models are provided in the following sections.

4.2.2 CANDU Model Description

The diffusion model for the 37-element and 43-element CANDU-type bundles was a 3D full core model. The geometry of the core was consistent with the geometry of a typical CANDU 6 core. Thus, it consisted of a total of 380 channels with 12 bundles per channel, located horizontally in the core. The channels were surrounded by a radial reflector approximately 65 cm thick, however no axial reflector was included. Because the CANDU uses online refuelling, a time-average core model was created.

The core was divided into nine regions with different exit irradiation values. The

regions used here are taken from an example of a typical arrangement for a CANDU reactor, from [20]. The regions are shown in the figure below.

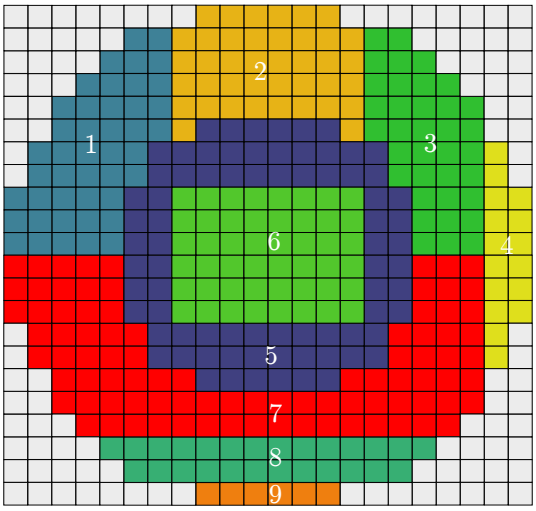

Figure 4.16: Thorium fuelled CANDU Burnup Regions [20]

The models developed here have no reactivity devices. Thus, modifying the exit burnups for each region to achieve $k_{eff} = 1$ would not provide an accurate estimate of the bundle burnups. Instead, a higher k_{eff} is chosen that accounts for absorption due to reactivity devices [43]. To determine the excess reactivity, and the required exit burnup values, a model of the typical natural uranium fuelled reactor was developed. Region exit burnup values from [20] were used in this model. The excess reactivity found for this case (≈20 mk) was then then assumed for the thoria plutonia fuelled CANDU cases. As an approximation, region exit burnup values for the natural uranium fuelled CANDU were scaled in order to achieve the required excess reactivity. Table 4.2.2 shows the exit burnups chosen for each core region.

Table 4.5: CANDU Regional Exit Burnups

	Regional Exit Burnup (kWd/kg)								
CANDU	R1	R2	R3	R4	R5	R6	R7	R8	R9
37-element	5200	5099	5200	5099	5099	5877	5215	4879	4879
43-element	5164	5063	5164	5063	5063	5836	5178	4845	4845

For the core snapshot, a refuelling sequence was used in order to simulate the core with a refuelling ripple. The sequence used was taken from [44].

The following table outlines the key input parameters for the CANDU cases.

Table 4.6: CANDU Diffusion Calculation Parameters

Parameter	Value
Total Core Power	2804.4 MW
Total Number of Channels	380
Bundles Per Channel	12
refuelling Bundle Shift	8
Bundle Length	49.53 cm
Reflector Thickness	65 cm

4.2.3 SCWR Model Description

The proposed Canadian SCWR consists of 336 channels with fuel channels located vertically in the core [45] and surrounded by a reflector. The reflector was assumed to be approximately 65 cm thick. As was described in Section 4.1.1.2, the fuel channel was divided into five regions, and for each region one DRAGON simulation was required. Thus, five CPO DRAGON output files containing homogenized and condensed cross sections were created. Each CPO file was used to represent two 50 cm sections of the SCWR channel in the DONJON model. In the current analysis, one quarter of the core was modelled and reflective boundary conditions were applied at the inner boundaries.

The SCWR is a batch-refuelled reactor with a 3-batch cycle. This means that the core has been divided into three different regions as shown in Figure 4.17. The regions and their corresponding colours in Figure 4.17 are: region 1 (fresh fuel, red), region 2 (once-irradiated, green), and region 3 (twice-irradiated, yellow). At each refuelling, fuel in region 3 is removed from the reactor, fuel in region 2 is moved to region 3, fuel in region 1 is moved to region 2, and fresh fuel is placed in region 1. The arrangement of the three regions is known as the fuelling scheme. When developing a fuelling scheme, one of the main goals is to ensure that the radial peaking factor (RPF) is minimized, where the RPF is:

$$\text{RPF} = \frac{\text{Maximum Channel Power}}{\text{Average Channel Power}} \tag{4.4}$$

The fuelling scheme used here was designed by iteratively simulating a number of different possible fuelling schemes in DONJON in an attempt to minimize the RPF. The final fuelling scheme chosen can be seen in the figure below. Note that optimization of this fuelling scheme to further decrease the RPF and flatten the flux is possible.

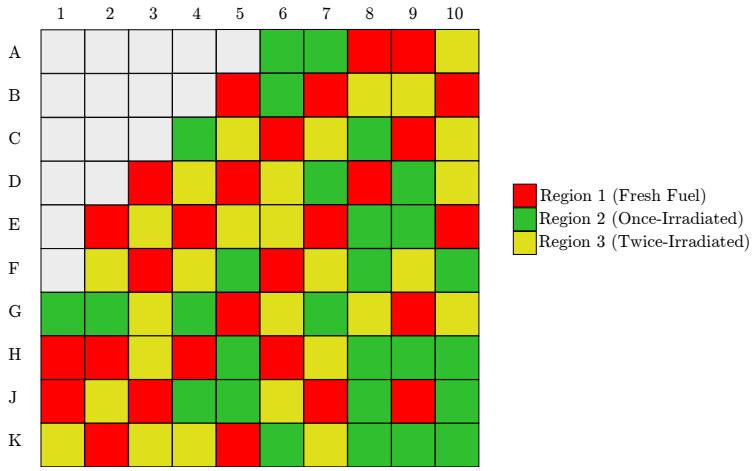

Figure 4.17: 78-Element SCWR Fuelling Scheme

In order to implement this fuelling scheme in DONJON the REFUEL: module with the shuffle option was used at the end of each cycle, allowing fuel to be moved from one channel location to another, replaced with fresh fuel, or removed from the core. For simplicity, the channels moved to a new location in the core at each refuelling were moved as follows. The fuel in each region 2 channel location starting with location A6 and following each row left to right until location K10, was moved to the right to the closest region 3 location to which fuel had not already been moved. If no more region 3 locations were available in the current row, the next row was analyzed from left to right and a position is chosen. For example, the fuel in location A6 was moved to A10, A7 was moved to B8, B6 was moved to B9, etc. The same process was then repeated to move the fuel from region 1 locations to the region 2 locations. By iterating the refuelling process until the DONJON k_{eff} result did not change, core results after a long period of operation were determined. To ensure convergence of the model, time was increased in 10-day increments until the cycle length was reached.

The key parameters used in the DONJON model are shown in the table below. The power per unit mass of heavy elements used here was 28 kW/kg [40]. This was how the total core power was determined.

Table 4.7: SCWR Diffusion Calculation Parameters

Parameter	Value
Total Core Power	2438.8 MW
Cycle Length	500 days
Total Number of Channels	336
Fuel Assembly Length	500 cm
Reflector Thickness	65 cm

4.2.4 Results

4.2.4.1 CANDU Results

A summary of some of the important results for the CANDU cores are as follows, assuming the power remains constant at 2804.4 MW and taking a snapshot of the core. The figure below shows a three dimensional image of the power of each channel in the core. Note that each (X,Y) coordinate represents the position of a channel in the reactor core.

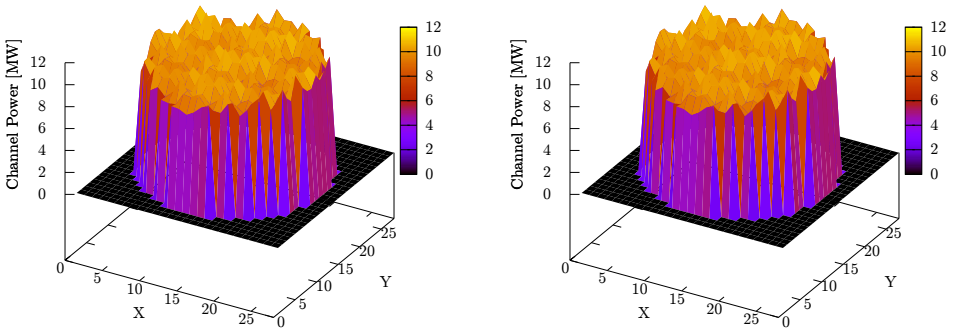

(a) 37-Element (b) 43-Element

Figure 4.18: CANDU-Type Reactor Channel Powers

The following plots show the axial power profile along the maximum channel power in the core.

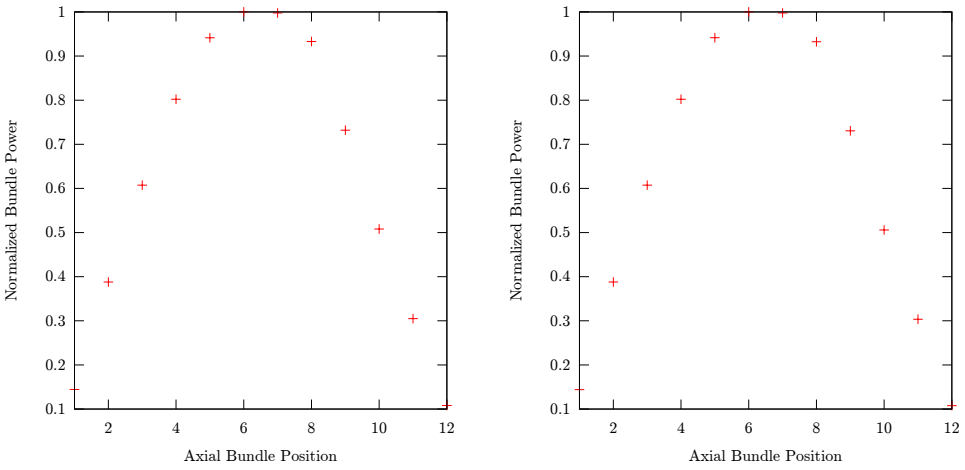

(a) 37-Element (b) 43-Element

Figure 4.19: CANDU-Type Reactor Axial Channel Power Profiles

As may be expected the axial power profile is peaked despite the differential fuelling in these cases due to the lack of adjuster rods in the simulations.

The following table lists some of the important results from the 3D core diffusion simulations. For the CANDU core, a quantity known as the channel power peaking factor (CPPF) which compares the instantaneous to time-average core powers is analyzed:

$$\text{CPPF} = max\left\{\frac{\text{Instantaneous Channel } i \text{ Power}}{\text{Time-Average Channel } i \text{ Power}}\right\} \tag{4.5}$$

where $i = 1, 2, ..., n$ and n is the total number of channels.

Table 4.8: DONJON Full Core CANDU Results

Parameter	37-Element	43-Element
Maximum Channel Power	13 127 kW	13 154 kW
CPPF	1.19	1.20
Average Exit Burnup	5257 kWd/kg	5220 kWd/kg

It is found that both thoria plutonia fuelled CANDU-type reactors have very similar results. As a comparison, results were found using an analagous method for a typical 37-element CANDU with natural uranium fuel. It is found that the uranium-fuelled CANDU bundles have a larger average exit burnup at 7359 MWd/kg. In addition, the CPPF is lower at 1.07.

4.2.4.2 SCWR Results

The 3D power profiles from the DONJON simulations are shown below.

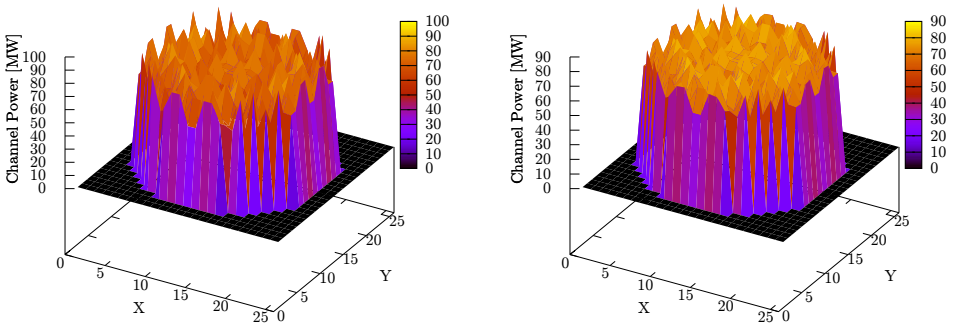

(a) BOC (b) EOC

Figure 4.20: 78-Element SCWR Channel Power

The axial power profile for the maximum power channel is shown below.

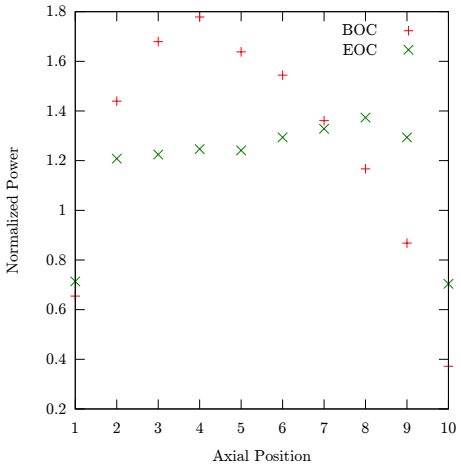

Figure 4.21: 78-Element SCWR Axial Channel Power Profile

As is to be expected, it is found that both the axial and radial power distributions are far flatter at the end of cycle than at the beginning of cycle. This is because the

fuel in the highest flux region is burned faster than the fuel in lower flux regions. The BOC axial power distribution in the maximum power channel is found to peak nearer to the inlet of the channel whereas the EOC distribution has a slight peak nearer to the outlet of the channel. The reason for this is that the maximum power channel at the BOC is a channel that has just been refuelled. Thus, as can be seen from Figure 4.9, the lower-density channel positions near the inlet have a higher reactivity, causing a power peak near the inlet. For burned fuel at the EOC, however, the reactivity of the higher density channel positions near the outlet have a higher reactivity, causing a power peak near the outlet of the channel.

The table below gives the key results from the DONJON core simulations. For the refuelling scheme used here, the radial peaking factor was found to be 1.25 at the BOC and 1.16 at the EOC. This yields a core with an average exit burnup of approximately 42 MWd/kg.

Table 4.9: DONJON Quarter Core SCWR Results

Parameter	BOC	EOC
Excess Reactivity	99 mk	7 mk
Maximum Channel Power	9075 kW	8440 kW
RPF	1.25	1.16
Average Exit Burnup	42 MWd/kg	

4.3 Power Reactor KENO V.a 3D Models

In order to create 3D Monte Carlo models of the power reactor designs with burned fuel using KENO V.a the inputs and the results from DRAGON and DONJON were combined and implemented in a KENO V.a model. The process of combining the results was presented in Section 3 of this thesis. For all of the KENO V.a simulations, quarter core models were used in order to decrease computation time. Thus, at the inner boundaries of the quarter core reflective conditions were used. The exit burnup map shown in Figure 4.2.2 for the full core CANDU simulations in DONJON was not completely symmetric. This was to account for the presence of devices in the core. However, it was assumed that using the DONJON results from the upper left quarter of the core provided sufficient accuracy for the KENO V.a simulations. This is reasonable considering the fact that the bundle burnups used in the KENO V.a simulations have been lumped into bins and the bins were chosen based on the full core results.

4.3.1 KENO V.a Models

The KENO V.a simulations performed here used the method to define the self-shielding geometry described in Section 4.1.3.

Some of the key parameters used in the KENO V.a simulations are outlined below. These include the neutrons per generation (NPG), number of generations (GEN), number of generations skipped to ensure source convergence (NSK), and the standard deviation in the multiplication factor, after which the simulation will stop (SIG). The simulation will stop at SIG only if at least NSK*2 active generations have run [46]. The indicated standard deviation overrides the number of generations. Note that the choice of these parameters was based on a compromise between computation time, available memory, and simulation accuracy.

Table 4.10: KENO V.a Simulation Parameters

Parameter	Value
NPG	100 000
GEN	350
NSK	100
SIG	0.0002

4.3.2 Reactivity Coefficient Results: KENO V.a and DONJON

Having simulated the full core in both KENO V.a and DONJON, a comparison of the reactivity coefficients calculated by the two codes was performed for each of the reactor designs. The reactivity coefficients analyzed here were the coolant temperature coefficient, the moderator temperature coefficient, the fuel temperature coefficient, and the moderator purity coefficient.

In order to calculate the reactivity coefficients using DONJON, for each coefficient two perturbed reactor states were examined (along with the normal-operating state). These perturbed states represented the core with an increase in a particular value (i.e. the fuel temperature) and the core with a decrease in that value. Using DRAGON, the homogenized cross section data for the perturbed reactor under each condition was determined as a function of burnup. To do so the DRAGON simulations used two separate material libraries [47]. One library consisted the normal-operation material data and the second was used to represent the perturbed reactor. At each burnup step, using the normal-operation library, the composition of the burned fuel was determined. The calculated fuel composition was then used to update the perturbed second library and calculate the k_{eff} of the second library

at this burnup step. In this way an instantaneous change in the property of interest was simulated.

Using the homogenized cross section data for the perturbed core calculated in DRAGON, the full core reactivity change due to the change in a particular parameter could be determined. This was done by simulating the core under normal conditions and then switching the homogenized cross section data from DRAGON from those for normal conditions to those for the perturbed state. Once again, by doing so the instantaneous affect of a change in a specific parameter can be found.

The process used to calculate the CVR in DONJON was analagous to the method used to calculate the reactivity coefficients, except only one perturbation is required.

Calculating the reactivity coefficients using KENO V.a was a simple matter of taking the core model designed and changing the specific parameter of interest.

The following tables outline the conditions used for each of the reactivity coefficient values calculated. Here ρ is a reactivity coefficient, T_{cool} is the coolant temperature, T_{fuel} is the fuel temperature, T_{mod} is the moderator temperature, and Pur_{mod} is the moderator purity.

Table 4.11: Reactivity Coefficient Calculations Conditions for CANDU Reactors

Coefficient	Case 1	Case 2	Case 3
$\rho_{T_{cool}}$*	T_{cool}=nominal	T_{cool}=nominal+10 K	T_{cool}=nominal-20
$\rho_{T_{fuel}}$	T_{fuel}=nominal	T_{fuel}=nominal+100 K	T_{fuel}=nominal-100 K
$\rho_{T_{mod}}$*	T_{mod}=nominal	T_{mod}=nominal+40 K	T_{mod}=nominal-40 K
$\rho_{Pur_{mod}}$	Pur_{mod}=nominal	Pur_{mod}=100%	Pur_{mod}=99.6%

Table 4.12: Reactivity Coefficient Calculations Conditions for SCWR

Coefficient	Case 1	Case 2	Case 3
$\rho_{T_{cool}}$*	T_{cool}=nominal	T_{cool}=nominal+30 K	T_{cool}=nominal-30
$\rho_{T_{fuel}}$	T_{fuel}=nominal	T_{fuel}=nominal+100 K	T_{fuel}=nominal-100 K
$\rho_{T_{mod}}$*	T_{mod}=nominal	T_{mod}=nominal+10 K	T_{mod}=nominal-10 K
$\rho_{Pur_{mod}}$	Pur_{mod}=nominal	Pur_{mod}=100%	Pur_{mod}=99.6%

* Note that for the coolant temperature and moderator temperature changes, the density of the coolant/moderator were changed accordingly using data from the NIST Thermophysical Properties of Fluid Systems tables [48].

The following tables show the reactivity coefficients as well as the CVR found using DRAGON/DONJON and KENO V.a for each of the power reactors studied. The uncertainties listed (for all cases except the CVR) are calculated as the un-

certainty in the slope of a least squares fitting. The KENO V.a simulation results have statistical uncertainties associated with them. However, for each reactivity coefficient the statistical uncertainties in the calculated reactivities were found to have approximately the same absolute value. Thus, the least squares uncertainty formula (which does not account for uncertainties in the data points) was sufficient [49]. The uncertainty in the CVR was calculated using the statistical uncertainties in the calculated k_{eff} and the standard formula for error propagation. Note that uncertainties in the k_{eff} due to nuclear data uncertainties are not considered here.

Table 4.13: DONJON and KENO V.a CANDU Reactivity Coefficients and CVR

	37-CANDU		43-CANDU	
	DONJON	KENO V.a	DONJON	KENO V.a
CVR (mk)	10.1±0.2	11.3±0.2	10.6±0.2	11.8±0.2
$\rho_{T_{cool}}$ (μk/K)	51.2±0.8	50.8±0.5	55±2	50±10
$\rho_{T_{fuel}}$ (μk/K)	-3.2±0.3	-5.0±0.4	-3.4±0.3	-2.7±1
$\rho_{T_{mod}}$ (μk/K)	105±1	118±5	106±15	123.0±0.6
$\rho_{Pur_{mod}}$ (mk/%)	22.4±0.4	23.709±0.006	21.7±3	23.3±0.6

Table 4.14: DONJON and KENO V.a SCWR Reactivity Coefficients and CVR

	SCWR BOC		SCWR EOC	
	DONJON	KENO V.a	DONJON	KENO V.a
CVR (mk)	-3.4±0.1	-1.2±0.1	-1.2±0.2	-2.3±0.2
$\rho_{T_{cool}}$ (μk/K)	-30±20	-26.3±0.6	-20±10	-9±6
$\rho_{T_{fuel}}$ (μk/K)	-19.1±0.2	-20.0±0.5	-21.0±0.2	-22±3
$\rho_{T_{mod}}$ (μk/K)	-43±8	-24±2	-33±8	-12±4
$\rho_{Pur_{mod}}$ (mk/%)	-0.67±0.3	-0.8±0.4	-1.45±0.09	-0.8±0.6

The results find that the CANDU-type reactors with 37-element and 43-element thoria plutonia fuel bundles exhibit very similar reactivity responses. For these reactors all of the reactivity coefficients analyzed were positive except for the fuel temperature coefficient. For the SCWR design, all of the reactivity coefficients were negative.

In general, the reactivity coefficient and CVR results from DRAGON/DONJON and KENO V.a were not found to agree within the listed uncertainties. However, they do tend to have similar trends. Discrepancies between the DRAGON/DONJON results and the KENO V.a results likely arise due to the following factors. First, as was mentioned in Section 4.1.3 the self-shielding method used may have been a factor. In addition, the KENO V.a model uses a larger number of groups in the cross section library (273 vs. 172). Thirdly, due to the burnup-bin method that was used, there are inherent differences in the model compositions.

Chapter 5

Similarity Analysis Results

The following outlines the results of a sensitivity and similarity analysis performed between the ZED-2 reactor and the power reactor designs. First, a brief description of the experimental reactor used in the analysis is provided.

5.1 ZED-2 Reactor KENO V.a Models

The ZED-2 heavy water critical facility located at Chalk River Laboratories is a zero-energy reactor used for lattice physics experiments. It was built in the late 1950's and is still operational today. It consists of a cylindrical tank of heavy water in which fuel rods are hung from beams located above the tank. Criticality is achieved by changing the moderator height in the tank. The power of the reactor is monitored by ion chambers located at the bottom of the tank just above the graphite reflector. [50]

The design of the ZED-2 reactor allows for a variable lattice arrangement and for many different fuel types to be easily tested in the reactor. In addition, absorber rods may be hung in the reactor and reactor measuring devices may also be used.

5.1.1 ZED-2 Experiments

In 1984 experiments were performed at the ZED-2 reactor in which (Th,Pu)O_2 fuel with 1.745 wt% PuO_2 was used in one channel in the center of the core [1]. The composition of the fuel used in this experiment is shown in Table 4.1. Experiments were performed in which the coolant in the (Th,Pu)O_2 fuelled channel was either water or air.

Other lattice positions in the ZED-2 reactor during these experiments were filled with ZEEP rods which are composed of natural uranium metal. A top view of the lattice arrangement used is shown in Figure 5.1.

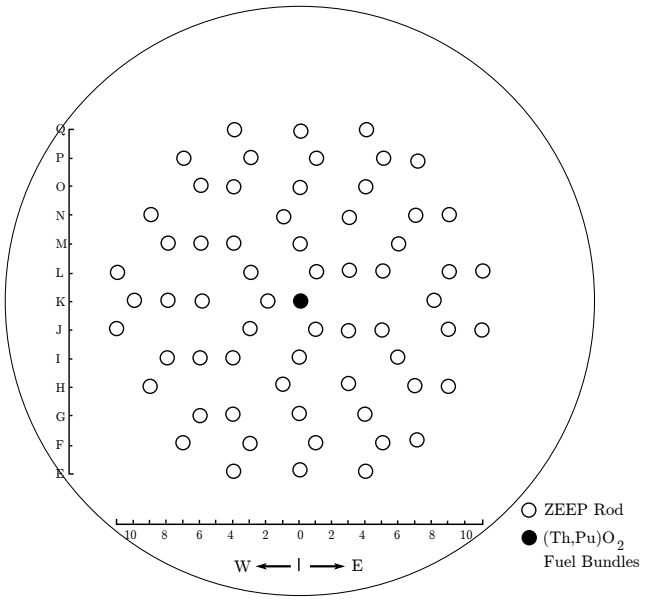

Figure 5.1: ZED-2 Lattice Arrangement for (Th,Pu)O_2 Fuel Experiments [1]

The central channel in the ZED-2 core contained five CANDU-type fuel bundles. The fuel bundles consisted of a 37-element arrangement, however in place of the central element a guide tube was used. The figure below shows the bundle and channel geometry and materials.

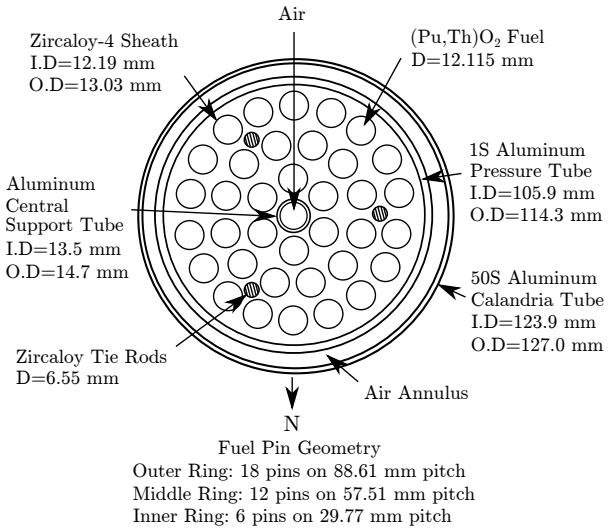

Figure 5.2: ZED-2 Bundle for (Th,Pu)O_2 Fuel Experiments [1]

Important aspects of the experiment design are listed in the table below.

Table 5.1: ZED-2 Experiment Layout

Parameter	Value
Number of Channels fuelled with the Test Fuel	1
Bundles in the Channel fuelled with the Test Fuel	5
Total Number of ZEEP Rods	63
Bundle Length	50.0 cm

In order to perform experiments in the ZED-2 reactor, a set of six Limiting Conditions for safe Operation (LCOs) must be met for safety reasons [50]. The LCOs were chosen to ensure that there is a 98.8% probability that the deposited energy in the experiment will not exceed an acceptance criterion [50]. These limits are reactor physics values that must be calculated prior to performing the experiment. These are listed in the table below.

Table 5.2: ZED-2 Limiting Conditions for Safe Operation [50]

Parameter	LCO
Moderator critical height (H_c)	$\leq$265 cm
Reactivity worth of temporary absorbers	$< \beta$+1
Actual core power (P_A)	$\leq$700 W at 200 W trip setpoint
Prompt neutron generation time (t_{gen})	>0.25 ms
Level coefficient of reactivity (LCR_c)	0.12$\leq$LCR$\leq$2.25 mk/cm
Submerged heavy element mass (M_f)	>1740 kg

5.1.2 KENO V.a Models

The original ZED-2 KENO V.a models that are used in the current work were created by T. Zhu [34]. These models simulated the ZED-2 thoria plutonia experiments described above. As with the power reactor KENO V.a models described in Section 4.3 for the purposes of self-shielding cross section correction, the bundles in the ZED-2 core were described as a 1D geometry consisting of concentric cylinders.

In addition to models of the original experiments, new potential experimental configurations for the ZED-2 reactor were also simulated and used in the similarity analysis. In these new configurations, several factors were changed. These include the number of lattice positions that use thoria plutonia fuel, the composition of the fuel used, and the arrangement of the lattice.

In order to develop a simulation that represents as closely as possible what the state of the actual experiment would be, the height of the moderator in the ZED-2 core was modified to ensure criticality. To accomplish this, a script was written to autonomously change the moderator height of the KENO V.a simulation input file, ensuring the height of the water is accurately represented on the fuel channels. Two initial cases are simulated and linear interpolation is used to predict the next moderator height. The new moderator height case is then simulated and the script repeats the linear interpolation of the moderator height until criticality is reached. To decrease the time this takes, the script was designed such that a small number of neutrons per generation (1000) are used initially. Once the reactor is close to critical, the number of neutrons per generation is increased to 100 000 and the script continues.

5.2 Sensitivity and Similarity Analysis Results

When performing a similarity analysis, the parameters of interest are the sensitivities and uncertainties of the experiments and the applications.

5.2.1 Sensitivities and Uncertainties

In order to determine the sensitivities of the systems modelled, the TSUNAMI-3D driver of the SCALE 6.1 code package was used. The sensitivity calculations are performed using perturbation theory in which the adjoint flux calculation is required. Thus, several simulation parameters are required in addition to those of the KENO V.a calculations. The simulation parameters used for the power reactor sensitivity analyses are listed in the table below. Here APG represents the number of neutrons per generation for the adjoint solution and PNM is the highest order of the flux moments calculated for the adjoint calculations. The TSUNAMI-3D simulations do not use flux meshing by default. Instead the flux is averaged over all of the repeated units. This means that all fuel bundles (or channel segments in the case of the SCWR) that have been lumped into the same burnup bin (and modelled as repeated units) will have an averaged flux. By introducing flux meshing, the accuracy of the calculated sensitivities tends to increase, however the computational expense increases dramatically. For this reason flux meshing was not feasible for the power reactor designs analyzed here, however calculating the flux moment to the third order was possible and this also contributes to accurate sensitivities [51].

Table 5.3: TSUNAMI Power Reactor Calculation Parameters

Parameter	Value
NPG	100 000
GEN	350
NSK	100
SIG	0.0002
APG	600 000
PNM	3

In addition to the above, it is important to mention that here a 44 group covariance library was used for the cross section uncertainty calculations.

As was described in Section 2.3.3, sensitivities represent the change in the multiplication factor with a small change in a particular cross section. Thus, it is effectively a representation of the 'importance' of a particular cross section to the multiplication factor of the core. This is because if a sensitivity is small, then a change in that particular cross section will have relatively little effect on the multiplication factor whereas if a sensitivity is large then a change in the cross section will have a relatively large effect on the multiplication factor.

It follows that it is more important to accurately know the value of cross sections with high sensitivities because any bias on the value being used in the simulations will have a greater effect on the results.

The following tables list the 10 largest sensitivities for each of the applications studied here. Reaction sensitivities that are combinations of other sensitivities (i.e. total, capture, scatter, and inelastic) are not listed. The uncertainties listed are the standard deviations of the sensitivities propagated from the statistical uncertainties in the forward and adjoint flux calculations and the k_{eff} calculation. They do not include the uncertainties resulting from uncertainties in the nuclear data used.

Table 5.4: 37-Element CANDU with (Th,Pu)O_2 Sensitivities

Reaction	Sensitivity
Pu-239 $\bar{\nu}$	0.8311 ± 0.00001
Pu-239 fission	0.4810 ± 0.0002
Th-232 (n,γ)	-0.3321 ± 0.0001
Pu-239 (n,γ)	-0.16739 ± 0.00006
Pu-241 $\bar{\nu}$	0.087983 ± 0.000001
H-2 elastic	0.08 ± 0.02
U-233 $\bar{\nu}$	0.068285 ± 0.000001
Pu-240 (n,γ)	-0.06152 ± 0.00002
Pu-241 fission	0.05298 ± 0.00002
U-233 fission	0.03775 ± 0.00002

Table 5.5: 43-Element CANDU with (Th,Pu)O_2 Sensitivities

Reaction	Sensitivity
Pu-239 $\bar{\nu}$	0.83476 ± 0.00001
Pu-239 fission	0.4828 ± 0.0002
Th-232 (n,γ)	-0.3363 ± 0.0001
Pu-239 (n,γ)	-0.16826 ± 0.00006
Pu-241 $\bar{\nu}$	0.087566 ± 0.000001
H-2 elastic	0.08 ± 0.02
U-233 $\bar{\nu}$	0.0656120 ± 0.0000009
Pu-240 (n,γ)	-0.06165 ± 0.00002
Pu-241 fission	0.05269 ± 0.00002
U-233 fission	0.03627 ± 0.00002

For both of the CANDU-type reactor cases, the highest sensitivities are to the Pu-239, Th-232, and H-2 cross sections, indicating that these are the most important sensitivities to cover by the test reactor experiments.

Table 5.6: SCWR (BOC) Sensitivities

Reaction	Sensitivity
Pu-239 $\bar{\nu}$	0.599350 ± 0.000004
Pu-241 $\bar{\nu}$	0.310580 ± 0.000002
Pu-239 fission	0.2952 ± 0.0003
Pu-241 fission	0.1613 ± 0.0001
Pu-239 (n,γ)	-0.1556 ± 0.0001
Th-232 (n,γ)	-0.13421 ± 0.00009
H-2 elastic	0.11 ± 0.05
Pu-240 (n,γ)	-0.09185 ± 0.00008
U-233 $\bar{\nu}$	0.0613120 ± 0.0000004
Pu-241 (n,γ)	-0.04863 ± 0.00005

Table 5.7: SCWR (EOC) Sensitivities

Reaction	Sensitivity
Pu-239 $\bar{\nu}$	0.501780 ± 0.000003
Pu-241 $\bar{\nu}$	0.324210 ± 0.000002
Pu-239 fission	0.26670 ± 0.0002
Pu-241 fission	0.1812 ± 0.0001
Th-232 (n,γ)	-0.14727 ± 0.00008
U-233 $\bar{\nu}$	0.137920 ± 0.000001
H-2 elastic	0.13 ± 0.05
Pu-239 (n,γ)	-0.12127 ± 0.00008
Pu-240 (n,γ)	-0.09799 ± 0.00007
U-233 fission	0.07353 ± 0.00005

For the SCWR, the highest sensitivities are to the Pu-239 and Pu-241 cross sections, both at the BOC and at the EOC. Unsurprisingly, the EOC case also has a high sensitivity to U-233, a result of the transmutation of the Th-232 in the fuel.

Thus, for all of the applications studied here, it is the fuel material that consists of the elements with the highest sensitivities.

To ensure the sensitivities calculated using TSUNAMI-3D are accurate and that the correct simulation parameters have been used, it is necessary to compare the sensitivities calculated using TSUNAMI to sensitivities calculated by direct perturbation (DP) [51]. To perform a direct perturbation, the number density of an isotope is changed from the nominal value and the forward calculation of the multiplication factor is repeated. Here, the number density ρ of the nuclide was changed by $\pm 3\%$

and the sensitivity was calculated using the following formula:

$$S_{k,\alpha} = \frac{(k_{\rho^+} - k_{\rho^-})/k_\rho}{(\rho^+ - \rho^-)/\rho} \tag{5.1}$$

Where ρ^+ and ρ^- are the perturbed number densities above and below ρ. This yields the total integrated sensitivity for all energies and reactions to the nuclide of interest.

It was assumed that within ±3% the sensitivity to a change in the number density of a nuclide is linear. Further analysis to confirm this assumption would be beneficial. It is suggested that direct perturbation should be performed for the primary fissile nuclide, absorber in the fuel, and moderating nuclide. [52]. Thus, a direct perturbation was performed for Pu-239, Pu-241, Th-232, and H-2 for each of the power reactors. The uncertainty listed in the sensitivity determined through direct perturbation is the standard deviation in the result resulting from statistical uncertainty in the k_{eff} and calculated using the standard error propagation formula.

Table 5.8: Sensitivity Verification for Thoria Plutonia fuelled CANDU Reactors

	CANDU (37)		CANDU (43)	
Reaction	DP	TSUNAMI	DP	TSUNAMI
Pu-239 total	0.313 ± 0.002	0.3135 ± 0.0002	0.312 ± 0.002	0.3141 ± 0.0002
Pu-241 total	0.038 ± 0.002	0.04092 ± 0.00002	0.039 ± 0.003	0.04066 ± 0.00002
Th-232 total	-0.323 ± 0.003	-0.3195 ± 0.0003	-0.322 ± 0.002	-0.3188 ± 0.0003
H-2 total	0.065 ± 0.002	0.08 ± 0.02	0.062 ± 0.002	0.08 ± 0.02

Table 5.9: Sensitivity Verification for Thoria Plutonia fuelled SCWR

	SCWR (BOC)		SCWR (EOC)	
Reaction	DP	TSUNAMI	DP	TSUNAMI
Pu-239 total	0.135 ± 0.003	0.1377 ± 0.0004	0.137 ± 0.003	0.1437 ± 0.0003
Pu-241 total	0.103 ± 0.003	0.1122 ± 0.0002	0.122 ± 0.003	0.1331 ± 0.0001
Th-232 total	-0.110 ± 0.003	-0.1136 ± 0.0003	-0.125 ± 0.002	-0.1236 ± 0.0003
H-2 total	0.119 ± 0.002	0.11 ± 0.05	0.128 ± 0.003	0.13 ± 0.05

It is found that the differences between total sensitivities calculated using direct perturbation versus those found using TSUNAMI were minimal. For the majority of the nuclides tested the results were equal or approximately equal within one standard deviation. The largest discrepancy outside of the range of one standard deviation was 6% in the Pu-241 cross section sensitivity of the EOC SCWR. This suggests that the TSUNAMI simulation input parameters used here allow the sensitivities to be calculated with a sufficient accuracy for the purposes of the current study. However, by modifying the parameters, the sensitivity accuracy likely could be improved.

From the sensitivity data and the cross section uncertainties, the uncertainty in

the multiplication factor due to cross section uncertainties is computed. These are shown below.

Table 5.10: 37-Element CANDU with (Th,Pu)O_2 Uncertainties

Power Reactor	Uncertainty (%Δk/k)
CANDU (37-element)	1.132 ± 0.004
CANDU (43-element)	1.137 ± 0.004
SCWR (BOC)	0.79 ± 0.01
SCWR (EOC)	0.73 ± 0.01

The reaction pairs with the highest contribution to this uncertainty for each power reactor are shown in the tables below.

Table 5.11: 37-Element CANDU with (Th,Pu)O_2 Uncertainties

Reaction 1	Reaction 2	Uncertainty (%Δk/k)
Pu-239 $\bar{\nu}$	Pu-239 $\bar{\nu}$	0.856250 ± 0.000003
Pu-239 fission	Pu-239 fission	0.45122 ± 0.00002
Th-232 (n,γ)	Th-232 (n,γ)	0.34368 ± 0.00001
Pu-239 fission	Pu-239 (n,γ)	0.271660 ± 0.000006
H-2 (n,2n)	H-2 (n,2n)	0.24221 ± 0.00004
Pu-239 (n,γ)	Pu-239 (n,γ)	0.201030 ± 0.000003
H-2 (n,2n)	H-2 elastic	-0.201 ± 0.003
H-2 elastic	H-2 elastic	0.164 ± 0.003
Zr-92 (n,γ)	Zr-92 (n,γ)	0.123430 ± 0.000002
Pu-240 (n,γ)	Pu-240 (n,γ)	0.114190 ± 0.000001

Table 5.12: 43-Element CANDU with (Th,Pu)O_2 Uncertainties

Reaction 1	Reaction 2	Uncertainty (%Δk/k)
Pu-239 $\bar{\nu}$	Pu-239 $\bar{\nu}$	0.860210 ± 0.000002
Pu-239 fission	Pu-239 fission	0.45302 ± 0.00002
Th-232 (n,γ)	Th-232 (n,γ)	0.34413 ± 0.00001
Pu-239 fission	Pu-239 (n,γ)	0.2734 ± 0.000005
H-2 (n,2n)	H-2 (n,2n)	0.24452 ± 0.00004
Pu-239 (n,γ)	Pu-239 (n,γ)	0.202490 ± 0.000004
H-2 (n,2n)	H-2 elastic	-0.201 ± 0.003
H-2 elastic	H-2 elastic	0.163 ± 0.003
Zr-92 (n,γ)	Zr-92 (n,γ)	0.126040 ± 0.000002
Pu-240 (n,γ)	Pu-240 (n,γ)	0.114170 ± 0.000001

Table 5.13: SCWR (BOC) Uncertainties

Reaction 1	Reaction 2	Uncertainty (%Δk/k)
Pu-239 $\bar{\nu}$	Pu-239 $\bar{\nu}$	0.6050400 ± 0.0000008
H-2 elastic	H-2 elastic	0.22 ± 0.01
Pu-239 fission	Pu-239 fission	0.20897 ± 0.00002
H-2 (n,2n)	H-2 elastic	-0.17918 ± 0.0056416
Zr-92 (n,γ)	Zr-92 (n,γ)	0.16535 ± 0.00002
Pu-239 (n,γ)	Pu-239 (n,γ)	0.1572 ± 0.00001
Pu-240 (n,γ)	Pu-240 (n,γ)	0.147190 ± 0.000009
Pu-239 fission	Pu-239 (n,γ)	0.144149 ± 0.000009
H-2 (n,2n)	H-2 (n,2n)	0.14003 ± 0.00005
Zr-91 (n,γ)	Zr-91 (n,γ)	0.1265 ± 0.00001

Table 5.14: SCWR (EOC) Uncertainties

Reaction 1	Reaction 2	Uncertainty (%Δk/k)
Pu-239 $\bar{\nu}$	Pu-239 $\bar{\nu}$	0.5057200 ± 0.0000006
H-2 elastic	H-2 elastic	0.25 ± 0.01
H-2 (n,2n)	H-2 elastic	-0.194 ± 0.007
Pu-239 fission	Pu-239 fission	0.18735 ± 0.00001
Pu-240 (n,γ)	Pu-240 (n,γ)	0.161830 ± 0.000009
Zr-92 (n,γ)	Zr-92 (n,γ)	0.15531 ± 0.00002
H-2 (n,2n)	H-2 (n,2n)	0.14303 ± 0.00005
Pu-241 fission	Pu-241 fission	0.122760 ± 0.000008
Pu-239 (n,γ)	Pu-239 (n,γ)	0.122000 ± 0.000005
Zr-91 (n,γ)	Zr-91 (n,γ)	0.121380 ± 0.000009

Once again, the largest uncertainties tend to occur as a result of the plutonium and thorium isotopes in the fuel. This is expected due to the high sensitivity of these values. However, zirconium in the pressure tubes is also found to have a high uncertainty despite its relatively low sensitivity, indicating that the uncertainty of the measured values for this cross section are high. This illustrates the fact that the final uncertainty in the multiplication factor due to cross section uncertainties is a combined effect of the sensitivities and cross section uncertainties.

5.2.2 Similarity (c_k) Scoping Study

For each application, a scoping study was performed analyzing its similarity to existing experiments performed in the ZED-2 reactor facility and examining the effect on the similarity of simulated changes to the experiments. In the interests of

decreasing computation time for this study, the ZED-2 sensitivity calculations used fewer neutrons per generation for the adjoint calculations than the power reactor simulations and the order of the flux moments was decreased to 1. Once again, flux meshing was not used.

Table 5.15: TSUNAMI ZED-2 Reactor Calculation Parameters

Parameter	Value
NPG	100 000
GEN	350
NSK	100
SIG	0.0002
APG	300 000
PNM	1

Here the similarity index used is the c_k factor that represents the similarity of the uncertainties in the nuclear data (as described in Section 2.3.5). A high similarity parameter is not necessarily a requirement for a GLLS calculation, however, as seen in Section 2.4, it is often used as a metric for the number of experiments required for the calculation. Thus, it is useful to analyze core configurations with a high similarity. The results a similarity analysis between the each power reactor type and the experiment performed in the ZED-2 reactor described in 5.1.1 in which water was used as the coolant are shown in the table below.

Table 5.16: Similarities to Test Experiment Performed in ZED-2

37-CANDU	43-CANDU	SCWR (BOC)	SCWR (EOC)
0.21 ± 0.06	0.21 ± 0.06	0.22 ± 0.08	0.23 ± 0.09

For these cases the similarity between the existing ZED-2 reactor experiment and the power reactors is low. In order to increase the similarity, this scoping study analyzed several potential simulated experimental setups in which the fuel in the ZED-2 reactor was changed and the number of channels fuelled with (Th,Pu)O_2 was varied. In particular, fuel with an increased PuO_2 content was tested. This was chosen because, as can be seen in Tables 5.4, 5.5, 5.6, and 5.7, all three applications have a large sensitivity to the plutonium isotopes.

The table below shows the fuel types that were used in this scoping study.

Table 5.17: Test Experiment Fuel Types for Scoping Study

Fuel Type	Fuel Description
Test Fuel 1	ZED-2 Test Experiment Fuel: (Th,Pu)O_2 fuel with 1.745 wt% PuO_2
Test Fuel 2	ZED-2 Test Experiment Fuel with Increased PuO_2 Content: (Th,Pu)O_2 fuel with 2.745 wt% PuO_2
Test Fuel 3	Proposed Fuel for Canadian SCWR: (Th,Pu)O_2 fuel with 13 wt% PuO_2

The top view of the ZED-2 lattice arrangements used in the scoping study are shown below for cases representing various numbers of fuelled channels. Solid dots represent channels fuelled with thoria plutonia bundles and hollow dots represent ZEEP rods.

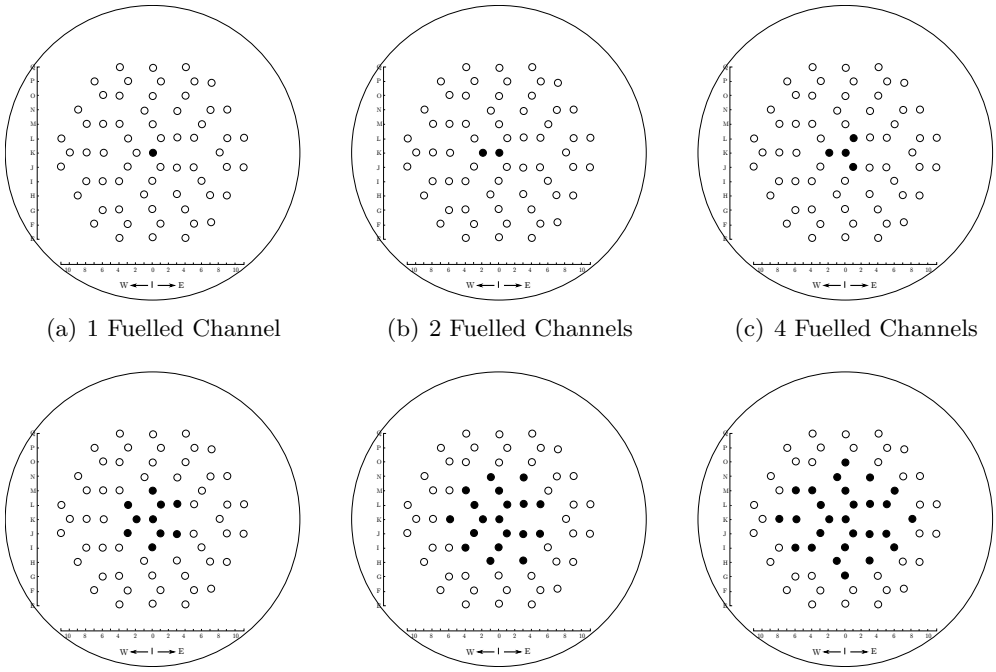

(a) 1 Fuelled Channel (b) 2 Fuelled Channels (c) 4 Fuelled Channels

(d) 10 Fuelled Channels (e) 19 Fuelled Channels (f) 27 Fuelled Channels

Figure 5.3: Test Experiment Lattice Arrangement for Scoping Study

The figures below show the similarity between the experiments and the applications with each fuel type used and with an increasing number of fuelled channels. Here F1 is test fuel 1, F2 is test fuel 2 and F3 is test fuel 3.

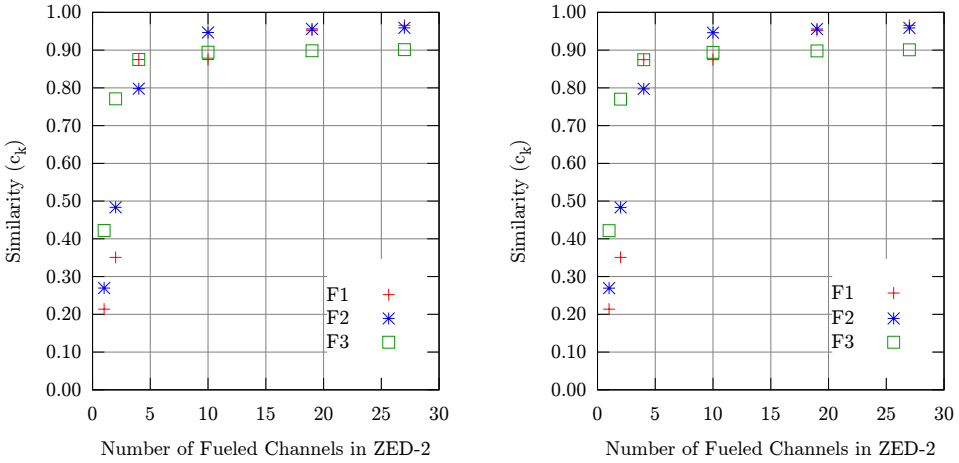

(a) 37-Element (b) 43-Element

Figure 5.4: Similarity between ZED-2 and CANDU Reactors

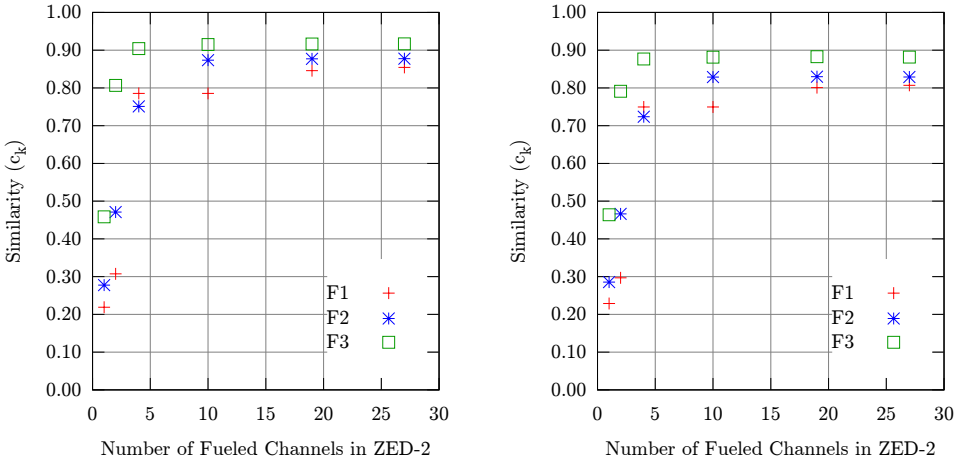

(a) BOC (b) EOC

Figure 5.5: Similarity between ZED-2 and SCWR

It is clear from the above that both the number of fuelled channels in the ZED-2 reactor experiment, and the type of fuel used in the experiment have a significant impact on the resulting similarity c_k. As the PuO_2 content in the fuel is increased from fuel type 1 to fuel type 3, the rate of increase in similarity with fuelled channels also increases for every application. This is likely because the highest contributing nuclides to the uncertainty for all of the power reactor designs analyzed are plutonium isotopes. Increasing the quantity of plutonium in the experiments increases the uncertainty due to the plutonium isotopes in the experiment, thereby increasing

the similarity while requiring fewer fuelled channels.

With an increasing number of fuelled channels, the similarity tends to converge to a maximum value for each fuel type. Once this maximum value has been reached, increasing the number of fuelled channels has little effect on the similarity. This indicates that the remaining dissimilarity is mainly a result of differences in the materials used in the experiment versus the application and differences in the neutron energy spectrum.

The maximum similarity that can be reached depends on the fuel composition used in the experiments and the application. For the CANDU-type reactors in which the fuel has the plutonium composition used in the original ZED-2 experiments, fuel types 1 and 2 (both of which contain plutonium with the original ZED-2 experiment composition) achieve the highest similarity at approximately 0.96. This is despite the fact that fuel type 3 has a higher plutonium content. Likewise, the SCWR has a higher similarity to fuel type 3 (the same fuel as used in the SCWR). The BOC SCWR has a higher maximum similarity (approximately 0.91) than the EOC (approximately 0.89). This is because at the EOC there are more fission products in the SCWR which are not being used in the experiments.

Using the TSAR module of SCALE 6.1, the sensitivities of the coolant void reactivity for the power reactors and the scoping study test experiments were also determined. These sensitivities were then used in a similarity study to determine the similarity of the void reactivity in the ZED-2 experiments and the power reactors. In the current work the multiplication factor is used as the response of interest throughout the majority of the analysis. However, if the void reactivity bias were desired, it would be the similarity data below that would be of interest.

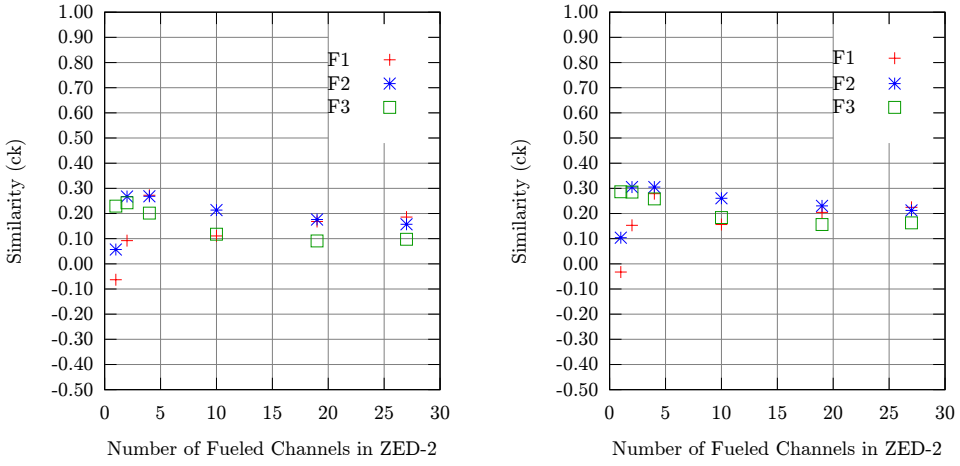

(a) 37-Element (b) 43-Element

Figure 5.6: Similarity between ZED-2 and CANDU Reactors CVR

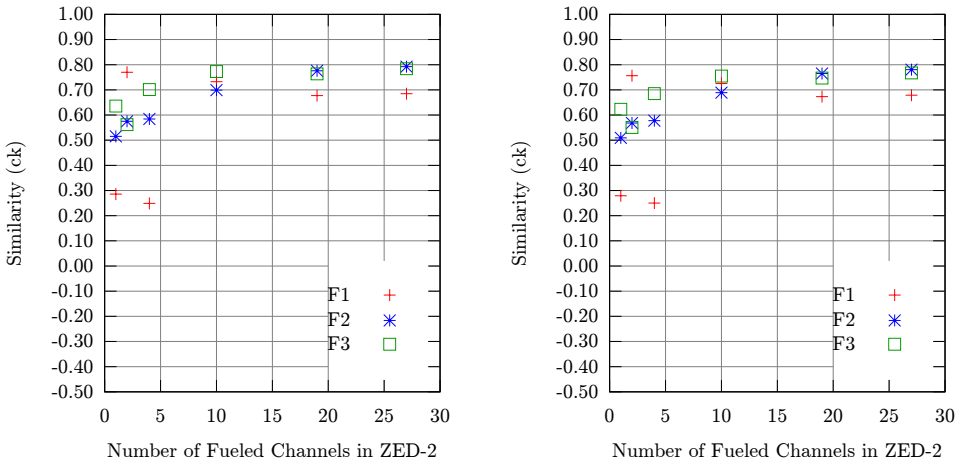

(a) BOC (b) EOC

Figure 5.7: Similarity between ZED-2 and SCWR CVR

The similarity between the CVR of the experiments and the applications does not have as simple a correlation as the reactivities of the experiments and applications. Despite the experiments and the CANDU-type reactors having a large similarity for many of the cases, the similarity between the CVR of the experiments and the CANDU-type reactors is low. This indicates that although the experiments may provide a good representation of the cooled reactor, the uncertainties associated with voiding the coolant are not well represented.

The similarities between the SCWR CVR and the experiment CVRs are much larger, indicating the contributions to the uncertainties in the experiments and the SCWR CVR tend to agree.

5.2.3 Completeness (R) Scoping Study

In addition to the similarity parameter between the experiments and the applications, the completeness is another factor used to determine if an experiment is useful for a bias calculation procedure. In particular, a high total completeness is required for a GLLS adjustment. For a GLLS analysis, the experiments are combined to determine the total completeness. However, here the completeness of each of the experiments used in the scoping study (described in Table 5.17 and Figure 5.3) to the power reactors is calculated individually assuming *senfac=0.9* (the experiment sensitivity must be $\geq 90\%$ of the application's sensitivity to be considered covered). This provides an indication of how well the sensitivities of each individual experiment used in the scoping study tend to cover the sensitivities of the applications.

From this, the effects of increasing the number of fuelled channels, and changing the fuel type can be analyzed. An analysis of a method of determining a set of experiments that, when combined, achieve a high completeness, is outlined in subsequent sections of this thesis.

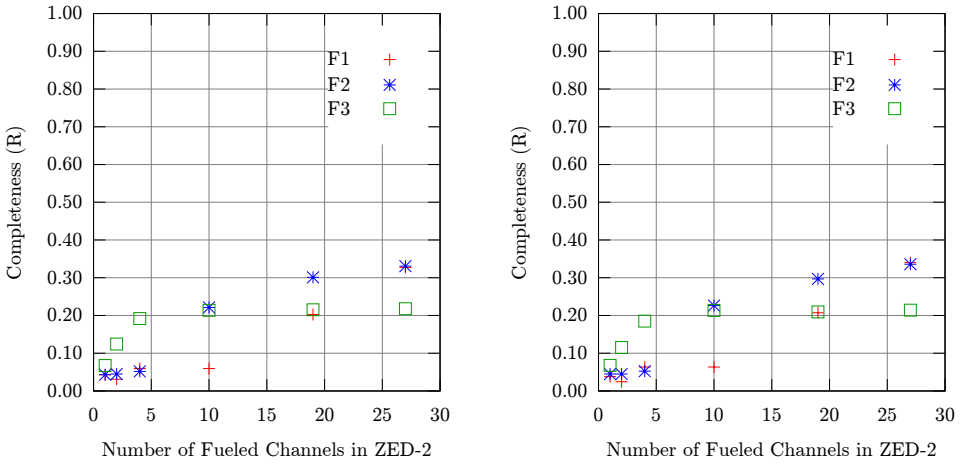

(a) 37-Element (b) 43-Element

Figure 5.8: Completeness between ZED-2 and CANDU Reactors

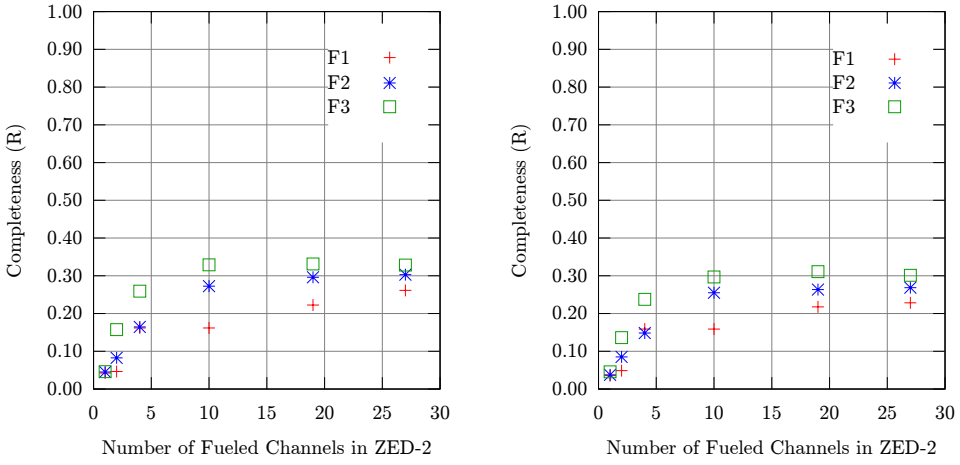

(a) BOC (b) EOC

Figure 5.9: Completeness between ZED-2 and SCWR

From the figures above, it is found for all power reactor designs and each test fuel type that as the number of fuelled channels increases, the individual completeness also tends to increase. However, this effect tends to plateau after a certain number of

fuelled channels. As with the similarity parameter, the fuel type with the maximum completeness for each power reactor corresponds to fuel that has the same plutonium composition as is used in the power reactor. The maximum completeness found for all of the power reactor designs and for each fuel type was between 0.2 and 0.4. This indicates that for each experiment no more than 20% to 40% of the application's sensitivities are covered. To achieve a completeness of 0.7 or higher, experiments must be chosen and combined such that together they cover the energy spectra of each cross section of the application.

5.3 Development of a Benchmark Set for a GLLS Adjustment

As has been described previously in this thesis, the overall goal of a similarity study is to determine if a set of benchmark experiments is applicable to a bias calculation procedure. The parameters that are useful in determining whether a benchmark set is applicable to a bias calculation procedure are the similarity index c_k and the completeness R which were defined in previous chapters.

For the current study, the focus when designing a set of benchmark experiments was to ensure the completeness was sufficiently high that a GLLS analysis could be performed for power reactor designs. Specifically, a completeness greater than 0.7 was used as a threshold beyond which a benchmark set is sufficient. The reason for this limiting choice is that the TSURFER user guide suggests a completeness between 0.7 and 0.8 is required for an adequate set of experiments for a GLLS adjustment. The similarity index c_k was also considered in this analysis, although it is not a requirement for a GLLS analysis set. The reason for including c_k in the analysis will be discussed in subsequent sections.

The similarity analysis performed here is of a theoretical nature. The goal is to determine a set of experiments that would be beneficial to perform in order to ensure that a bias calculation procedure would be sufficiently accurate. However, an in depth study of considerations such as specific experiment limits, the difficulty in obtaining the fuel materials, and the cost of the experiments was not analyzed to a large degree. In the final development of an appropriate benchmark set, these considerations would need to be given a higher importance.

5.3.1 Benchmark Set Development Methodology

One of the difficulties when designing a benchmark set of experiments in a case such as this is that there are a large number of variables that can be altered. For the ZED-2 reactor, the location of the channels in the core, the number of channels in the core, and the coolant can be modified, and new or different materials can be introduced to the core by modifying existing experiments or designing new experiments. This means that, when purely considering the simulations of the cases (and not considering some of the more practical limitations such as availability of materials, etc.) there are essentially an unlimited number of core arrangement possibilities. Thus, it was important to determine exactly what is required to increase the completeness, and to develop a methodology that streamlines the process of developing an appropriate set.

The ultimate goal of the experiment design methodology is to analyze the affect of core modifications on the magnitude of the cross section sensitivities and the energy spectrum of the cross section sensitivities. In general, changing the amount of a specific isotope in the fuel tends to increase the magnitude of the cross section sensitivities. Modifying the core to change the energy spectrum of the neutrons tends to modify the energy spectrum of the sensitivities. However, for each modification to the core geometry there are several effects. For example, increasing the amount of a fissile element in the fuel may mean that the moderator height becomes very low. Thus, it is beneficial to establish guidelines for the construction of an experiment set to help establish the effects of changes to the test reactor setup.

The methodology developed and used here is listed below in a step-by-step fashion. Note that while these guidelines were created to assist in gathering experiment sets for a k_{eff} bias calculation, they would also be useful for gathering experiments for other integral response bias calculations.

- ♢ Step 1: Examine largest application sensitivities
- ♢ Step 2: Choose possible fuel types based on sensitivities and the application's fuel
- ♢ Step 3: Choose basic lattice arrangement and geometry
- ♢ Step 4: Modify the lattice pitch and fuelled channels to examine effect on sensitivity spectrum coverage
- ♢ Step 5: Modify coolant type to examine effect on sensitivity spectrum coverage

♢ Step 6: Based on the results of the previous steps, begin iteratively accumulating a set of experiments that achieves an adequate completeness

Using the TSUNAMI-IP code module, the final value for the completeness can be obtained, however it does not indicate what is required to increase the completeness. Thus, a script was written that recalculates the completeness using the same method as is described by TSUNAMI-IP, but that also allows the user access to more information concerning the contribution to this final completeness value.

Recall that the completeness is a ratio of the sum of the application's sensitivities covered by the experiment to the total sum of the application's sensitivities, where the covered sensitivities are region integrated, but energy and reaction specific. Coverage of a specific sensitivity is assumed if the magnitude of the experiment's sensitivity is within a specified factor of the magnitude of the application's sensitivity. From the definition of the completeness it is clear the higher the magnitude of one of the application's sensitivities, the larger the weight it has in the completeness calculation. It follows that the most effective way to increase the completeness is to ensure that the largest (in magnitude) of the application's sensitivities are covered.

In the script written here to calculate completeness, an output file is created that lists which of the application's sensitivities are covered and, for those that are not, what the application's sensitivity value is. In addition, the script outputs a list of the isotopes for which the sum of the uncovered sensitivities was the largest. Finally, for a user-specified isotope and reaction, plots of the sensitivity vs. energy for each experiment compared to the application are created automatically. Using this information, the user can determine which uncovered sensitivities are the most important to address, and the energy range of these sensitivities. The user can then make educated changes to the experimental set in order to attempt to cover the 'most important' isotopes.

While developing the script, it was discovered through testing that the completeness that is calculated by TSUNAMI-IP only includes sensitivity information for capture, scatter, and fission reactions rather than the components of these reactions. Because the TSURFER module adjusts each component of the reaction, it was decided that the following reactions will be included in the script written here: $\bar{\nu}$, fission, (n,γ), elastic, (n,2n), χ, (n,α), (n,n'), (n,p), (n,d), and (n,he-3). This ensures that the completeness is not overestimated or underestimated as a result of lumping reaction sensitivities together. The result is only a small change in the completeness value calculated. The table below describes each reaction in more detail [25]:

Table 5.18: Reactions Considered in Completeness Calculation

Reaction	Description
$\bar{\nu}$	Number of neutrons born from fission
fission	Fission
(n,γ)	Neutron capture and γ release
elastic	Elastic scattering
(n,2n)	Neutron capture and 2 neutron release
χ	Fission spectrum
(n,α)	Neutron capture and alpha release
(n,n')	Neutron capture and neutron release
(n,p)	Neutron capture and proton release
(n,d)	Neutron capture and deuteron release
(n,he-3)	Neutron capture and He-3 release

5.3.2 Benchmark Set

Here, a benchmark set of experiments in the ZED-2 reactor is developed that together cover the thorium-fuelled CANDU-type reactors and the SCWR analyzed throughout this thesis. To do so, the steps listed above were used.

Step 1: Examine largest application sensitivities

As was mentioned above, to increase the completeness of a benchmark set of experiments, it is key to ensure that the largest sensitivities are covered. From Tables 5.4, 5.5, 5.6, and 5.7 it was found that the highest sensitivities tend to be those of the fissile materials (Pu-241 and Pu-239), and the heavy water (H-2). Because the SCWR models were averaged core models for the BOC and EOC cores, it was expected that the fission products would have an effect on the completeness. However, it was found that because the magnitude of the sensitivities for the fresh fuel isotopes (i.e. Pu-240, Th-232, etc.) were so high, the presence of the majority of these fission products did not have a significant effect on the completeness. Thus, when building the benchmark set, the isotopes listed above were the main focus.

Step 2: Choose possible fuel types based on sensitivities and the application's fuel

Based on the fact that the highest sensitivities were to the Pu-241 and Pu-239 isotope cross sections, it is clearly important to choose fuel types that incorporate plutonium fuel. The fuel in the CANDU-type reactors used in this study contained plutonium with a lower percentage of Pu-241 than was used in the SCWR fuel, and correspondingly, the CANDU-type reactors have a lower sensitivity to Pu-241 than the SCWR. Thus, it was decided that fuel types containing each of the plutonium

types would be used. As an example of the differences in the sensitivity coverage, the figures below illustrate the effects of using two fuel types. Fuel A is the thoria plutonia fuel used here in the CANDU-type reactors. Fuel B is a modification of the thoria plutonia fuel used here in the SCWR. It uses the same plutonium type as the SCWR but at 2.5 wt% PuO_2. Note that the rectangular nature of the plots is a consequence of the multi-group structure of the cross section data used.

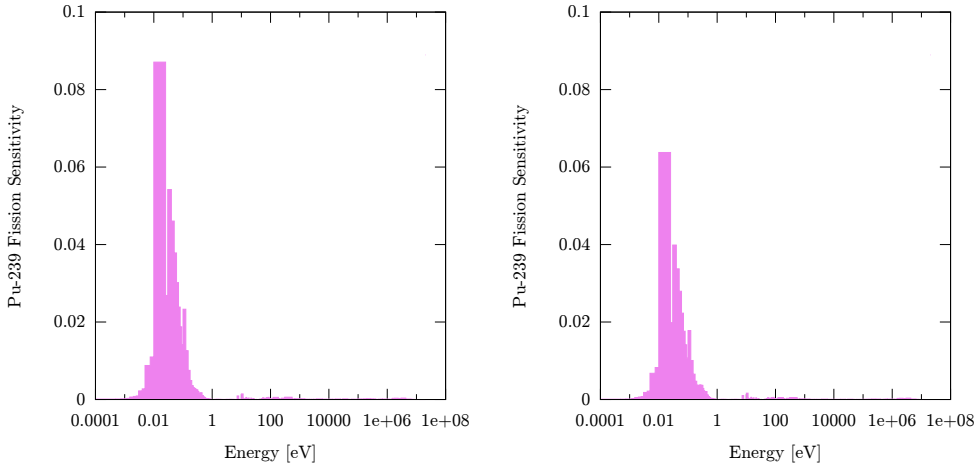

(a) Fuel A (b) Fuel B

Figure 5.10: Pu-239 Fission Sensitivity Spectrum with Fuel Type

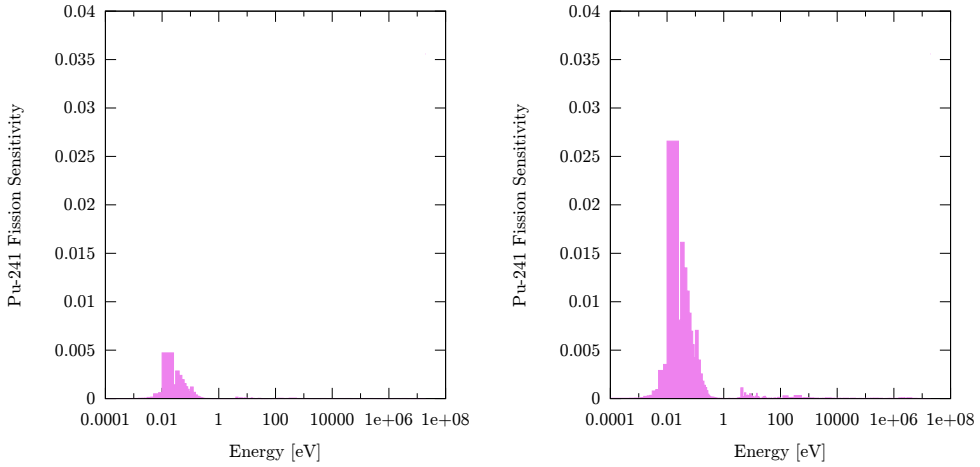

(a) Fuel A (b) Fuel B

Figure 5.11: Pu-241 Fission Sensitivity Spectrum with Fuel Type

For each of the nuclide/reaction pairs, the general shape of the curve tends to be the

same for the experiments while the height of the sensitivity for the various energy groups changes. This is because the general shape of the curve is mainly dependent on the values of the cross section data itself (the relative sensitivity coefficient is directly proportional to the cross section) while its magnitude depends on several factors. These include the value of the cross section data, the quantity of the isotope of interest in the system, and the energies of the neutrons in the system.

For example, the Fuel A above contains plutonium with a larger percentage of Pu-239 than Fuel B and a lower percentage of Pu-241. This causes the Pu-239 sensitivities for the Fuel A to be larger than for Fuel B and the Pu-241 sensitivities for Fuel B to be larger than for Fuel A.

Step 3: Choose basic lattice arrangement and geometry

For the benchmark set that was developed here, the basic setup of the ZED-2 core was used. In addition, despite the fact that the SCWR has a 78-element fuel assembly with a Zirconia center pin and insulator materials, the experiments simulated all used the original channel and bundle geometry and the original channel and bundle materials. The only difference was a substitution of the fuel materials, and a substitution of the coolant type. Because the sensitivity of the application to the fuel materials was relatively low, excluding them did not significantly decrease the completeness.

The core arrangement used for the benchmark sets was not the same as those used in the ZED-2 experiments described above. Instead, a square lattice arrangement that is more typical of recent ZED-2 experiments [50] was used. The reason this lattice arrangement was used is that it makes increasing the lattice pitch simpler. An image of the square lattice core arrangement is shown below.

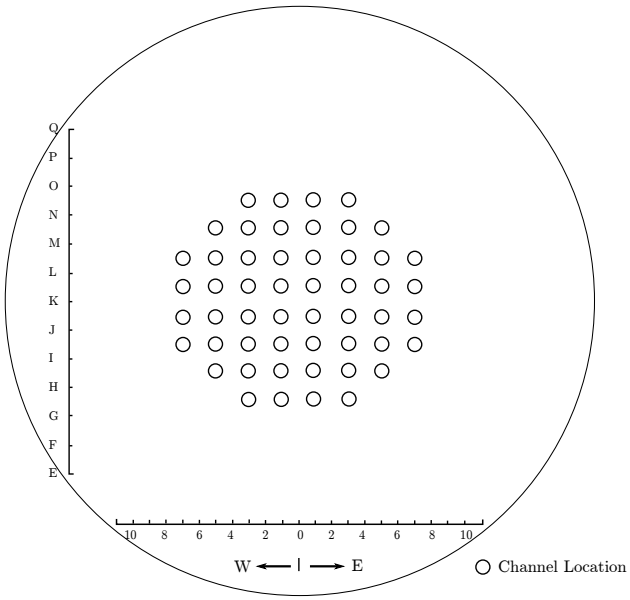

Figure 5.12: ZED-2 Lattice Arrangement for Benchmark Construction

For the various chosen experiments, the lattice pitch and the number of fuelled channels were modified. In addition, in some cases ZEEP rods were used in addition to the fuelled channels. This was used as a relatively simple way to increase the reactivity and submerged fuel mass in the ZED-2 reactor so the moderator height was acceptable for cases where a small number of channels were fuelled.

Step 4: Modify the lattice pitch and fuelled channels to examine effect on sensitivity spectrum coverage

Having determined possible fuel types and the basic arrangement of the lattice, simulations were performed to analyze the effects of changing the lattice pitch and arrangement. It was found that the lattice pitch has a significant effect on the cross section energy range that is covered by the experiment. As an example, the figure below shows the difference in the Pu-239 sensitivity with a 14 cm lattice pitch and a 38 cm lattice pitch for cases where all other factors except the moderator height were held constant.

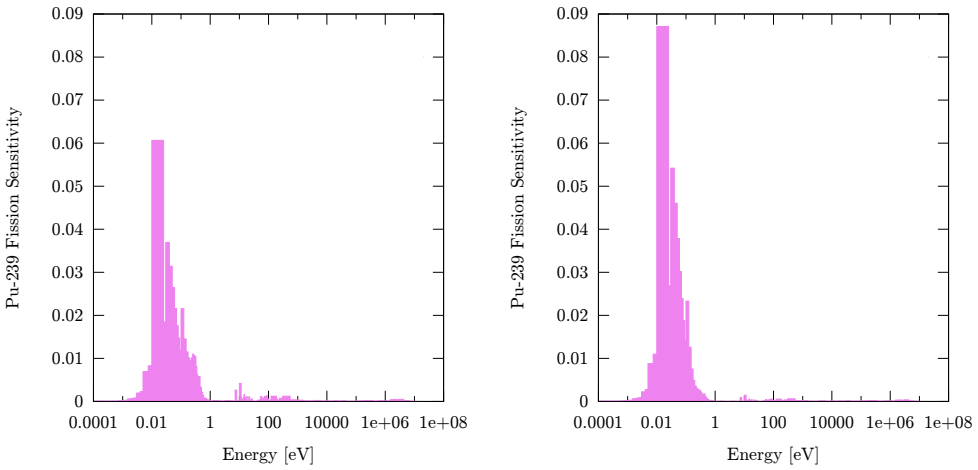

(a) 14.0 cm lattice pitch

(b) 38.0 cm lattice pitch

Figure 5.13: Pu-239 Fission Sensitivity Spectrum with Lattice Pitch

It was found that in general with a small lattice pitch, the simulation tends to have a higher sensitivity to high energy cross section data, whereas with a large lattice pitch the simulation has a higher sensitivity to low energy cross section data. The reason for this is that when the lattice pitch is small and the fuel is spaced closer together, the fast flux is higher, while the opposite is true for a large lattice pitch.

Step 5: Modify coolant type to examine effect on sensitivity spectrum coverage

In addition to modifying the lattice pitch, a second modification to the simulated experiments that was used as a relatively simple way of changing the coverage of the experiment sensitivities was to change the coolant type used. The following plots show an example of the change in the Pu-239 sensitivities when using air versus heavy water as coolant for cases with a lattice pitch of 38.0 cm.

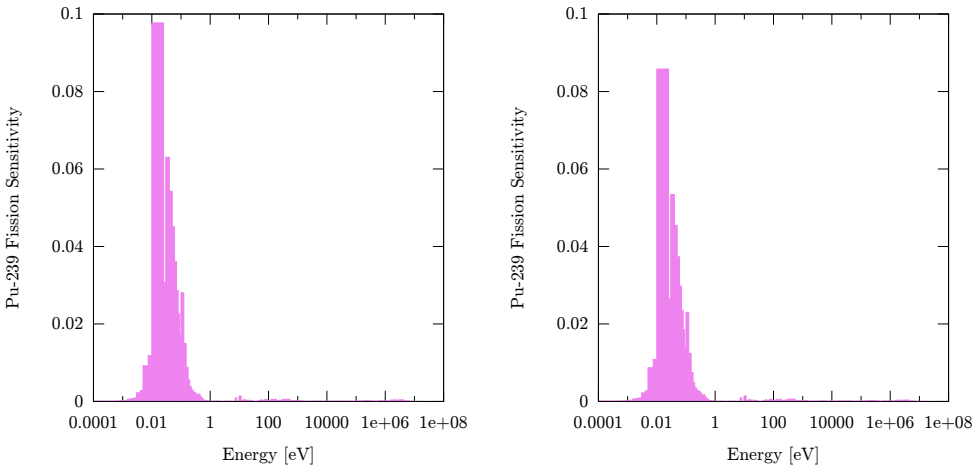

(a) Air cooled

(b) D_2O cooled

Figure 5.14: Pu-239 Fission Sensitivity Spectrum with Coolant Type

Using air as the coolant (i.e. voiding the channel) the sensitivities tend to be higher. This may seem counter intuitive because air is a poorer moderator than D_2O. However, in order to maintain criticality in the core with air as coolant, the moderator height must be increased. The result of this is that overall there is more D_2O in the core, despite being cooled with air. This could result in a more thermalized neutron spectrum and may be the reason for the increased sensitivity. This illustrates how there are multiple factors contributing to the sensitivity changes in the test reactor.

Step 6: Based on the results of the previous steps, begin iteratively accumulating a set of experiments that achieves an adequate completeness

From the above results, the effects of modifications to certain aspects of the experiments can be examined. Having done so, the next step is to accumulate a complete set of experiments that together achieve a high completeness, while also meeting the safety limits of the test reactor. This is done by iteratively examining the sensitivity coverage and modifying the experiments accordingly. Note that when performing this step, it is generally necessary to repeat the previous steps (for example, a new fuel choice may be deemed necessary).

5.3.2.1 Final Set

For the final set of experiments made to achieve a high completeness for all of the power reactors, three fuel types were used: the (Pu, Th)O_2 fuel used in the CANDU-

type reactors, and two variations of the SCWR fuel. The SCWR fuel variations used plutonium fuel with the same isotopic content as that of the SCWR fuel. However, rather than 13 wt% plutonium, these fuels had 2.5 wt% and 7.0 wt% plutonium. The composition of each of the fuel types chosen are listed in the table below. The density of Fuel 1 is 9.46 g/cm^3, while the density of Fuel 2 and Fuel 3 is 9.88 g/cm^3

Table 5.19: Experiment Set Fuel Compositions

	Fuel 1	Fuel 2	Fuel 3
Nuclide	wt%	wt%	wt%
Th-232	86.051	85.682	81.727
Pu-238	0.002	0.061	0.169
Pu-239	1.181	1.146	3.209
Pu-240	0.303	0.506	1.418
Pu-241	0.045	0.336	0.941
Pu-242	0.008	0.157	0.438
O-16	12.410	12.113	12.097

The reason fuel types with the same plutonium as the SCWR but at a lower weight percent were used in the experiments was to allow for the safety limits to be met. With a high plutonium content, criticality in the ZED-2 reactor core is reached at a very low moderator height. This means that the limit concerning the minimum mass of submerged heavy elements cannot be met.

The reason two fuel types with SCWR plutonium were used was to allow for both the low energy and the high energy Pu-241 sensitivities to be covered (both of which are large for the SCWR). Using only the 2.5 wt% plutonium fuel, the high energy sensitivities are not covered, and using only the 7 wt% plutonium, the low energy sensitivities cannot be covered while meeting the submerged fuel mass limit.

The lattice geometry arrangements used for these ZED-2 reactor experiment simulations are shown in the figure below. Note that the lattice pitch used was varied in the experiments.

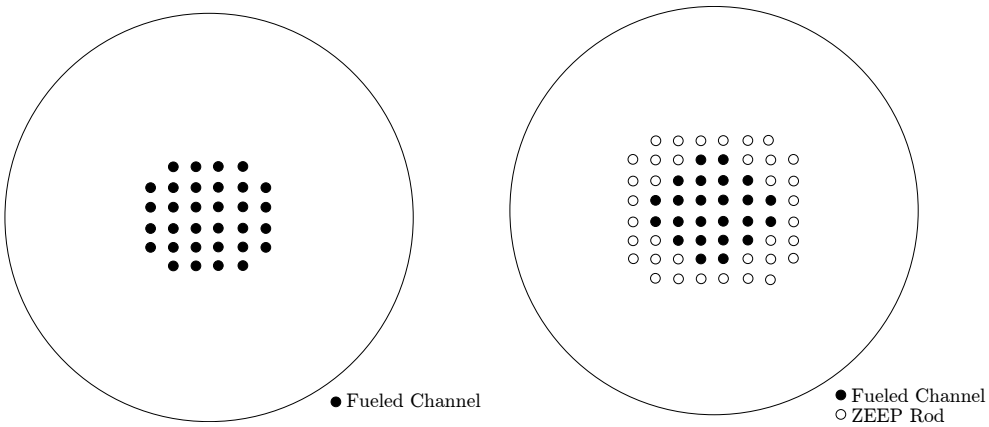

(a) Geometry 1 (b) Geometry 2

Figure 5.15: ZED-2 Simulated Benchmark Set Geometries

The simulation parameters used for the final set are the same as those indicated in Table 5.3.

A description of the final set of potential experiments (Exp # 1 through 6) chosen is provided in Table 5.20, where the fuel type refers to those listed in Table 5.19, the geometry refers to those shown in Figure 5.15, and H_c is the critical height found from the simulations. Note that it was assumed that the number of experiments required with a sensitivity that covers the application's sensitivity was 1 ($nixlim = 0$) and that the experiment cross section must be at least 90% of that of the application to be considered covered ($senfac = 0.9$). Along with the experiment specifications, the importance of each experiment as it pertains to the large cross section sensitivity coverage is also listed.

Table 5.20: Final Set of Potential Test Experiments

Exp #	Fuel Type	Fuelled Channels	Coolant	Pitch	H_c	Importance
Exp 1	Fuel 1	32 (Geometry 1)	H_2O	14.0 cm	176 cm	Pu-239 fission low energy
Exp 2	Fuel 1	32 (Geometry 1)	D_2O	38.0 cm	175 cm	Pu-239 fission high energy
Exp 3	Fuel 1	32 (Geometry 1)	Air	38.0 cm	219 cm	Th-232 capture
Exp 4	Fuel 2	32 (Geometry 1)	H_2O	38.0 cm	196 cm	Pu-241 fission low energy
Exp 5	Fuel 2	24 and 36 ZEEP (Geometry 2)	Air	20.0 cm	150 cm	Pu-241 fission low energy
Exp 6	Fuel 3	32 (Geometry 1)	D_2O	13.0 cm	200 cm	Pu-241 fission high energy

These simulated experiments were chosen primarily to be an example of an experiment set that meets the completeness requirements for a GLLS analysis. Considerations of the difficulty in obtaining particular materials and the expense of the experiments were not examined, nor were particular operating concerns. In an effort to ensure the experiments used in this study are feasible, all of the experiments above have been chosen such that the safety limits of the ZED-2 reactor have been met as closely as possible. However, particulars such as the uncertainty in the lattice pitch of experiments, and the potential effect this would have on the experiment compliance with safety limits were not considered. In particular, for experiments with a small lattice pitch, a change of 2.0 cm can result in a failure to meet the safety limits.

A difficulty with ensuring the safety limits were met was in the calculation of the actual core power at an indicated power of 200 W. In order to determine the actual core power, the locations and sizes of the ion chambers are required, and these were not known here. Thus, the surface flux was estimated using a large region in the center of the core at the graphite reflector, and the total area was estimated as 80 cm^2. This was chosen to ensure the existing experiments available [1] were within the power limit (compliance with the LCO's was assumed). The following formula was then used:

$$\text{Power} = \frac{\text{Fission Power}}{\text{Ion Chamber Surface Flux}} \left(4.554 \times 10^7 \frac{n}{cm^2 \cdot s}\right) \left(\frac{200W}{50W}\right) \tag{5.2}$$

Here, $4.554 \times 10^7 n/cm^2 \cdot s$ is the measured flux at the detector locations for an indicated power of 50 W [53]. If these experiments were to be performed, recalculating the actual core power with more accurate information would be required.

The level coefficient of reactivity (LCR) calculated here was determined by taking the change in the reactivity with a ΔH=2 cm increase in moderator height:

$$LCR = \frac{\Delta\rho}{\Delta H} \tag{5.3}$$

This value was then corrected using a Taylor expansion to the first order (this correction is used at the ZED-2 facility) [53]:

$$LCR_c = LCR\left(1 + 3 \times \frac{H_m - H_c}{H_m + H_c} + \frac{k_m - k_c}{k_m + k_c}\right) \tag{5.4}$$

Where H_c and k_c represent the critical moderator height and H_m and k_m represent the moderator height and k_{eff} for the case where the moderator height was changed.

The prompt generation time listed is actually the lifespan to fission. It has been used as an estimate of the prompt generation time. In general this is not a good approximation [54] and therefore the validity of the neutron generation time should be further analyzed.

A final note is that here it was assumed that the submerged fuel mass limit was still sufficient when two different fuel types are used. This assumption would need to be verified if the experiments were being performed.

The tables below list the values of the LCO's for each of the experiments chosen. The experiments were simulated such that they are within approximately 2.5 mk of criticality (i.e. between 1.025 and 1.0). This was an assumed computational bias on the ZED-2 simulations based on work by T. Zhu [34]. No absorber rods were used in these experiments so the absorber worth limit was not necessary.

Table 5.21: Experiment LCO acceptability (Part A)

	Experiment 1	Experiment 2	Experiment 3
H_c (cm)	176	175	219
P_A (W)	612±4	449±1	613±3
t_{gen} (ms)	0.3544±0.0007	1.4489±0.0004	1.4636±0.0005
LCR_c (mk/cm)	0.4±0.1	1.0±0.1	0.8±0.1
M_f (kg)	1768	1760	2244

Table 5.22: Experiment LCO acceptability (Part B)

	Experiment 4	Experiment 5	Experiment 6
H_c (cm)	196	150	200
P_A (W)	580±3	362±1	421±1
t_{gen} (ms)	1.3535±0.0007	0.7317±0.0006	0.737±0.001
LCR_c (mk/cm)	0.6±0.1	0.9±0.1	0.2±0.1
M_f (kg)	2087	1936	2133

The uncertainties listed above assume that the critical height (and therefore the submerged mass) are accurate and have no uncertainty. The actual critical height would depend on the bias of the experiment, which is currently unknown. However, in these experiments the main limiting value was found to be the mass of submerged fuel, and keeping the moderator height high enough for an acceptable M_f was more of a concern than the moderator height being too high. Using the calculated LCR_c value, a simple calculation finds that all of the experiments remain just over the minimum submerged fuel height when the multiplication factor is equal to or greater than 1.0. Thus, as long as the bias is positive (which was assumed based on experiments analyzed by T. Zhu [34]) these experiments have an acceptable submerged fuel height.

The uncertainty in P_A, t_{gen}, and LCR_c are statistical uncertainties based on the simulation with the listed moderator height. These values are calculated using the standard error formula and the standard deviation values output by the KENO V.a code module.

To test the accuracy of the sensitivities calculated using TSUNAMI, a direct perturbation study was performed for each experiment (this is recommended when using experiments to perform a bias calculation [52]). The direct perturbation verification is shown in the tables below.

Table 5.23: Sensitivity Verification for Experiment Set (Part A)

	Experiment 1		Experiment 2	
Reaction	DP	TSUNAMI	DP	TSUNAMI
Pu-239 total	0.343 ± 0.003	0.3470 ± 0.0004	0.215 ± 0.003	0.2202 ± 0.0007
Pu-241 total	0.022 ± 0.003	0.02042 ± 0.00002	0.098 ± 0.003	0.1019 ± 0.0003
Th-232 total	-0.292 ± 0.003	-0.2892 ± 0.0003	-0.230 ± 0.003	-0.2237 ± 0.0006
H-2 total	0.068 ± 0.004	0.1 ± 0.2	0.061 ± 0.004	0.1 ± 0.3

Table 5.24: Sensitivity Verification for Experiment Set (Part B)

	Experiment 3		Experiment 4	
Reaction	DP	TSUNAMI	DP	TSUNAMI
Pu-239 total	0.343 ± 0.003	0.3470 ± 0.0004	0.215 ± 0.003	0.2202 ± 0.0007
Pu-241 total	0.022 ± 0.003	0.02042 ± 0.00002	0.098 ± 0.003	0.1019 ± 0.0003
Th-232 total	-0.292 ± 0.003	-0.2892 ± 0.0003	-0.230 ± 0.003	-0.2237 ± 0.0006
H-2 total	0.068 ± 0.004	0.1 ± 0.2	0.061 ± 0.004	0.1 ± 0.3

Table 5.25: Sensitivity Verification for Experiment Set (Part C)

	Experiment 5		Experiment 6	
Reaction	DP	TSUNAMI	DP	TSUNAMI
Pu-239 total	0.152 ± 0.003	0.1615 ± 0.0002	0.137 ± 0.003	0.1369 ± 0.0005
Pu-241 total	0.079 ± 0.003	0.0814 ± 0.0001	0.090 ± 0.003	0.1011 ± 0.0002
Th-232 total	-0.192 ± 0.004	-0.1952 ± 0.0002	-0.201 ± 0.004	-0.1974 ± 0.0006
H-2 total	0.217 ± 0.003	0.20 ± 0.09	0.184 ± 0.003	0.2 ± 0.8

The agreement between the TSUNAMI and direct perturbation sensitivities for the experiments was similar to that found for the power reactor simulations. That is, the sensitivities found using TSUNAMI were either equal within one standard deviation to the sensitivities found using the direct perturbation technique, or lie slightly outside of the range of the standard deviation. The largest discrepancy outside of the standard deviations was 7% difference in the Pu-241 cross section sensitivity of Experiment 6. Because the experiments are smaller, it may have been expected that the experiments would exhibit better agreement than the power reactors. However, for the power reactor calculations multiple bundles/channel segments (6 for the CANDU-type reactors and 15 for the SCWR) were used so as to achieve different burnups values. Thus, the power reactor flux tallies were taken over multiple bundles/channel segments, which has a similar effect to introducing a flux mesh. For the ZED-2 simulations all of the bundles were simulated as repeated units and the flux in the bundles was calculated by averaging the tally from each bundle. This means that there was poor spatial refinement in the flux solution. It is therefore likely that the introduction of flux meshing to the experiment simulations would increase the agreement of the sensitivities. In addition, in some cases the standard deviation in the H-2 total sensitivity found for the experiments was larger than the value itself. Flux meshing would also be beneficial in decreasing this statistical uncertainty. This was not performed here due to computation time constraints.

Using these experiments, the following completeness values were achieved for each of the applications analyzed here. The uncertainty listed is the standard deviation of the completeness, calculated using the standard error formula.

Table 5.26: Completeness Results

Application	Completeness
CANDU (37-element)	0.76 ± 0.01
CANDU (43-element)	0.75 ± 0.01
SCWR (BOC)	0.77 ± 0.03
SCWR (EOC)	0.70 ± 0.02

The completeness values for the CANDU-type reactors and the SCWR reached the goal of 0.7-0.8 using these experiments. The value of the SCWR (EOC) completeness

was significantly lower than that of the SCWR (BOC). This was because there is a large sensitivity to U-233, which was not included in the experiment fuel used here.

The figures below indicate the coverage for each power reactor of some the largest sensitivities (specifically, Pu-239 fission, Pu-239 $\bar{\nu}$, Pu-241 fission, and Pu-241 $\bar{\nu}$). In these figures, the combined coverage over the energy spectrum of all of the experiments together is shown. The application sensitivities have been outlined so in cases of full coverage of a particular sensitivity, it is clear how much higher the experiment sensitivities are.

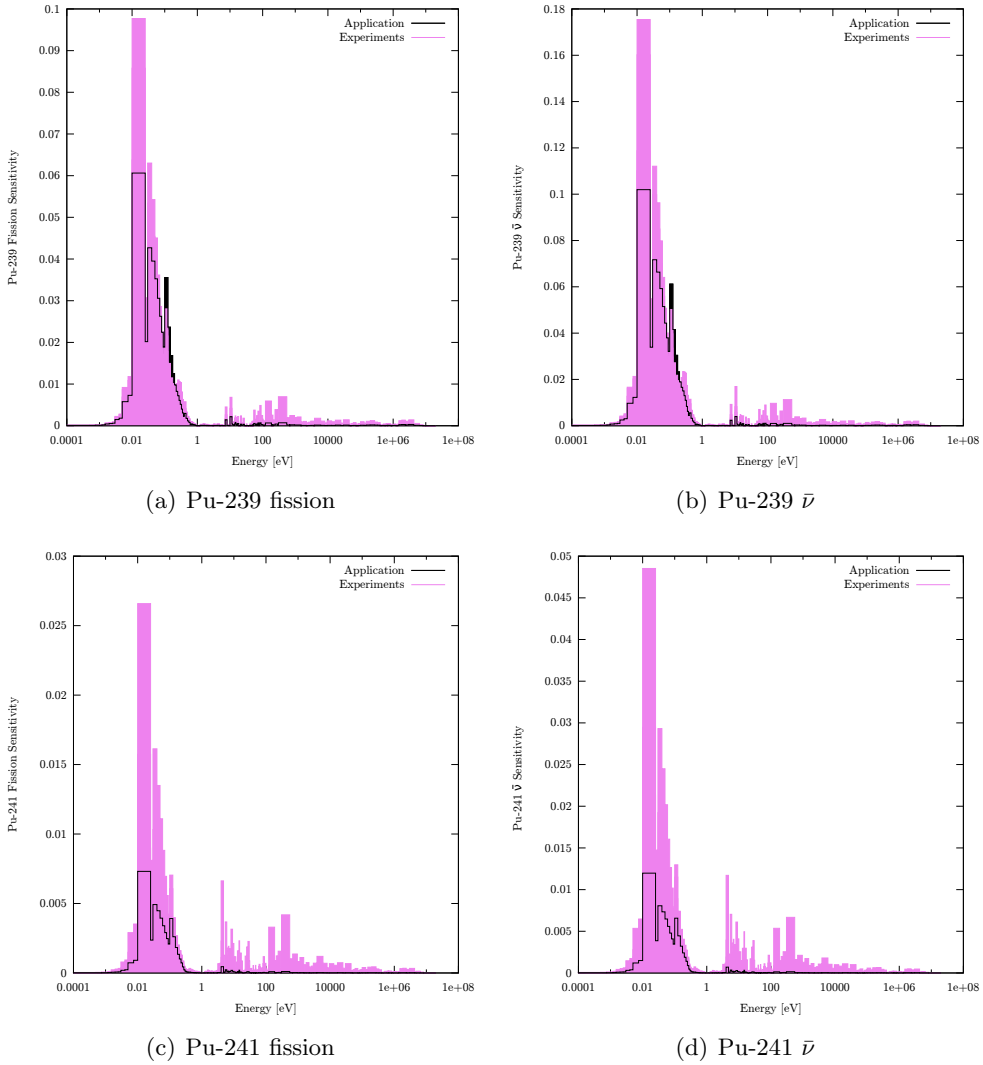

(a) Pu-239 fission

(b) Pu-239 $\bar{\nu}$

(c) Pu-241 fission

(d) Pu-241 $\bar{\nu}$

Figure 5.16: Sensitivity Spectrum Coverage for 37-Element CANDU Cross Sections

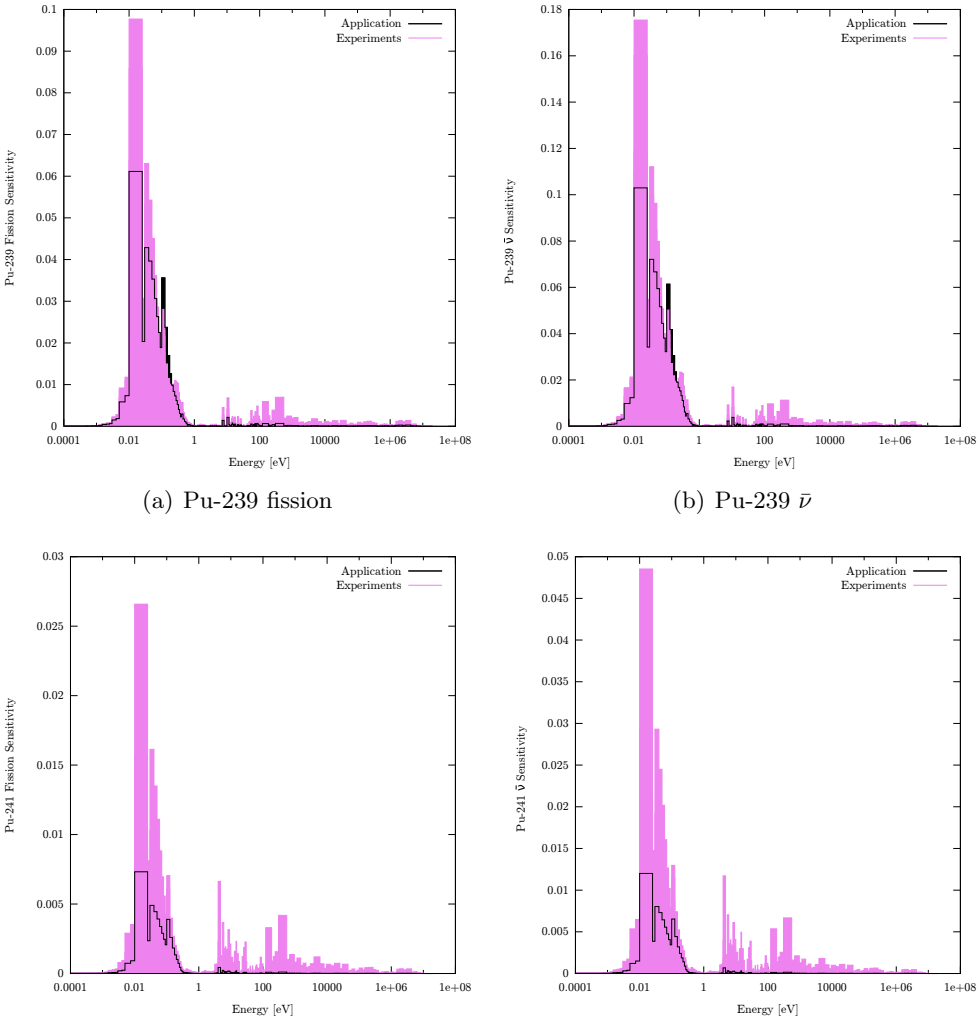

(a) Pu-239 fission

(b) Pu-239 $\bar{\nu}$

(c) Pu-241 fission

(d) Pu-241 $\bar{\nu}$

Figure 5.17: Sensitivity Spectrum Coverage for 43-Element CANDU Cross Sections

The results show that for the CANDU-type (Pu,Th)O_2 fuelled reactors, the experiment set simulated provides full coverage of the Pu-241 cross section sensitivities listed. The Pu-239 cross sections (which are the largest cross sections for this application) are covered in the low energy and high energy ranges, however for energies near approximately 0.1 eV, there is a large uncovered region.

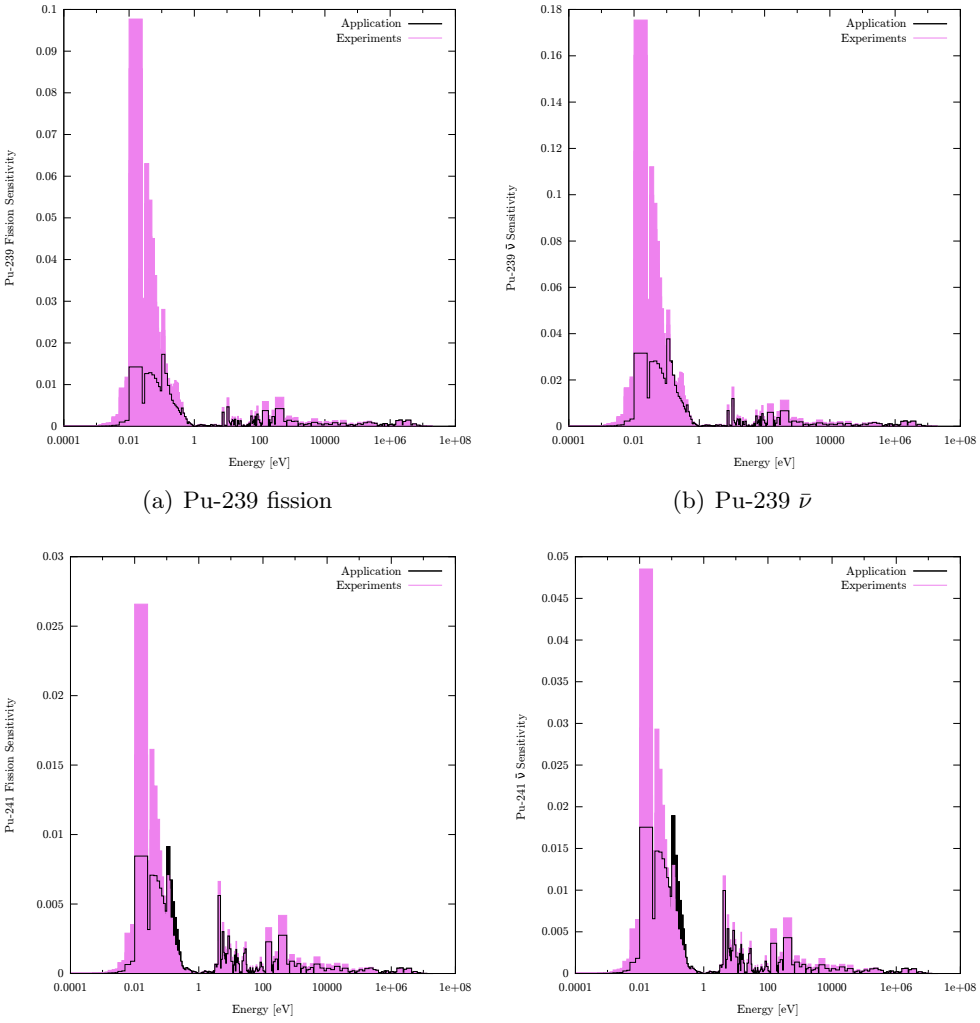

(a) Pu-239 fission

(b) Pu-239 $\bar{\nu}$

(c) Pu-241 fission

(d) Pu-241 $\bar{\nu}$

Figure 5.18: Sensitivity Spectrum Coverage for SCWR (BOC) Cross Sections

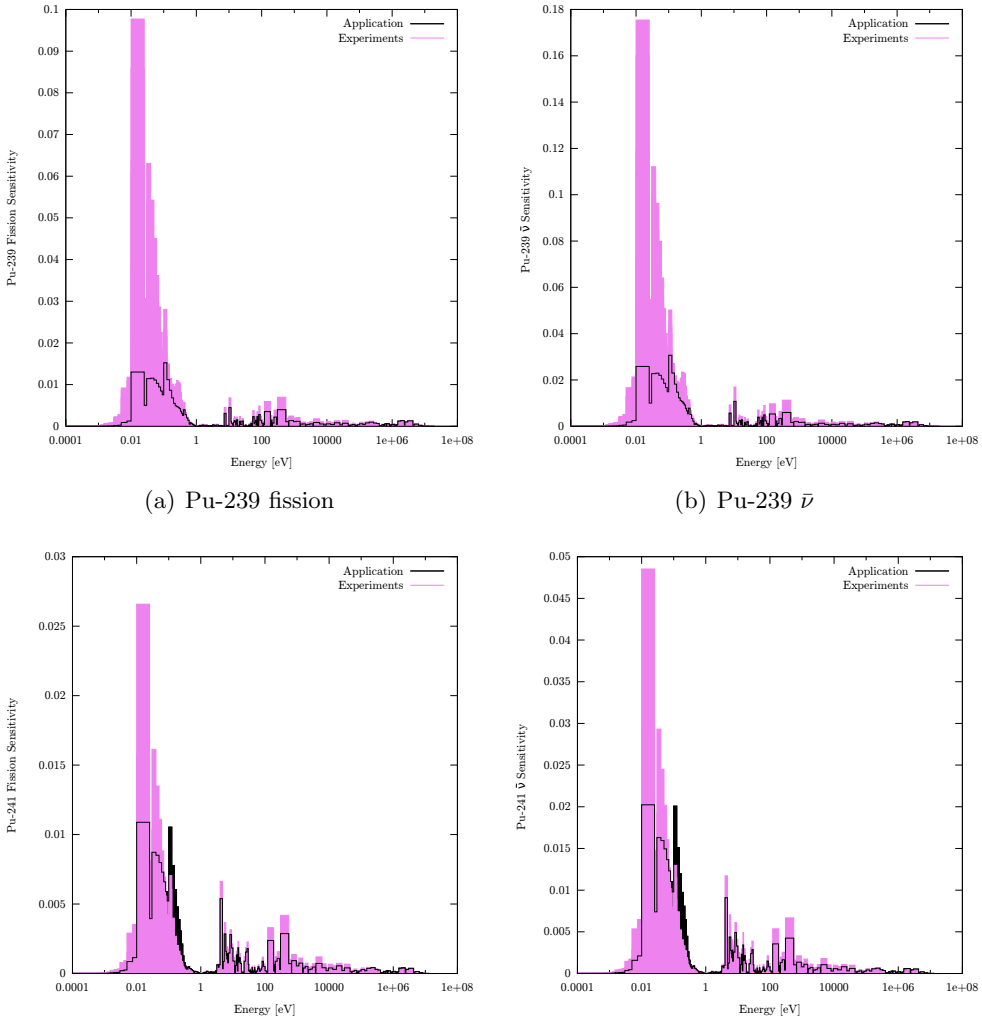

(a) Pu-239 fission

(b) Pu-239 $\bar{\nu}$

(c) Pu-241 fission

(d) Pu-241 $\bar{\nu}$

Figure 5.19: Sensitivity Spectrum Coverage for SCWR (EOC) Cross Sections

For both the BOC and EOC SCWR, the Pu-239 cross sections sensitivities shown here have been fully covered whereas the Pu-241 sensitivities (which were much larger for the SCWR than for the CANDU-type reactors) are not fully covered. Again, the uncovered sensitivities lie at energies of approximately 0.1 eV.

For subsequent additions to the potential experiment set analyzed here, both the CANDU and SCWR results suggest that it would be useful to focus on coverage of sensitivities at energies close to 0.1 eV. To do so, an attempt could be made to modify the lattice arrangement of the fuel types used here in order to increase the number of neutrons in the core that have an energy in this range. By increasing the number of neutrons in that energy range, the sensitivity to changes in cross sections

at that energy would also tend to increase.

The following tables list the sum over all energies of the uncovered region integrated sensitivities for the reactions with the largest uncovered sensitivities for each power reactor. This indicates the nuclide-reaction pairs that have the largest effect on the remaining uncovered sensitivities in the completeness calculation for this set of experiments.

The results find that in addition to the plutonium reactions, there are also large uncovered sensitivities from Th-232, U-233, Xe-135, Zr-91, and others. To increase the coverage of the Th-232 and Zr-91 cross sections, once again an analysis of the sensitivity energy spectrum coverage could be performed, and the lattice modified to cover uncovered sensitivities. Coverage of the U-233 and Xe-135 cross sections would require the introduction of these nuclides to the experiments.

Table 5.27: 37-Element CANDU with (Th,Pu)O_2 Integrated Uncovered Sensitivities

Reaction	Integrated Uncovered Sensitivity
Pu-239 $\bar{\nu}$	0.156459 ± 0.000006
Pu-239 fission	0.08866 ± 0.00007
Th-232 (n,γ)	-0.08163 ± 0.00005
U-233 $\bar{\nu}$	0.068434 ± 0.000002
Pu-239 (n,γ)	-0.03872 ± 0.00003
U-233 fission	0.03788 ± 0.00002
Xe-135 (n,γ)	-0.02575 ± 0.00001
H-2 elastic	-0.025 ± 0.007
Pu-240 (n,γ)	-0.01653 ± 0.00001
Zr-91 (n,γ)	-0.009280 ± 0.000005

Table 5.28: 43-Element CANDU with (Th,Pu)O_2 Integrated Uncovered Sensitivities

Reaction	Integrated Uncovered Sensitivity
Pu-239 $\bar{\nu}$	0.156820 ± 0.000007
Pu-239 fission	0.08889 ± 0.00007
Th-232 (n,γ)	-0.08201 ± 0.00005
U-233 $\bar{\nu}$	0.067479 ± 0.000002
Pu-239 (n,γ)	-0.03880 ± 0.00003
U-233 fission	0.03732 ± 0.00002
Xe-135 (n,γ)	-0.02585 ± 0.00001
H-2 elastic	-0.024 ± 0.005
Pu-240 (n,γ)	-0.01684 ± 0.00001
Zr-91 (n,γ)	-0.009498 ± 0.000005

Table 5.29: SCWR (BOC) Integrated Uncovered Sensitivities

Reaction	Integrated Uncovered Sensitivity
Pu-241 $\bar{\nu}$	0.091887 ± 0.000001
U-233 $\bar{\nu}$	0.0611389 ± 0.0000004
Pu-241 fission	0.04076 ± 0.00007
Pu-240 (n,γ)	-0.03373 ± 0.00004
U-233 fission	0.03108 ± 0.00003
Zr-91 (n,γ)	-0.02030 ± 0.00002
Pu-241 (n,γ)	-0.01806 ± 0.00002
Pu-239 $\bar{\nu}$	0.0174466 ± 0.0000002
Pu-239 (n,γ)	-0.01664 ± 0.00004
Fe-56 (n,γ)	-0.01602 ± 0.00001

Table 5.30: SCWR (EOC) Integrated Uncovered Sensitivities

Reaction	Integrated Uncovered Sensitivity
U-233 $\bar{\nu}$	0.134652 ± 0.000001
Pu-241 $\bar{\nu}$	0.103497 ± 0.00002
U-233 fission	0.07146 ± 0.00005
Pu-241 fission	0.05417 ± 0.00008
Pu-240 (n,γ)	-0.04425 ± 0.00005
Zr-91 (n,γ)	-0.02031 ± 0.00002
Pu-241 (n,γ)	-0.01937 ± 0.00003
Fe-56 (n,γ)	-0.01793 ± 0.00002
Xe-135 (n,γ)	-0.01468 ± 0.00002
Am-241 (n,γ)	-0.013499 ± 0.000009

Although a high similarity (c_k) is not required, it is still a useful parameter. The reason for this is as follows: in the completeness study performed, it was assumed that having only one experiment that covered a particular sensitivity was sufficient. This means that if this cross section had a very small effect in all of the other experiments, the cross section adjustment would be based primarily on one experiment. To prevent this, experiments can be chosen such that each sensitivity is covered by multiple experiments. However, for the current study it was found that the experiments had a very high similarity (correlation of cross section uncertainties) both to each other and to the applications. The similarity between experiments was >0.8 for all cases and the similarity between the experiments and the applications was >0.75. This indicates that, while not all of the experiments cover all of the sensitivities, all of the experiments do tend to use the same materials between them, and to use materials important to the power reactor uncertainty. This means that a change in a particular cross section will have an effect on multiple experiments. This makes the use of only one experiment required to cover each sensitivity reasonable for the current study as the purpose of this study is to determine how to find a set with a

high completeness, not to build a large database of experiments.

The similarity between the experiments are listed in the table below.

Table 5.31: Similarity Between Experiments

Exp #	1	2	3	4	5	6
1	———	0.97 ± 0.03	0.89 ± 0.02	0.96 ± 0.03	0.82 ± 0.05	0.9 ± 0.1
2	0.97 ± 0.03	———	0.92 ± 0.04	1.0 ± 0.1	0.9 ± 0.1	0.8 ± 0.2
3	0.89 ± 0.02	0.92 ± 0.04	———	0.9 ± 0.1	0.92 ± 0.04	0.9 ± 0.2
4	0.96 ± 0.03	1.0 ± 0.1	0.9 ± 0.1	———	0.9 ± 0.1	0.9 ± 0.2
5	0.82 ± 0.05	0.9 ± 0.1	0.92 ± 0.04	0.9 ± 0.1	———	0.9 ± 0.3
6	0.9 ± 0.1	0.8 ± 0.2	0.9 ± 0.2	0.9 ± 0.2	0.9 ± 0.3	———

The similarity between the experiments and the applications are listed in the table below.

Table 5.32: Similarity Between Experiments and Applications

Exp #	CANDU (37)	CANDU (43)	SCWR (BOC)	SCWR (EOC)
1	0.88 ± 0.03	0.88 ± 0.03	0.80 ± 0.04	0.76 ± 0.04
2	0.89 ± 0.03	0.89 ± 0.04	0.79 ± 0.05	0.76 ± 0.05
3	0.97 ± 0.02	0.97 ± 0.02	0.85 ± 0.04	0.81 ± 0.04
4	0.92 ± 0.06	0.92 ± 0.06	0.85 ± 0.09	0.82 ± 0.09
5	0.90 ± 0.02	0.89 ± 0.02	0.88 ± 0.04	0.86 ± 0.04
6	0.8 ± 0.2	0.8 ± 0.2	0.9 ± 0.3	0.9 ± 0.3

Here the value of an experiment set to a GLLS adjustment was mainly represented by the completeness factor. However, there are some considerations that are not addressed in the completeness factor that may affect the legitimacy of applying a particular set to a GLLS adjustment for an application.

As has been mentioned before, the completeness parameter that is calculated here is based solely on the relative sensitivity values. Cross section nuclide/reaction/energy sensitivities are weighted in the completeness formula such that larger sensitivities have a greater effect on the calculated completeness value. This is useful because it ensures cross section values that have high sensitivities in the application are more important to the adjustment procedure. However, another consideration in the cross section adjustment is the uncertainty of each individual cross section. As was found in Section 5.2.1, a large cross section uncertainty range can mean that cross sections with small sensitivities can result in a large uncertainty on the multiplication factor. The GLLS method adjusts the cross sections such that they remain within their uncertainty range so as to minimize χ^2. Thus, if an application has a cross section with a small relative sensitivity and a large relative uncertainty and this sensitivity is not covered by the experiments, then, despite being small, its effect may still be

underestimated and it may be over-adjusted.

For this reason, it may be useful to weight the sensitivities in the completeness formula by their relative cross section variance values for the specific nuclide/reaction/energy. This would ensure sensitivity coverage of cross sections with a relatively low sensitivity but high uncertainty as well as those with a high sensitivity. The covariances between the cross sections further complicate the determination of the cross section adjustments and the consideration of their weight in the adjustment procedure and the potential effect on the validity of the completeness factor has been left for future study.

A second factor that is not considered in the completeness but that may affect the accuracy of the bias calculation is as follows. If all of the experiments being used in the adjustment procedure have very high sensitivities to particular cross sections (higher than in the application) then this may skew the adjustment of all of the cross sections. This is because in a GLLS adjustment, adjusting data with a high sensitivity means that the increase in χ^2 is less than if data with a low sensitivity is adjusted. If all of the experiments are very sensitive to particular shared cross sections then these may be given far more weight in the adjustment procedure while the cross sections important to the application are given little consideration, despite being 'covered' by the completeness factor.

An implication of observed limitations above is that the completeness factor can be used as a guideline for finding an applicable experiment set, however other factors should be considered before deeming a set appropriate to a bias calculation using the GLLS method. A GLLS method is a complex procedure and has a number of conflicting effects that are ignored if only the completeness factor is used. A more mathematical analysis of the qualitative considerations listed above has not been performed here, but may be useful for future study.

Chapter 6

Summary and Conclusions

In order to perform a validation study of a power reactor simulation, it is necessary to use test reactor experiments to predict the simulation bias. When choosing test reactor experiments for this purpose it is important to ensure that the experiments are applicable to the power reactor. The goal of the work performed here was therefore to analyze a method for designing a set of applicable experiments that could be used in a bias calculation procedure to validate a simulation.

To accurately design a relevant set of experiments it is first necessary to develop models of the power reactors of interest. Here, the power reactor designs studied were CANDU-type reactors using a 37-element bundle and a 43-element bundle, both containing (Th,Pu)O_2 fuel, and a Canadian supercritical water reactor design in which there are 78-element fuel assemblies containing (Th,Pu)O_2 fuel.

6.1 Core Models

To perform a similarity study, core models representative of the state of the reactors after a long period of time were created for the Monte Carlo code module KENO V.a. These models could then be used in the sensitivity and uncertainty analysis TSUNAMI code modules. To develop core models for use in KENO V.a, results from the transport code DRAGON and the diffusion code DONJON were combined to determine the composition of the core. Due to the computational intensity of large scale simulations using the Monte Carlo method, quarter core models were created and the burnup states were lumped into a set number of groups.

Simulations performed in DRAGON were used to compare the agreement between the KENO V.a and DRAGON codes. It was found that for the CANDU-type reactor designs the discrepancy between the KENO V.a and DRAGON results for both the multiplication factor and the coolant void reactivity results were small (up to approximately 5 mk difference in the multiplication factor and 2 mk in the CVR). For the SCWR, there was a larger discrepancy between the results (up to approximately 10 mk difference in the multiplication factor and 5 mk in the void reactivity). It is hypothesized that this may be a result of self-shielding methods used by the

various codes. In addition, the linear element ratings of each of the power reactor designs were studied. It was found that the 43-element bundle has a lower maximum LER than the 37-element bundle. Because other results with the two bundle types are very similar, this decrease in the maximum LER provides a reason to use this bundle type over the more traditional 37-element bundle.

6.2 Similarity Study

A similarity study was performed in which a set of experiments was designed for the purpose of effectively representing the power reactor designs described above for the purposes of a multiplication factor bias calculation. The experiment set was designed for the ZED-2 reactor at Chalk River laboratories. The metric used to indicate the adequacy of an experiment set was a parameter called the completeness which represents how well the application sensitivities are being covered by a set of experiments. A high completeness (0.7-0.8) is an indication that a set of experiments has an adequate cross section coverage to be used in a GLLS adjustment.

To assist in the design of an appropriate set of experiments, the following procedure was developed: (1) Examine largest application sensitivities (2) Choose possible fuel types based on sensitivities and the application's fuel (3) Choose basic lattice arrangement and geometry (4) Modify the lattice pitch and fuelled channels to examine effect on sensitivity spectrum coverage (5) Modify coolant type to examine effect on sensitivity spectrum coverage (6) Based on the results of the previous steps, begin iteratively accumulating a set of experiments that achieves an adequate completeness.

Ultimately, the purpose of the above steps is to analyze the changes in the sensitivity profile that result from changes in experimental design parameters (i.e. affecting the neutron spectrum or critical height of the core). These are the major contributors to the sensitivity magnitudes.

Using this procedure a potential set of experiments that is within the ZED-2 safety limits was designed. It was found that for the CANDU-type reactors and the BOC and EOC SCWR this set of experiments was adequate to ensure the completeness is above the 0.7 threshold. In addition, between the experiments and the applications there is a high similarity index c_k. This suggests that using a smaller number of experiments for a bias calculation may be acceptable because the largest uncertainty contributors are common to the experiments and the applications. However, adding further experiments to the set would be useful, as would further analysis of the validity of the completeness factor.

The work performed here focused on the development of experiment sets for the calculation of the bias in the multiplication factor of a power reactor design. How-

ever, the same set of guidelines could be applied to the determination of experiment sets for the calculation of the bias in a different integral parameter, or for use in criticality safety studies.

Chapter 7

Future Work

The current work leaves several areas of work for the future. The first, and most obvious, future goal would be to perform experiments such as those designed here so that they can be used in a bias calculation procedure. If this were to be attempted, considerations of the cost and availability of the fuel materials used in the current study would likely need to be re-examined, and more specific licencing and safety limitations would need to be analyzed. This could result in a re-working of the chosen experiments, however the same process as that used here could be applied to the benchmark experiment set design.

Alternatively, experiments that have already been performed could be accumulated in an attempt to achieve a high completeness. The difficulty here would be in obtaining the necessary experimental data, and ensuring that the experiments have an adequate similarity or that an adequate number of experiments are used.

If an adequate set of experiments was accumulated, the generalized linear least squares adjustment procedure that was described here but could not be executed could be performed. This would require that the uncertainties in the experiments performed are well documented.

In addition, several factors involved in the simulations of the power reactors could be improved. First, to develop more accurate power reactor models, reactivity devices could be included in the various designs. In addition, the SCWR design used in the current study is for the Canadian SCWR that is currently in the conceptual design stage. Since the completion of the simulations performed here, the fuel assembly design has changed, so this could be re-modelled to see if the acceptable experiment set changes.

There are also concerns with the SCWR lattice cell simulations that need to be addressed. The first is the discrepancies in the multiplication factor results between the various reactor physics codes used. It was found that between the DRAGON and KENO versions used here there is a significant discrepancy, particularly for the voided cases. Benchmark simulations have been performed, and continue to be performed, to analyze these code discrepancies [38]. A second concern with the SCWR is the choice of the energy group boundaries for the cross section condensation and homogenization. An analysis of which energy boundaries to choose would be bene-

ficial in increasing the accuracy of the DONJON diffusion calculation.

To improve upon the Monte Carlo simulations, more burnup bins could be applied. In addition, flux meshing could be applied to increase the accuracy of the sensitivity calculations. Here computation time and memory were limiting factors for these improvements.

Finally, additions could be made to the experiment set developed here that increase the completeness and provide further coverage of each sensitivity. In addition, a study concerning the limiting completeness value for adequate set completeness (which here was assumed to be 0.7) and the potential benefits of ensuring the experiments have a high similarity index c_k would be beneficial, as would further analysis concerning the limitations when using the completeness factor to develop a set of experiments for a bias calculation.

Bibliography

[1] R. T. Jones, "Experiments performed in ZED-2 in support of the irradiation of (Th,Pu)O2 fuel (BDL-422) in NRU," Tech. Rep. AECL-7918, Atomic Energy of Canada Limited, January 1984.

[2] K. Kok, *Nuclear engineering handbook*. USA: Taylor and Francis Group, LLC, 2009.

[3] International Atomic Energy Agency, "Thorium fuel cycle - potential benefits and challenges," Tech. Rep. IAEA-TECDOC-1450, May 2005.

[4] J. Kang and F. von Hippel, "U-232 and the proliferation-resistance of u-233 in spent fuel," *Science & Global Security*, vol. 9, pp. 1–32, 2001.

[5] J. Whitlock, "The evolution of CANDU fuel cycles and their potential contribution to world peace," in *International Youth Nuclear Congress 2000*, (Bratislava, Slovakia), April 2000.

[6] Z. Yang, "Experiment of heat transfer to supercritical water flowing in vertical annular channels," *Journal of Heat Transfer*, vol. 135, 2013.

[7] H. Khartabil, "SCWR: Overview," in *GIF Symposium*, (Paris, France), September 2009.

[8] R. P. Corcuera, "Covariance matrices in evaluated nuclear data," Tech. Rep. IEAv/NT-007/83, Aerospace Technical Centre Institute of Advanced Studies, 1983.

[9] G. M. A. Hébert and R. Roy, "A user guide for DRAGON 3.06," Tech. Rep. IGE-174 Rev. 7, École Polytechnique de Montréal, March 2008.

[10] T. Kulikowska, "An introduction to the neutron transport phenomena," in *Workshop on nuclear data and nuclear reactors: physics, design and safety*, (Trieste, Italy), April 2000.

[11] J. J. Duderstadt and L. J. Hamilton, *Nuclear reactor analysis*. Canada: John Wiley & Sons, 1976.

[12] G. Marleau, "DRAGON theory manual part 1: collision probability calculations," Tech. Rep. IGE-236 Revision 1, École Polytechnique de Montréal, October 2001.

[13] R. Matavosian, *Complex problems arising in the collision probability theory for neutron transport*. PhD thesis, University of Texas, 2007.

[14] S. Dabiran, "Modeling and sensitivity/uncertainty analyses of ZED-2 benchmark experiment using DRAGON, DONJON & SUSD3D," Master's thesis, McMaster University, 2011.

[15] A. Hébert, *Applied reactor physics*, ch. 4. Canada: Presses Internationales Polytechnique, 2009.

[16] National Nuclear Data Center, "Evaluated nuclear data file ENDF/B-VII.0." `http://www.nndc.bnl.gov/`, December 2006.

[17] A. Salmon, *The nuclear reactor*, ch. 4. Edinburgh: T. and A. Constable Ltd., 1964.

[18] E. B. Podgoršak, *Radiation physics for medical physicists*, ch. 8. Germany: Springer, 2006.

[19] E. Varin, A. Hébert R Roy and J Koclas, "A user guide for DONJON version 3.01," Tech. Rep. IGE-208 Rev. 4, École Polytechnique de Montréal, August 2005.

[20] B. Rouben, "CANDU fuel management." Atomic Energy of Canada Limited, Presented to McMaster University, November 2003.

[21] Radiation Safety Information Computational Center. `https://rsicc.ornl.gov`, 2013.

[22] W. M. Stacey, *Nuclear reactor physics*, ch. 9. Georgia Institute of Technology: John Wiley & Sons, Inc., 2001.

[23] M. L. Williams, M. Asgari and D. F. Hollenbach, "CENTRM: A one-dimensional neutron transport code for computing pointwise energy spectra," Tech. Rep. ORNL/TM-2005/39 Version 6.1 Sect. F18, Oak Ridge National Laboratory, June 2011.

[24] N.M. Greene, "BONAMI: Resonance self-shielding by the Bondarenko method," Tech. Rep. ORNL/TM-2005/39 Version 6.1 Sect. F1, Oak Ridge National Laboratory, June 2011.

[25] B. T. Rearden *et al.*, "SAMS: Sensitivity analysis module for SCALE," Tech. Rep. ORNL/TM-2005/39 Version 6.1 Sect. F22, Oak Ridge National Laboratory, June 2011.

[26] B. T. Rearden M. A. Jessee, "TSUNAMI utility modules," Tech. Rep. ORNL/TM-2005/39 Version 6.1 Sect. M18, Oak Ridge National Laboratory, June 2011.

[27] D. A. McQuarrie, *Mathematical methods for scientists and engineers*, ch. 21. California: University Science Books, 2003.

[28] S. Goluoglu and C. M. Hopper, "Assessment of degree of applicability of benchmarks for gadolinium using KENO V.a and the 238-group SCALE cross-section library," Tech. Rep. ORNL/TM-2003/106, Oak Ridge National Laboratory, December 2003.

[29] B. L. Broadhead, B. T. Rearden, and C. M. Hopper, "Sensitivity and uncertainty based criticality safety validation techniques," *Nuclear Science and Engineering*, vol. 146, pp. 340–366, 2004.

[30] T. Kugo, "Recent application of nuclear data to reactor core analysis in JAEA," *Journal of the Korean Physical Society*, vol. 59, pp. 1347–1352, August 2011.

[31] W. Press *et al.*, *Numerical recipes in FORTRAN 77: The art of scientific computing*. Cambridge: Press Syndicate of the University of Cambridge, 1986.

[32] M. L. Williams, B. L. Broadhead, M. E. Jessee, and J. J. Wagschal, "TSURFER: An adjustment code to determine biases and uncertainties in nuclear system responses by consolidating differential data and benchmark integral experiments," Tech. Rep. ORNL/TM-2005/39 Version 6.1 Sect. M21, Oak Ridge National Laboratory, June 2011.

[33] B. T. Rearden, "TSUNAMI-3D: Control module for three-dimensional cross-section sensitivity and uncertainty analysis for criticality," Tech. Rep. ORNL/TM-2005/39 Version 6.1 Sect. C9, Oak Ridge National Laboratory, June 2011.

[34] T. Zhu, "Sensitivity and uncertainty analysis of (Th, Pu)O2 benchmark ex-

periments in ZED-2 using TSUNAMI," Master's thesis, McMaster University, 2011.

[35] B. L. Broadhead, C.M. Hopper, R. L. Childs, and C.V. Parks, "Sensitivity and uncertainty analyses applied to criticality safety validation, volume 1," Tech. Rep. NUREG/CR-6655, Vol 1, ORNL/TM-13692/V1, Oak Ridge National Laboratory, November 1999.

[36] B. L. Broadhead, C.M. Hopper, R. L. Childs, and C.V. Parks, "Sensitivity and uncertainty analyses applied to criticality safety validation, volume 2," Tech. Rep. NUREG/CR-6655, Vol. 2, ORNL/TM-13692/V2, Oak Ridge National Laboratory, November 1999.

[37] B. L. Broadhead *et al.*, "Criticality safety applications of S/U validation methods," in *ANS/ENS 2000 International Winter Meeting and Embedded Topical Meetings*, (Washington DC, USA), November 2000.

[38] J. Pencer, "Preliminary specifications for a 2D lattice-level SCWR benchmark," Tech. Rep. 217-123700-REPT-005, Atomic Energy of Canada Limited, June 2012.

[39] P. Boczar, "ACR Technology base: fuel." Atomic Energy of Canada Limited, Presented to US Nuclear Reulatory Commission, September 2002.

[40] J. Pencer, "SCWR 78-element bundle reference model," Tech. Rep. 217-123700-REPT-001, Atomic Energy of Canada Limited, September 2011.

[41] W. Inch *et al.*, "Increasing CANDU operating margins with CANFLEX fuel," in *6th COG/IAEA Technical Committee Meeting on Exchange of Operational Safety Experience of PHWRs*, (Trois Rivieres, Quebec), September 2000.

[42] W. Shen, "Evaluation of the adequacy of using few-group lattice-homogenized properties for the diffusion analysis of the super critical water reactor," in *PHYSOR-2012 - Advances in Reactor Physis - Linking Research, Industry, and Education*, (Knoxville Tennessee USA), April 2012.

[43] A. Nuttin *et al.*, "Study of CANDU thorium-based fuel cycles by deterministic and Monte Carlo methods," in *PHYSOR-2006, ANS Topical Meeting on Reactor Physics*, (Vancouver British Columbia Canada), September 2006.

[44] B. Rouben, "DIFC6 computer program." Nuclear fuel management EP704, McMaster University, 2011.

[45] M. McDonald, "Fuel and core physics considerations for a pressure tube supercritical water cooled reactor," Master's thesis, McMaster University, 2011.

[46] L. M. Petrie *et al.*, "KENO V.a: An improved Monte Carlo criticality program," Tech. Rep. ORNL/TM-2005/39 Version 6.1 Sect. F11, Oak Ridge National Laboratory, June 2011.

[47] G. Marleau, "DRAGON today and tomorrow," in *ANL DRAGON Workshop*, (Argonne, Illinois), 2005.

[48] National Institute of Standards and Technology, "Thermophysical properties of fluid systems." `http://webbook.nist.gov/chemistry/fluid/`, 2011.

[49] J. Fox, *Applied regression analysis and generalized linear models*, ch. 11. California, USA: Sage Publications Inc., 2nd ed., 2008.

[50] G.B. Wilkin, "ZED-2 reactor capabilities and the new license safety case," in *ZED-2 Winter School*, (Chalk River, Ontario), December 2011.

[51] B. T. Rearden, "Improvements in KENO V.a to support TSUNAMI-3D sensitivity calculations," in *The Monte Carlo method: versatility unbounded in a dynamic computing world*, (Chattanooga, Tennessee), April 2005.

[52] D. E. Mueller and B. T. Rearden, "Sensitivity coefficient generation for a burnup credit cask model using TSUNAMI-3D," in *Integrating criticality safety into the resurgence of nuclear power*, (Knoxville, Tennessee), September 2005.

[53] ZED-2 Winter School, "Simulations of reactor experiments with MCNP." Atomic Energy of Canada Limited, 2011.

[54] L. Petrie *et al.*, "KENO Lifetimes," in *American Nuclear Society Meeting*, (Orlando, Florida), June 1997.